Characterizing Forest Structure Using Terrestrial LiDAR Remote Sensing

by

Leila Taheriazad

A thesis submitted in partial fulfillment of the requirements for the degree of

Doctor of Philosophy

Department of Earth and Atmospheric Science
University of Alberta

ABSTRACT

Forests are one of the important natural resources, because of their benefits toward the economy and ecosystem services including goods, climate control, pollution reduction, carbon storage, wildlife habitat protection, nutrient cycling, social and cultural benefits. Hence, sustainable development requires assessment of forest structure with the goal of efficient resource management. The goal of this thesis is to investigate forest structure using Light Detection and Ranging (LiDAR) technology. LiDAR is an active remote sensing method that is suitable for this purpose due to its capability to capture both distribution and three-dimensional structure of canopies into a 3D point cloud with millions of points. This thesis introduces new simple algorithms for automatic processing of the point cloud data collected by ground-based LiDAR and simple assessment of forest structure. Also, the major challenges in handling the huge amount of data generated by LiDAR are discussed and proper solutions are offered and examined. In this light, chapter one reviews the background and capabilities of the LiDAR technology. In chapter two, an algorithm is developed for processing LiDAR data to generate Digital Terrain Model (DTM). Chapter three targets separation of photosynthetic components from non-photosynthetic components using a combination of distance and intensity attribute which are both provided by LiDAR. A comprehensive qualitative/quantitative error analysis is also presented along with the chapters on DTM and separation methods. Chapter four deals with Leaf Area Index (LAI) which makes one of the important assessment parameters of any forest. The drawbacks of current methods for calculation of LAI including the application of uniform voxels of arbitrary size and ignoring the effect of LiDAR scan resolution are discussed. Then, LAI is calculated by non-uniform voxels based on local sampling resolution of LiDAR. This technique avoids using the common radiative transfer model and gap fraction model which

involve a high level of approximation. Hence, LAI is calculated directly from the LiDAR data and without intermediate auxiliary models. Finally, chapter five reviews the main contributions and significance of this study. Collectively, ground-based LiDAR is demonstrated as a suitable technology for forest survey. The 3D point cloud data from LiDAR can be processed by proper algorithms to generate DTM, separate leaves from wood, and calculate LAI with high precision.

هر کجا برگی هست شور من می شکفد (سهراب سپهری)

Wherever there is a leaf, my passion blossoms
(S. Sepehri)

For my Love

ACKNOWLEDGEMENTS

I would like to express my deeply gratitude to my supervisor, Dr. Arturo Sánchez-Azofeifa for all his support, guidance, comments, patience, motivation, and immense knowledge that finally lead to the successful completion of this dissertation. I am thankful for the opportunity he provided to students to develop as researchers.

Besides my supervisor, I would like also to thank my committee members, Dr. Benoit Rivard and Dr. Mike MacGregor, for their support, insightful comments and scientific advices.

My thesis could not have been completed without the financial support of the University of Alberta (2013-2017), National Science and Research Council of Canada (NSERC) and the Inter-American Institute for Global Change Research (CRN3-025). The Ecosystem Management Emulating Natural Disturbance (EMEND) is also acknowledged for providing facilities in the study area in boreal forest, north of Alberta.

All this would not have been possible without the constant encouragement and support provided by my dear husband, my parents, and my siblings throughout my studies.

I would also like to thank my fellow graduate students and office/lab mates for the stimulating discussions and all the people who contributed in some way to the work described in this thesis including Dr. Bradley D. Danielson, Dr. Virginia Garcia Millan, Dr. Kati Laakso, Dr. Iman Entezari Najafabadi, Sarah Freitas Magalhães Silva, Dominica Harrison, Marissa Castro Magnani, Wei Li, Lindong Zou, Branko Hilje Rodriquez, Felipe Alencastro, Sofia Calvo Rodriguez, Mei Mei Chong, Michael Hesketh at the Centre for Earth Observation Sciences (CEOS), University of Alberta.

Finally, I would like to dedicate this dissertation to my love, Hamid, who has been a constant source of support and encouragement through my studies.

This work is also dedicated to my parents, who have always loved me unconditionally and whose good examples have taught me to work hard for the things that I aspire to achieve.

Table of Contents

List of Tables

List of Figures

CHAPTER 1

Introduction

1.1 Background

The life cycle on planet earth is dependent upon forest ecosystems. Forests cover about 30% of Earth's land area (~4.03 billion hectares) (FAO 2010). The forests are responsible for 50% of terrestrial photosynthesis and contain 80% of the total plant biomass on the earth (FAO 2010, Beer et al. 2010; Kindermann et al. 2008). Forests are one of the most important components in global CO_2 exchange in terrestrial ecosystems with main reservoirs on soils and standing biomass (Zheng et al. 2007). Furthermore, forests offer high levels of biodiversity and provide a wide variety of direct and indirect goods and ecosystem services to humanity such as fiber, timber, food, medicine, fresh air and water, control of climate and disease, protection of habitats, soils, watersheds, fisheries, and also cultural, spiritual and recreational benefits (Jackson et al. 2005; McKinley et al. 2011; Millennium Ecosystem Assessment, 2005; Gullison et al., 2007). In addition, forests constitute a fundamental source of raw materials, both for industry and for rural societies that depend on forest products to meet basic living needs (FAO, 2006). Understanding the forest canopy structure is a key factor for ecosystem assessment, management, modeling, and monitoring (Sexton et al. 2009). A forest canopy is a complex volume that it is composed of leaves, twigs, branches, and stems with gaps between them (Andersen et al. 2006). Canopy structure is described by several parameters such as canopy height, Diameter at Breast Height (DBH), crown height, crown volume, plant area, etc. These aforementioned parameters affect the interaction between the atmosphere and land surface, especially in the case of interception of precipitation, radiation absorption, and photosynthetic activity (Baldocchi and Harley, 1995; Parker, 1995). As an example, the canopy height which is an initial canopy parameter can affect the microclimate, the wildlife habitat value, and the plant composition (Welden et al. 1991; Kruger et al. 1997; Raupach, 2004; James, 1971). Also, the leaf area which is a significant canopy parameter is an indicator of the global carbon cycle (Beland et al. 2014).

Ecosystem service management requires the forest resource information at different scales from national to stand-scale and also at various user levels, from global governmental decision making to operational forest management (Liang et al. 2016). At the national scale and global level, the main goal of a forest inventory is to collect and assess data of some forest attributes such as biodiversity, stem volume, and biomass. On the other hand, at the forest stand scale, data collection is necessary for forest operations and finding timber harvesting potential. Based on the required accuracy and the available resources, forest inventory techniques include field measurements and remote sensing tools. Conventionally, field measurements have been done using simple tools, such as calipers and clinometers, and the progress of forest inventories has been slow. Recently, advanced remote sensing techniques enable researchers to measure properties and monitor processes of ecosystems quickly, accurately, and in different scales (Prince and Goward, 1995; Goetz et al. 2000; Running et al. 2000; Zheng et al. 2004). With the advent of the ground-based Light Detection and Ranging (LiDAR) in the past two decades, significant changes have occurred in forest inventory.

LiDAR has been a promising active remote sensing tool to deliver various parameters of the canopy in detail. LiDAR can be used to effectively estimate the 3D canopy parameters as an alternative to conventional passive methods (Yu et al. 2004; Næsset, 1997; Hyyppa¨ et al. 2001; Næsset et al. 2004; Reutebuch et al. 2005; Omasa et al. 2006). Due to the three following reasons, LiDAR emerged as a suitable and effective alternative for field measurements inventory:

(1) Field inventory is time-consuming and labor- intensive both in data collecting and data interpreting;

(2) The LiDAR accuracy is higher than the conventional techniques;

(3) LiDAR provides more details on tree attributes which are important for forest management and decision-making at any scale (Liang et al. 2016).

Typical remote sensing methods represent the forest ecosystem attributes in two-dimensional space while LiDAR technology offers 3D forest structure attributes such as canopy structure, crown volume, biomass, stem density, sub-canopy topography, vertical foliage diversity, and leaf area index through direct and indirect retrievals (Behera and Roy, 2002).

The LiDAR scanner emits a laser beam in the spectrum of visible to near-infrared light (Beland et al. 2014). When the pulse hits the surface of an object, part of energy reflects back to

the scanner and based on the time interval between the pulse emission and reception, the distance between the object and the instrument is calculated. Finally, the 3D coordinate of each point of the surrounding objects will be calculated and collected in a Point Cloud Data (PCD) set.

Various LiDAR sensors use different laser's wavelength, power, pulse duration, pulse repetition rate, beam size and divergence angle. The wavelength of the laser for ground applications usually is between 500 to 1064 nanometers (Lefsky et al. 2002). LiDAR can be used in three platforms: spaceborne LiDAR such as Deformation, Ecosystem Structure, and Dynamics of Ice (DESDynI) and Ice, Cloud, and Land Elevation Satellite (ICESat) with a resolution of 50-150 m (NCR, 2007), airborne LiDAR with a resolution of 0.1–1 m and ground-based (terrestrial) LiDAR with a resolution of 0.05–10 cm.

Ground-based LiDAR emits small laser pulses with high rate and small angular resolution. The current Terrestrial Laser Scanner (TLS) systems usually have a high spatial resolution in the range of millimeters at several meters from the scanner, for example, ±2 mm at 25 m. The smallest angular resolution in both horizontal and vertical direction is less than 0.01 degree (Liang et al. 2016). The intensity of the return beam depends on several factors including the power of the transmitted laser pulse, the portion of the laser pulse that is captured by an object, and the reflected pulse which is backscattered toward the sensor (Lefsky et al. 2002).

From the aspect of signal processing and sampling, LiDAR systems are classified into the discrete return or full waveform (Dubayah and Drake, 2000; Wulder et al. 2008, 2012). Discrete return LiDAR systems usually record only one (first or last), two (first and last), or a few returns per pulse footprint (Lim et al. 2003; Wulder et al. 2008). The result of discrete return scanning is a 3D cloud of points where the points of lower altitude show the land surface (Lim et al. 2003; Wulder et al. 2008). Also, the distance between the surface of an object and the LiDAR scan station is calculated based on the flight time of the pulse. In contrast, a full waveform LiDAR system measures the quantity of energy reflected toward the sensor for a series of equal time intervals. Full-waveform LiDAR systems deliver a vertical vegetation profile and normally have a larger footprint of 10 m to 100 m (Lefsky et al. 2001; Harding et al. 2001). The large peaks in a full waveform profile are interpreted as discrete objects. Therefore, within a forest ecosystem, full waveform systems record the total waveform for structural analysis, while discrete return systems record clouds of points showing intercepted topographies (Lefsky et al. 2001; Harding et al. 2001).

Applications of LiDAR in forestry are generating Digital Terrain Model (DTM), 3D forest structure assessment, and assessment of the forest attributes such as volume and aboveground biomass (Lefsky et al. 2002).

Generating a DTM with traditional surveying techniques such as photogrammetry and field measurement creates a high accuracy DTM. However, it is time-consuming and labor-intensive (Lefsky et al. 2002). Generating DTM by LiDAR is of commercial benefits (Flood and Gutelis, 1997). Recently, LiDAR has been applied in DTM generation (Chen et al. 2016; Nurunnabi et al. 2016; Beumier and Idrissa, 2016; Maguya et al. 2014; Reutebuch et al. 2003).

Canopy structure is the vertical and horizontal distribution of all the foliage elements with a variety of shape, size, and orientation of different species groups above-ground in a forest stand (Norman and Campbell, 1989; McIntosh et al. 2009). Canopy structure contains substantial information about the state of development of plant communities and canopy function (Lefsky et al. 1999; Brownd and Prker, 1994). Forest structure assessment is of ultimate significance for resource management and sustainable development. The investigation into the 3D canopy structure is necessary for their accurate quantitative assessment (Martínez et al. 2009).

LiDAR has been used increasingly as an effective tool to provide data on aboveground biomass in forest areas (Wulder et al. 2012a, 2012b). Margolis et al. (2015) estimated above ground biomass using LiDAR in the boreal forest of North America. Zhou and Hemstrom (2009) used LiDAR data to develop a model for estimation of tree biomass on forest land in the Pacific Northwest (USA). Other studies focused on estimating aboveground biomass in the forest using airborne LiDAR data are performed by Chang et al. (2012) and Kim et al. (2012).

1.2 Thesis Objectives and Hypotheses

The current study aims to develop new methods for analyzing ground-based LiDAR data to assess the structure of the boreal forest and overcome some of the current limitations of this new technology for forest research and management. In this context, the three main specific objectives and hypotheses of my doctoral dissertation are:

1- To develop a simple model for extracting Digital Terrain Model (DTM) in a dense boreal forest with high spatial resolution using ground-based LiDAR data, and evaluate the effect of surface topography on DTM retrievals. To carry out this task, I am proposing to use non-linear

median digital filters and local slope analysis. The processing steps are selecting lowest altitude points, applying median filters of high order (>15). In addition, to find the optimum order of median filter, a new criterion is developed which monitors the gradient in slope of DTM profile. It is hypothesized that the PCD collected by terrestrial provides sufficient information on land properties for extraction of DTM with spatial resolution as small as 20 cm using the above-mentioned processing steps.

2- To assess the potential of terrestrial LiDAR data for detection of photosynthetic components from non-photosynthetic components and to develop an automatic, simple, and efficient algorithm for separating photosynthetic components from the non-photosynthetic components. It is hypothesized that both intensity and (*x, y, z*) coordinates provided by the terrestrial LiDAR for each point in the PCD are required for extraction of a suitable scale with a single threshold value for separation of leaves from wood.

3- To develop a new method to calculate LAI from LiDAR PCD directly and simply by addressing the drawbacks of previous methods in literature such as radiative transfer model. It is hypothesized LAI can be calculated directly (without using radiative transfer model) from terrestrial LiDAR PCD using non-uniform voxelization based on local spatial scan resolution.

1.3 Thesis Outline

In order to achieve the goals and hypotheses associated to this doctoral dissertation, I have divided this work into three chapters. The following is the description of each individual contribution.

Chapter 2. *Retrieving a Digital Terrain Model (DTM) in a boreal forest using ground-based LiDAR.* In this chapter, a new simple algorithm is developed for automatic DTM generation in MATLAB® software based on median filtering along with a new score for assessment of the quality of DTM profile based on local slope. The input of the algorithm is a high spatial resolution PCD which is slightly post processed. The algorithm is applied to cross-sections of boreal forests in north of Canada with surface areas up to 40×40 m^2. Also, qualita

tive and quantitative (omission/commission) errors associated with DTM profile are calculated and analyzed. This chapter is ready for submission as a publication. The authors are Leila Taheriazad, Arturo Sanchez Azofeifa, and Hamid Moghadas. Extraction of a Digital Terrain Model (DTM) from point cloud data of ground-based LiDAR.

Chapter 3. *Automatic separation of photosynthetic and non-photosynthetic components in a point cloud data from a boreal forest canopy*. A new simple efficient algorithm is developed for automatic separation of photosynthetic and non-photosynthetic features in a canopy. The algorithm input is the raw PCD collected by terrestrial LiDAR from a Canadian boreal forest. The algorithm uses point intensity provided by LiDAR. The raw intensity is processed using the distance of a point to the scan station. It is shown that photosynthetic and non-photosynthetic features of a PCD can be separated with a very low commission and omission error using the proposed method. This work is ready for submission as a publication. The authors are Leila Taheriazad, Arturo Sanchez Azofeifa, and Hamid Moghadas. Automatic separation of photosynthetic and non-photosynthetic components in point cloud of ground based LiDAR using intensity parameter.

Chapter 4. *Calculation of leaf area index in a Canadian boreal forest using ground-based LiDAR*. The 3D PCD collected by terrestrial LiDAR has been used to extract canopy structure parameters such as Leaf Area Index (LAI). To calculate LAI, state of the art methods divide the PCD into smaller equisize cubic collections called voxels (Hancock et al. 2014; Hosoi et al. 2013; Côté et al. 2012; Song et al. 2011; Hosoi and Omasa, 2009; Wang et al. 2008;). Then, they take advantage of auxiliary mathematical models such as radiative transfer and gap fraction model in order to calculate LAI. The mentioned methods are prone to a high level of error. Besides, the effect of LiDAR scan sampling resolution is ignored in present studies. Chapter 4 is dedicated to enhancing current methods for extracting LAI from LiDAR PCD by considering the effect of scan sampling resolution in voxelization, offering an improved voxel system, and without using radiative transfer or gap fraction model. This can simplify the computations while improving the calculation accuracy. This chapter is ready for submission as a publication. The authors are Leila Taheriazad, Arturo Sanchez Azofeifa, and Hamid Moghadas. Adaptive voxelization for direct calculation of leaf area index using terrestrial LiDAR.

1.4 Significance

The results and findings of the studies in this thesis are to be used to broaden the knowledge of monitoring in forest ecosystems with the purpose of sustainable resource management. As monitoring forests with traditional inventory is time-consuming, labor-intensive and costly, remote sensing technologies such as LiDAR have been receiving much attention. However, processing the huge amount of data and images collected by LiDAR for extraction of forest ecosystem parameters isn't a straightforward task. This thesis focuses on algorithms for automatic and effective extraction of the forest parameters. These algorithms are of commercial value since they can be integrated with LiDAR scan stations for on-site application toward sustainable management and development.

References

Andersen, H.E., Reutebuch, R.E., and McGaughey, R.J. 2006. A rigorous assessment of tree height measurements obtained using airborne lidar and conventional field methods. *Canadian Journal of Remote Sensing*, 32, 355-366.

Anjin, C., Yongmin, K., Yongil, K. and Yangdam, E. 2012. Estimation of individual tree biomass from airborne lidar data using tree height and crown diameter. *Disaster Advances*, 5(4), 360-365.

Beer, C., Reichstein, M., Tomelleri, E., Ciais, P., Jung, M., Carvalhais, N., Rödenbeck, C., Arain, M.A., Baldocchi, D., Bonan, G.B. and Bondeau, A. 2010. Terrestrial gross carbon dioxide uptake: global distribution and covariation with climate. *Science*, 329(5993), 834-838.

Behera, M. D., and Roy, P. S. 2002. Lidar remote sensing for forestry applications: The Indian context. *Current Science*, 83 (11), 1320-1328.

Beland, M., Baldocchi, D.D., Widlowski, J.L., Fournier, R.A. and Verstraete, M.M. 2014b. On seeing the wood from the leaves and the role of voxel size in determining leaf area distribution of forests with terrestrial LiDAR. *Agricultural and Forest Meteorology*, 184, 82-97.

Beumier, C., and Idrissa, M. 2016. Digital terrain models derived from digital surface model uniform regions in urban areas. *International Journal of Remote Sensing*, 37 (15), 3477-3493.

Brown, M.J., and Parker, G.G. 1994. Canopy light transmittance in a chronosequence of mixed-species deciduous forests. *Canadian Journal of Forest Research*, *24*(8), 1694-1703.

Chen, Z., Xu, B., and Gao, B. 2016. An Image-Segmentation-Based Urban DTM Generation Method Using Airborne LiDAR Data. *IEEE, journal of selected topics in applied earth observations and remote sensing*, 9 (1), 496-506.

Côté, J.F., Fournier, R.A., Frazer, G.W. and Niemann, K.O. 2012. A fine-scale architectural model of trees to enhance LiDAR-derived measurements of forest canopy structure. *Agricultural and Forest Meteorology*, 166, 72-85.

Dubayah R.O., and Drake J.B. (2000). LiDAR Remote Sensing for Forestry. *Journal of Forestry*, 98 (6), 44-46.

FAO, 2006. Global Forest Resources Assessment 2005. FAO Forestry Paper 147, Food and Agriculture Organization of the United Nations, Rome, Italy.

Flood, M., and Gutelis, B. 1997. Commercial implications of topographic terrain mapping using scanning airborne laser radar. *Photogrammetric Engineering and Remote Sensing*, 63, 327-366.

Food Agric. Organ. (FAO). 2010. Global forest resources assessment. *Forestry Paper* 163, FAO, Rome, Italy.

Goetz, S.J., Prince, S.D., Small, J., and Gleason, A.C.R., 2000. Interannual variability of global terrestrial primary production: results of a model driven with satellite observations. *Journal of Geophysical Research-Atmospheres,* 105, 20077-20091.

Gullison, R.E., Frumhoff, P., Canadell, J., Field, C.B., Nepstad, D.C., Hayhoe, K., Avissar, R., Curran, L.M., Friedlingstein, P., Jones, C.D., and Nobre, C. 2007. Tropical forests and climate policy. *Science*, 316, 985-986.

Hancock, S., Essery, R., Reid, T., Carle, J., Baxter, R., Rutter, N. and Huntley, B. 2014. Characterising forest gap fraction with terrestrial lidar and photography: An examination of relative limitations. *Agricultural and forest meteorology*, 189, 105-114.

Harding, D.J., Lefsky, M.A., Parker, G.G., and Blair J.B. 2001. Laser altimeter canopy height profiles: methods and validation for closed-canopy, broadleaf forests. *Remote Sensing of Environment*, 76 (3), 283-297.

Hosoi, F. and Omasa, K. 2012. Estimation of vertical plant area density profiles in a rice canopy at different growth stages by high-resolution portable scanning LiDAR with a lightweight mirror. *ISPRS journal of photogrammetry and remote sensing*, 74, 11-19.

Hosoi, F., Nakai, Y. and Omasa, K. 2013. 3-D voxel-based solid modeling of a broad-leaved tree for accurate volume estimation using portable scanning LiDAR. *ISPRS journal of photogrammetry and remote sensing*, 82, 41-48.

Hyyppa, J., Kelle, O., Lehikoinen, M. and Inkinen, M. 2001. A segmentation-based method to retrieve stem volume estimates from 3-D tree height models produced by laser scanners. *IEEE Transactions on geoscience and remote sensing*, 39, 969-975.

Jackson, R.B., Jobbágy, E.G., Avissar, R., Roy, S.B., Barrett, D.J., Cook, C.W., Farley, K.A., Le Maitre, D.C., McCarl, B.A. and Murray, B.C. 2005. Trading water for carbon with biological carbon sequestration. *Science*, 310(5756), 1944-1947.

Kim, Y., Chang, A., Kim, Y., Song, J. and Kim, C. 2012. Estimation of forest biomass from airborne LiDAR data as measures against Global Warming-Individual Tree Unit and Forest Stand Unit. *Disaster Advances*, *5*(4), 295-299.

Kindermann, G., McCallum, I., Fritz, S. and Obersteiner, M. 2008. A global forest growing stock, biomass and carbon map based on FAO statistics. *Silva Fennica*, 42(3), 387-396.

Lefsky, M.A., Cohen W.B., Parker G.G., and Harding D.J. 2002. LiDAR Remote Sensing for Ecosystem Studies. *BioScience*, 52(1), 19-30.

Lefsky, M.A., Cohen, W.B. and Spies, T.A. 2001. An evaluation of alternate remote sensing products for forest inventory, monitoring, and mapping of Douglas-fir forests in western Oregon. *Canadian journal of forest research*, 31(1), 78-87.

Lefsky, M.A., Cohen, W.B., Acker, S.A., Parker, G.G., Spies, T.A., and Harding, D.J. 1999. LiDAR remote sensing of the canopy structure and biophysical properties of Douglas-fir western hemlock forests. *Remote Sensing of Environment*, 70(3), 339-361.

Liang, X., Kankare, V., Hyyppä, J., Wang, Y., Kukko, A., Haggrén, H., Yu, X., Kaartinen, H., Jaakkola, A., Guan, F., Holopainen, M., Vastaranta, M. 2016. Terrestrial laser scanning in forest inventories. *ISPRS Journal of Photogrammetry and Remote Sensing*, 115, 63-77.

Lim, K., Treitz, P., Wulder, M., St-Onge, B. and Flood, M. 2003. LiDAR remote sensing of forest structure. *Progress in physical geography*, 27(1), 88-106.

Maguya, A.S., Junttila, V. and Kauranne, T. 2014. Algorithm for Extracting Digital Terrain Models under Forest Canopy from Airborne LiDAR Data. *Remote Sensing*, 6, 6524-6548.

Margolis, H.A., Nelson, R.F., Montesano, P.M., Beaudoin, A., Sun, G., Andersen, H.E. and Wulder, M.A. 2015. Combining satellite lidar, airborne lidar, and ground plots to estimate the amount and distribution of aboveground biomass in the boreal forest of North America. *Canadian Journal of Forest Research*, 45(7), 838-855.

Martínez, B., García-Haro, F.J. and Camacho-de Coca, F. 2009. Derivation of high-resolution leaf area index maps in support of validation activities: Application to the cropland Barrax site. *Agricultural and forest meteorology*, 149(1), 130-145.

McIntosh, A.C., Gray, A.N. and Garman, S.L. 2009. Canopy structure on forest lands in western Oregon: Differences among forest types and stand ages. United States Department of Agriculture, Forest Service, Pacific Northwest Research Station, General Technical Report PNW-GTR-794 August 2009.

McKinley, D.C., Ryan, M.G., Birdsey, R.A., Giardina, C.P., Harmon, M.E., Heath, L.S., Houghton, R.A., Jackson, R.B., Morrison, J.F., Murray, B.C. and Pataki, D.E. 2011. A synthesis of current knowledge on forests and carbon storage in the United States. *Ecological Applications*, 21(6), pp.1902-1924.

MEA, M.E.A. 2005. Ecosystems and human well-being: synthesis. *Island, Washington, DC*.

Næsset, E. 1997. Determination of mean tree height of forest stands using airborne laser scanner data. *ISPRS Journal of Photogrammetry and Remote Sensing,* 52, 49-56.

Næsset, E., Gobakken, T., Holmgren, J., Hyyppä, H., Hyyppä, J., Maltamo, M., Nilsson, M., Olsson, H., Persson, Å. and Söderman, U. 2004. Laser scanning of forest resources: the Nordic experience. *Scandinavian Journal of Forest Research*, 19(6), 482-499.

NRC (2007). Earth science and applications from space: National imperatives for the next decade and beyond, 2007. Washington, D.C., The National Academies Press, 426 pp.

Norman, J.M. and Campbell, G.S. 1989. "Canopy structure," in Plant Physiological Ecology. Field Methods and Instrumentation, J. E. R. W. Pearcy, H. A. Mooney, and P. W. Rundel, Eds. New York: Chapman and Hall, 301-325.

Norman, J.M. and Campbell, G.S. 1989. Canopy structure. In 'Plant physiological ecology: field methods and instrumentation'. (Eds RW Pearcy, J Ehleringer, HA Mooney, PW Rundel) 301-325.

Nurunnabi, A., West, G., and Belton, D. 2016. Robust Locally Weighted Regression Techniques for Ground Surface Points Filtering in Mobile Laser Scanning Three Dimensional Point Cloud Data. *IEEE, transactions on geoscience and remote sensing*, 54 (4), 2181-2193.

Omasa, K., Hosoi, F., and Konishi, A. 2006. 3D lidar imaging for detecting and understanding plant responses and canopy structure. *Journal of experimental botany*, 58(4), 881-898.

Pan, Y., Birdsey, R.A., Fang, J., Houghton, R., Kauppi, P.E., Kurz, W.A., Phillips, O.L., Shvidenko, A., Lewis, S.L., Canadell, J.G. and Ciais, P. 2011. A large and persistent carbon sink in the world's forests. *Science*, 333(6045), 988-993.

Prince, S.D., and Goward, S.N. 1995. Global primary production: a remote sensing approach. *Journal of Biogeography,* 22, 815-835.

Reutebuch, S.E., Andersen, H.E. and McGaughey, R.J. 2005. Light detection and ranging (LIDAR): an emerging tool for multiple resource inventory. *Journal of Forestry*, 103(6), 286-292.

Reutebuch, S.E., McGaughey, R. J., Andersen, H. E., and Carson, W.W. 2003. Accuracy of a high-resolution LiDAR terrain model under a conifer forest canopy. *Canadian Journal of Remote Sensing*, 29 (5), 527-535.

Running, S.W., Thornton, P.E., Nemani, R. and Glassy, J.M. 2000. Global terrestrial gross and net primary productivity from the Earth Observing System. *Methods in ecosystem science*, 3, 44-45.

Sexton, J.O., Bax, T., Siqueir, Paul., Swenson, J.J., and Hensley, S. 2009.A comparison of lidar, radar, and field measurements of canopy height in pine and hardwood forests of southeastern North America. *Forest Ecology and Management*, 257, 1136-1147.

Song, Y., Maki, M., Imanishi, J. and Morimoto, Y. 2011. Voxel-based estimation of plant area density from airborne laser scanner data. In Proceedings of the ISPRS Workshop Laser Scanning, Calgary, Canada 38 (5/W12).

Wang, Y., Weinacker, H. and Koch, B. 2008. A lidar point cloud based procedure for vertical canopy structure analysis and 3D single tree modeling in forest. *Sensors*, 8(6), 3938-3951.

Wulder, M.A., Bater, C.W., Coops, N.C., Hilker, T. and White, J.C. 2008. The role of LiDAR in sustainable forest management. *The Forestry Chronicle*, 84(6), 807-826.

Wulder, M.A., White, J.C., Bater, C.W., Coops, N.C., Hopkinson, C. and Chen, G. 2012a. Lidar plots -A new large-area data collection option: Context, concepts, and case study. *Canadian Journal of Remote Sensing*, 38(05), 600-618.

Wulder, M.A., White, J.C., Nelson, R.F., Næsset, E., Ørka, H.O., Coops, N.C., Hilker, T., Bater, C.W. and Gobakken, T. 2012. Lidar sampling for large-area forest characterization: A review. *Remote Sensing of Environment*, 121, 196-209.

Yu, X., Hyyppä, J., Kaartinen, H. and Maltamo, M. 2004. Automatic detection of harvested trees and determination of forest growth using airborne laser scanning. *Remote Sensing of Environment*, 90(4), 451-462.

Zheng, D.L., Rademacher, J., Chen, J.Q., Crow, T., Bresee, M., le Moine, J., and Ryu, S.R. 2004. Estimating aboveground biomass using Landsat 7 ETM+ data across a managed landscape in northern Wisconsin, USA. *Remote Sensing of Environment,* 93, 402-411.

Zhou, X. and Hemstrom, M.A. 2009. Estimating aboveground tree biomass on forest land in the Pacific Northwest: a comparison of approaches.

CHAPTER 2

Retrieving a Digital Terrain Model (DTM) in a Boreal Forest Using Ground-Based LiDAR

2.1 Introduction

Digital Terrain Model (DTM) is the 3D demonstration of the ground surface. According to Miller and LaFelamme (1985), DTM represents the ground surface points which are statistically continuous and has known (*x, y,* and *z*) Cartesian coordinates. Geometrically, DTM maps *x, y* coordinates as a function of terrain elevation $z = f(x,y)$. Here, the terrain is defined as the boundary surface between the solid ground and the air (Pfeifer and Mandlburger, 2009; Sithole and Vosselman, 2004). There are several other terms for description of terrain such as Digital Terrain Elevation Model (DTEM), Digital Elevation Model (DEM), Digital Height Model (DHM), and Digital Ground Model (DGM), which should be carefully used (Petrie and Kennie, 1990). Among those, only DEM is the same as DTM. But the other terms should not be mistaken with DTM (El-Sheimy et al. 2005; Pfeifer and Mandlburger, 2009).

DTM is widely used in Global Positioning System (GPS), Geographical Information System (GIS), and forestry. Traditionally, data collection for DTM is carried out by field measurement and photogrammetry which are time-consuming and labor-intensive (Kraus and Pfeifer, 1998). Furthermore, in remote and dense forested areas, these methods are not possible. As an alternative, airborne and satellite-based technologies such as optical satellites, satellite altimetry, and Interferometric Synthetic Aperture Radar (InSAR) are used (Bamber and Rivera, 2007; Haugerud and Harding, 2001; Raber et al. 2002; Maguya et al. 2014; Reutebuch et al. 2003). These airborne and satellite-based technologies offer limited spatial resolution and very low precision (Herzfeld et al. 1993; Moholdt et al. 2010).

Recently, Light Detection and Ranging (LiDAR) technology has been widely used in landscape and environmental assessment, road management, indoor modeling, urban mapping, urban street maintenance, and geology (Kraus et al. 2006; Chehata et al. 2009; Yu et al. 2010; Hong et al. 2015; Jones, 2006; Wang et al. 2010; Jaboyedoff et al. 2012). LiDAR is an active remote sensing system which is minimally affected by the external light conditions. Airborne

LiDAR can offer a decimeter precision that outperforms satellite techniques (Woolard and Colby, 2002; Arnold et al. 2006; Chen, 2007; Roering et al. 2009). The accuracy of DTM by airborne LiDAR in forested areas is equal to photogrammetry in open areas (Kraus and Pfeifer 1998). However, weak signal return from the sky to ground and rolling of LiDAR platform may cause miscalculation in surface features (Liu, 2008; Pope et al. 2013). Chen et al. (2016) used airborne LiDAR data to generate urban DTM; Nurunnabi et al. (2016) have extracted surface points from mobile laser scanning data; a high-resolution terrain model under a conifer forest canopy was produced by Reutebuch et al. (2003); Beumier and Idrissa (2016) extracted DTM from DSM using airborne laser scanning in urban area; Maguya et al. (2014) has driven DTM in steep forested terrain from airborne LiDAR data; Tyagur and Hollaus (2016) create an automatic DTM for road environment of the nature reserve. As an alternative, ground-based LiDAR has the potential to provide precise DTM with high spatial resolution even from dense forest-covered grounds due to its fixed platform and high-density point cloud (Slob and Hack, 2004; Prokop, 2008; Entwistle et al, 2009; Ergun, 2010; Abellán e al. 2014). Another important feature of ground-based LiDAR is its quick scan which outperforms other technologies; as an example, the Leica Scan Station C10 has a data acquisition rate of 50000 samples/sec and acquisition time of 6 min and 45 sec.

The initial step in processing ground-based LiDAR data is separating ground and non-ground points. However, this procedure is challenging in dense environments such as forest due to occlusion effect (Tyagur and Hollaus, 2016). Occlusion happens where some portions of the ground are missing because of other features such as trunks, branches or leaves (Bauwens et al. 2016).

Many algorithms have been developed for LiDAR ground filtering during the past decade. Sithole and Vosselman (2004) examined and compared several ground filtering algorithms for processing airborne LiDAR data. Zhang and Whitman (2005) used three algorithms to separate ground and non-ground points from airborne LiDAR data. Bartels and Wei (2010) have developed an unsupervised classification algorithm (skewness balancing) for separation of ground and non-ground point.

Different filters for generating DTM are classified into four major classes: morphological, surface-based, progressive densification and segmentation (Pfeifer and Mandlburger, 2009; Nurunnabi et al. 2016). The International Society for Photogrammetry and Remote Sensing

(ISPRS) Working Group 3 (WGIII) has compared these filters and shown that the performance of different filters is not the same for various landscape topology (Pfeifer and Mandlburger, 2009; Sithole and Vosselman, 2004). These filter classes are elaborated as follows.

Morphological filters and its variants: The basic of the DTM morphological filter is derived from mathematical morphology presented by Haralick and Shapiro (1992). In this method, the ground points are first separated based on lowest *z*-value within the data set and then followed by an auto-regression analysis to refine the initial results (Shan and Sampath, 2005). Since the size of the object elements on the ground can affect the result of this method, Kilian et al. (1996) improved it by applying a group of morphologic functions with a diversity of size to detect the ground points.

Vosselman (2000) and Sithole (2001) developed a variant of morphological filter named slope-based filter to consider the local relief. This filter works based on the terrain slope threshold (Sithole, 2001). This method is not applicable to steep areas (Vosselman, 2000; Sithole, 2001; Zakˇsek and Pfeifer, 2006). Morphological filters have been used by Kilian et al. 1996; Vosselman, 2000; Lohmann et al. 2000; Zhang et al. 2003; and Filin and Pfeifer, 2006. Some variants of morphological methods are terrain slope (Axelsson, 1999; Sithole, 2001), local elevation difference (Wang et al. 2001), and Despike Virtual Deforestation (VDF) algorithm (Haugerud and Harding, 2001; Raber et al. 2002).

Surface-based filters: Surface-based filters work based on the assumption that initially, all points belong to the ground surface and gradually the points that are not fit to the general surface model will be removed. The general surface model is created to approach the DTM (Pfeifer and Mandlburger, 2009). Kraus and Pfeifer (1998) developed an iterative robust interpolation surface-based filter using linear least squares interpolation to describe the surface in wooded areas. In the linear-prediction methods (Kraus and Pfeifer, 1998; Pfeifer et al. 1999) a surface was divided into several patches and computed with equal weights for all points. Lee and Younan, (2003) generated DTM in commercial forestland with variable terrain, canopy densities, and heights near Bellingham, WA. They demonstrated that although the linear prediction methods are the robust methods to generate a DTM, they are not capable of generating an

effective one in steep or varying slopes. Lee and Younan, (2003) have improved the linear prediction methods with adaptive processing methods.

Polynomial function algorithms are another surface method which has been used to extract ground points. In this method, the ground surface is assumed as a continuous surface and points with a defined vertical distance are selected as the ground points (Kraus and Pfeifer, 1998; Elmqvist, 2002). Since using the above algorithms requires complex computation and is applied only to continuous terrain surface, a Triangulated Irregular Network (TIN) for discontinuous terrain surface and easier computation is developed by Vosselman, 2000; Axelsson, 2000; Vosselman and Mass, 2001; and Haugerud and Harding, 2001.

Progressive densification filters: Algorithms in progressive densification class reconstruct the grounds points progressively (Sohn and Dowman, 2002). Axelsson (2000) developed a Triangular Irregular Network (TIN) algorithm to generate the DTM. In this method, the lowest elevation points in large grid cells are assigned as the ground point. Next, the ground points are triangulated to construct a reference surface. Then, by investigating through the TIN for each triangle, an additional ground point is determined. This process will continue till no more points can be added to the TIN.

Segmentation-based filters: Segmentation is defined as collecting and clustering points with similar attributes (Nardinocchi et al. 2003; Jacobsen and Lohmann, 2003; Tóvári and Pfeifer, 2005; Sithole, 2005). This method is suitable for analyzing of LiDAR PCD rather than individual points. In Segmentation algorithms, the whole homogeneous area is classified into segments based on the local geometry of points such as slope, height or twist in a neighborhood instead of single points in point cloud data set. Each point in the same segment belongs to the same class. Briefly, this algorithm uses the geometric information to classify points (Filin and Pfeifer, 2006).

Other algorithms: Sithole and Vosselman; Pfeifer and Mandlburger, 2009; and Nurunnabi et al. 2016; have shown that many of above-mentioned methods work well in flat areas with less vegetation and small constructions but they don't perform efficiently in complex environments, steep sloped terrain, dense vegetation, ramp, sharp edges and multiple buildings. To resolve these issues in boundaries and areas with a high twist, the Locally Weighted Regression (LWR)

with many suitable statistical properties has been proposed by Cleveland and Loader (1996). Parametric filtering models may result in misclassification in steep slopes. Hence, the local weighting is more efficient. Nurunnabi et al. (2016) proposed a new algorithm based on robust LWR (RLWR). In this algorithm for each point, a locally weighted interpolation function has been used. Many algorithms for ground filtering to generate DTM have been explored; an overview of some of them is given in Table 2.1.

All the above-mentioned studies applied airborne LiDAR for the generation of DTM in a forest area. For the first time, the present study investigates the potentials of terrestrial LiDAR remote sensing for DTM extraction in a dense forest where the ground points are barely visible. In such conditions, quick and simple generation of DTM is a challenging task. A new algorithm is developed here for automatic extraction of DTM based on the correction of the local slopes. The algorithm mathematical tools are different from the above-mentioned techniques. This simple algorithm uses median filters and *Angle Score* (*AS*). The *AS* parameter is calculated based on the variations in DTM local surface gradients for automatic monitoring of the performance of median filter and finding the optimum filter order. In this chapter, experimental design and methodology are presented in section 2. The result and discussion are described in section 3 and 4, respectively. The conclusion is drawn as section 5.

2.2 Materials and Methods

2.2.1 Study Area and Data Explanation

The study area in this project is a plot with 50 m × 50 m in size and located in northwestern Alberta, Canada (Latitude: 56.744223◦ N; Longitude: -118.344673◦ W; Altitude: 871 m) at the Peace River Environmental Monitoring Super Site (PR-EMSS) which consist of an old-growth stand of Trembling Aspen (*Populus tremuloides*) with a broad leaf deciduous canopy (Figure 2.1). The supersite is situated in the joint industry-research forestry region. The PCD was collected using a ground-based LiDAR -Leica Scan Station C10- and the scanning process was performed in summer and fall seasons of 2014 to 2016. The characteristics of the Leica Scan Station C10 are summarized in Table 2.2.

2.2.2 Experimental Design and Methodology

The schematic field setup is depicted in Figure 2.2. The rectangular plot study was scanned from four locations in order to find the comprehensive PCD. Meanwhile, five targets were set as reference points to align the four scans. The target locations were made observable in most of the scans. Scanner locations are indicated alphabetically. T_1 to T_5 shows the location of reference targets with white and blue squares. In this study, the distance between stations was 25 m and the distance between reference targets and stations was 11 m. The reference targets for co-registration are depicted in Figure 2.3. To have a comprehensive and integrated point cloud in the co-registering process, at least three reference targets are required. All reference targets should be observable from all scan stations. During the installation of reference targets, steep relief was avoided to minimize the occlusion effect by understory. In this plan, north is shown. All four scans from the plot study were co-registered using the standing targets. The collection, registration, and processing of PCD were performed in the Cyclone 8.1 software and MATLAB Software (MATLAB R2016b).

The Leica Scan Station C10 scanner emits laser beam pulses at 532 nm (green laser) and captures high resolution of point cloud data in 360^o coverage of the environment. It has high intensity and its effective range varies from 300 m to 134 m at 90% and 18% albedo respectively (Leica guide). The Leica C10 is provided with a dual-axis compensator to correct the horizontal angle and balance the device when the instrument is not leveled (Cothrun, 1995). In addition, Leica Scan Station C10 is equipped with a high-resolution camera which provides an RGB image with point cloud data.

Final accuracy of point cloud data can be affected by several parameters such as operation, co-registration, and geo-referencing (GSA_BIM Guide, 2009). By co-registering, a multiple LiDAR scanning data is transferred into a single PCD with a reference coordinate system. In this process, having a sufficient number of matched points which are arranged in pairs is necessary to have the high precision of co-registration.

2.2.3 Co-Registration

There are two approaches to the co-registration process: with and without reference targets. The target base approach is the most popular method as it is easy to use and more accurate than

the target-free approach (GSA_BIM Guide, 2009). The target-free approach is utilized when reference targets are not available. In this method, natural features are used in a point cloud for co-registering (Jaw and Chuang, 2008). For target-based co-registration, blue and white square planar targets have been used to match the points.

2.2.4 Data Preprocessing

Before any data processing, all noisy data in the point cloud such as sun beam noise and any devices in the field were filtered manually in the Cyclone software to have the better quality of PCD. Figure 2.4 shows some samples of these interrupting noise and removal of them in Cyclone. After filtering the noisy points, an algorithm is implemented in MATLAB to create DTM.

2.2.5 DTM Generation and Algorithm

In the present study, an algorithm was developed in MATLAB to create the DTM. The algorithm flowchart is shown in Figure 2.5. The initial step is to make a template for data processing in PCD by generating a mesh grid network with arbitrary step size (Δ) in the x-y plane. Then, in each grid, the point with the lowest elevation (z) is detected and assumed as a draft ground point. The draft collection of ground points needs to be further processed since it still contains many points from foliage which result in spike noise in its profile. For the first time, the proposed algorithm applies median filters for the effective elimination of spike noise and creating DTM. The median filter is a nonlinear digital filter (Roncella et al. 1991).This filter goes through the draft ground point collection one-by-one using a square matrix window of size [$M \times M$] and replaces each data point with the median of neighbors inside the window.

The algorithm starts with $M = 3$. DTM is analyzed and M increases to the next odd number ($M = 5$). To study the effect of filter order, the algorithm is applied to the PCD from an area of $41 \times 41\ m^2$ with a grid spacing of $0.2 \times 0.2\ m^2$. Spike noise around the boundaries of DTM is the most difficult one to remove and is usually handled by increasing the filter order. For $M = 3$, $M = 5$, $M = 7$, and $M = 27$, boundary spike noise is effectively removed.

In order to find the optimum *M*, the algorithm calculates an *Angle Score* (*AS*) for DTM at each *M*, in addition to visual inspection of the DTM profile. *AS* is defined as the maximum DTM profile slope angle among all pixels. The pixel slope angle is calculated by the derivative of DTM profile in main planes of *x*-*z* and *y*-*z*. Hence, the gradient of DTM has to be calculated along both *x* and *y* axes as in equation (1), (2) respectively:

$$AS_{M,y} = \frac{\partial(DTM_M)}{\partial y} \qquad (1)$$

$$AS_{M,x} = \frac{\partial(DTM_M)}{\partial x} \qquad (2)$$

Then, for the whole DTM, a single *AS* is defined as equation (3):

$$AS_M = \arctan(\max\{AS_{M,x}, AS_{M,y}\}) \qquad (3)$$

If the variation of *AS* is smaller than 1° when *M* increases by two units, the optimum *M* is found and the algorithm stops. This is verified by equation (4):

$$if \quad |AS_M - AS_{M-2}| < 1^\circ \rightarrow M\ is\ optimum\ and\ algorithm\ flowchart\ stops \qquad (4)$$

2.2.6 Accuracy Assessment

To evaluate the performance of filtering method and examine the errors, both qualitative and quantitative approaches have been used (Zhang, 2003; Serifoglu et al. 2016). In the qualitative method, the errors are checked by comparing the distinct features before and after filtering. It is not practical to compare all filtered and unfiltered points for finding the errors. Hence, Zhang et al. (2003), and Zhang and Whitman (2005) suggest a random selection of a sample of data sets for the test. To examine the errors in a qualitative approach, a random sample of test points is chosen and then two sets of data including filtered and non-filtered are compared to see if the points are correctly separated (Zhang and Whitman 2005; Serifoglu et al. 2016).

In the qualitative approach in this study, a sample of test points with a predefined radius of sample area with an obvious feature such as tree trunk or device box is selected. Since the LiDAR scanner in this study (Leica C10) is capturing the points in high density, a sample test point with 1-meter radius is selected in this qualitative approach.

Quantitative errors are categorized to omission (type I) and commission (type II) errors. Type I (omission error) refers to ground points which have been removed mistakenly and type II (commission error) relates to non-ground points that classify as ground points (Zhang and Whitman 2005; Serifoglu et al. 2016). In the quantitative evaluation, the method proposed by Zhang et al. (2003) and Zhang and Whitman (2005) was used to examine the ground filtering results. Three sample sets of points, each including different points with high, medium and low density and with the area of 1 m^2 are subset randomly from the whole point cloud. In sample set 1, the slope is heavily covered by understory vegetation. Sample set 2 is covered by low vegetation and located in a flat area. Sample set 3 is located in steep slope with distinguishable big tree trunks and low understory vegetation. To evaluate the accuracy of test points, the method proposed by Sithole and Vosselman (2004) is used here. In this method, two types of error are proposed. Error type I or omission error and error type II or commission error as below:

$$\text{Error type I} = \frac{a}{GP} \quad (5)$$

$$\text{Error type II} = \frac{b}{NGP} \quad (6)$$

where *a* stands for the number of ground points separated as non-ground (omission error) and *b* stands for the number of non-ground points classified as ground (commission error). GP shows the total number of ground points and NGP shows the total number of non-ground points (Montealegre et al. 2015).

In previous studies, most filters focus on minimizing type II errors (as shown in Table 2.3), rather than type I errors because in type I errors, many valid ground points are removed, while type II errors attempt to remove as many object points as possible, even objects that are small and close to the ground by choosing the proper filter parameters (Elmqvist, 2002; Roggero, 2001; Sohn, and Dowman, 2002; Wack and Wimmer, 2002; Brovelli et al. 2002; Sithole and Vosselman, 2004; Pfeifer and Mandlburger, 2009).

2.3 Results

The result of co-registration precision for each pair of stations is shown in Table 2.4. From each station, at least three reference targets were observable. The Root Mean Square Error (RMSE) ranges from 0 to 3 mm among stations for the co-registering process. The maximum RMSE (3 mm) happened between station 1 and 3 using T_2 as a reference target. It was because of the larger distance between station 3 and T_2 (13 m). LiDAR PCD in this study is made of 50,000,000 points (Figure 2.6 a). Figure 2.6 shows the color-coded PCD. Figure 2.6 b helps to separate some above ground objects with arbitrary elevation. Figure 2.6 c shows a portion of PCD with color-coded intensity and Figure 2.6 d is the real color image scan.

To study the effect of filter order, the algorithm is applied to the PCD from an area of 41×41 m^2 with a grid spacing of 0.2×0.2 m^2. Figure 2.7 shows the 2D and 3D view of the DTM without median filtering which includes strong spike noise all over the profile. Figure 2.8 shows how the noise is minimized by applying the median filter, resulting in a smooth profile. Spike noise around the boundaries of DTM is the most difficult one to remove and is usually handled by increasing the filter order. For M = 3, M = 5, M = 7, M = 13, M = 17, and M = 27, boundary spike noise is effectively removed, as depicted in Figure 2.8.

Mongus et al. (2012) demonstrated that the separation of vegetation from their neighboring ground points on the steep slopes is limited as the vegetation points are not necessarily higher than ground points. The spike noise in Figure 2.7 demonstrates high density of understory vegetation or steep slopes that cover the ground points. To remove these types of noise, applying a median filter is necessary. Comparing Figure 2.7 and Figure 2.8 shows how applying different median filter removes noise in generated DTM at the edges where there is not enough data to interpolate or where the ground points are covered by the vegetation objects such as fallen dead trunks. However, for each Δ value, M has to be adjusted. To demonstrate this effect, for a test area of 41×41 m^2 and for constant M = 7, DTM is acquired for Δ = 0.2 and 0.5 m (Figure 2.9). In Figure 2.10 a, it is observed that M = 7 is not enough for a resolution of 0.2 m since there are some large spikes and the elevation is not uniform in many spots. However, the resolution of 0.5 m has achieved a better color uniformity (Figure 2.10b) and the effective removal of spike noise in the graph for the resolution of 0.5 m is observed.

Figure 2.11 shows *Angle Score* (*AS*) as a function of the order of the median filter (*M*) in fall and summer seasons. As can be seen, *AS* decreases as *M* increases. As Figure 2.11 shows, the *AS* of DTM has very small variations for $M > 27$ in both fall and summer seasons. Such trend can also be observed in in Figure 2.12. In Figure 2.11 the red dashed circle highlights the change in the trend of *AS* for $M \geq 27$. Since *AS* doesn't vary much for $M > 27$, therefore it can be concluded the best median filter for creating DTM with the grid size of 0.2 *m* is of order 27 (Figure 2.13). With $M = 27$ and $\Delta = 0.2$, the 3D DTM of an m × m land area is generated in both fall and summer season and depicted in Figure 2.14.

2.3.1 Qualitative Evaluation Results

The non-ground objects in this study area include tree trunks, fallen trees and some devices such as Wireless Sensor Network (WSN) nodes, soil flux box, and LiDAR Box. The result of the qualitative evaluation is shown in Figure 2.15. Figure 2.15a shows the raw data with high density. As it can be seen in Figure 2.15 c, the ground points (yellow dots) are separated very well from non-ground points such as the tree trunk and the red box.

2.3.2 Quantitative Evaluation Results

To analyze the commission error, several combinations of land features including *point density*, *cover type*, and *terrain slope* were applied. The commission error of the proposed algorithm is summarized in Table 2.5. The point density for sample sets varies from 33,849 points/m^2 to 14,697 points/m^2 from low to high density. The total commission error (type II) is 0.07%. To analyze the effects of the *point density*, *cover type*, and *terrain slope* parameters on error rates, three comparative experiments, which are depicted in Figure 2.16, were performed. The circles in this figure indicate some instances of commission error. Based on equation (1) the numbers of non-ground points (b in equation 1) for sample sets with high, medium and low density are 11, 4 and 56 respectively.

Point Density: The effect of the changes in point density on the performance of the proposed algorithm was evaluated quantitatively (Table 2.5). Theoretically, if the LiDAR resolution decreases, separating the ground surface from the objects is more difficult (Sithole and

Vosselman, 2004). Point density evaluation results indicate that the commission error decreased with increasing point density from 0.171% to 0.009%. The results in Table 2.5 indicate that the set area with highest point density (sample set 1) had the lowest commission error of 0.009%.

Cover Types: We also compared the performance of the proposed algorithm within each of the test areas. As can be observed in Figure 2.16 and the results from Table 2.5, the performance of the proposed filter was better in the area covered with grasses, dead tree trunks, and fallen branches than those covered with single trees in terms of commission error. However, our results do not allow us to draw firm conclusions on the effect of the cover type on the algorithm performance.

Terrain Slope: The influence of the terrain slope was assessed using three classes: smooth slopes ranging from 0 to 5°, medium slopes from 5 to 20°, and steep slopes higher than 20° (Figure 2.16). Point`s height differences is a key assumption to separate the ground surface from objects. Therefore, points above their neighbors are supposed to belong to objects, but this assumption becomes difficult in steep slopes (Sithole and Vosselman, 2004). Hence, most filtering methods had difficulties on steep slope higher than 15° and their error rates increased with the terrain complexity (Kraus and Pfeifer, 1998; Axelsson, 2000; Evans and Hudak, 2007; Vosselman, 2000; Zhang et al. 2003; Streutker and Glenn, 2006). The commission error in this study significantly increased with the change in slope. In summary, it can be concluded that the steep slopes with low point density result in the largest error (sample set 3).

2.4 Discussion

LiDAR has been shown as a powerful and cost-effective tool for data collection with the purpose of DTM generation in forest area (Vosselman and Maas, 2010). Every forest LiDAR scan results in millions of points representing leaves, branches, trunks, and the ground surface. DTM generation necessitates classification of the points and extraction of ground surface points from the whole PCD. This study tried to develop a new algorithm for the classification of discrete return LiDAR PCD into two classes of ground and non-ground points, in a Boreal forest environment. In this study, error associated with LiDAR classification on different data contexts, such as *point density*, *terrain slope*, *shadowing effect,* and *land cover type* of LiDAR data, was

assessed. Furthermore, the effect of two parameters including *grid size (Δ)* and the *order of median filter (M)* on the effectiveness of the proposed algorithm is discussed in both fall and summer seasons. The absence of severe biases in classified ground returns (with total commission error of 0.07%) suggests that the proposed algorithm is an effective method to generate DTM in this environment with ground-based LiDAR.

LiDAR sampling resolution is inversely proportional to the distance between the scan station and the objects. Hence, further objects are sampled with lower *point density*. For the special application of DTM generation in large land extents, this results in reduced number of ground points on the border areas of each scan and reduces the accuracy of interpolation and surface fitting. The corners of the generated DTM in Figure 2.12 and Figure 2.14 depict this effect. It implies that even median filtering can't eliminate this effect completely. As a future research, to address this problem, several reference targets can be added to the scan plot in the maximum reachable distance by LiDAR. Since reference targets are highly reflective, they add reference points to PCD boundaries which are advantageous in surface fitting and removing the border spike noise.

Terrain slope strongly affects the accuracy and quality of the generated DTM. Zhang and Lin (2013) pointed out that the ground points in steep slopes may be classified as plants as located at the same height, increasing commission errors. Meng et al. (2010) demonstrated that methods based on the slope may mislabel ground points as non-ground in areas with slopes larger than the maximum ground slope threshold. On this topic, the study area, with various situations, from flat areas to steep ones, is challenging to process because of the difficulty in choosing suitable slope and elevation thresholds. In this study, implementation of the proposed algorithm for steep slopes resulted in the higher error. This is shown in Table 2.5 and Figure 2.16 where the commission error in the steep slope is much higher than the flat area.

Vegetation density determines the ratio of ground to plants returns (Evans and Hudak, 2007). Evans and Hudak (2007) demonstrated that the effect of point density on filter performance is also influenced by vegetation types such as grasses, shrubs, or trees. The point density is not only dependent on the amount of emitted laser pulses but also by the existence or lack of vegetation. Meng et al. (2010) showed that the commission error increases due to the presence of attached and low objects such as small seedlings, stumps, and shrubs, which produce the classification of points as the ground surface. Evans and Hudak (2007) showed that their

filtering algorithm had the best performance in the low vegetation condition. However, in this regard, our results demonstrate that the effects of the vegetation are most likely minor compared to the errors introduced by the complexity of the scene, such as low point density on steep slopes.

The *shadowing* effect is another factor that causes the ground points to be missed behind or underneath the trees and understory. To minimize the shadowing effect, scans are performed on four different stations. Nevertheless, shadowing effect is still present and reduces DTM accuracy. Besides, having a discrete return LiDAR in this study (Leica C10) makes the scans more prone to shadowing. To avoid this, other studies apply multi-wavelength LiDAR (Morsdorf et al. 2009; (Sheng et al. 2003).

The proposed algorithm developed in this study successfully generated DTM from LiDAR PCD in a forest area using median filtering. The quality of DTM is controlled by two parameters in the algorithm which is the mesh *grid size* (Δ) and the order of *median filter* (M). Δ represents the DTM resolution which can be as small as the spatial resolution of LiDAR scan. Due to the high point density of LiDAR PCD, Δ can be reduced down to several centimeters. Δ is usually selected based on the application in demand. However, it should be noted that small Δ can result in longer processing time even for limited land areas. The proposed algorithm has been compared for Δ of 0.2 m and 0.5 m in Figure 2.9 with a fixed value of M. As can be observed, larger Δ results in lower spike noise. Regardless of the value selected for Δ, a certain level of spike noise will be present in the generated DTM.

On the other hand, M is an odd integer larger than 2 which defines the size of median filter operation window. The median filter is applied for the elimination of the spike noise from the initially extracted PCD. As Figure 2.7 shows, the unfiltered 2D and 3D DTM profile have a high level of spike noise. In the algorithm, a parameter is defined for quantifying and comparing the noise level as *Angle Score* (*AS*). Smaller Δ results in stronger spikes and higher *Angle Score*. Higher M values are more effective in removal of spike noise. Figure 2.8 demonstrates the 2D DTM for the unfiltered data in fall for M values of 3, 5, 7, and 27 and in summer for M values of 3, 13, 17, and 27. The strong spike noise in unfiltered data is gradually reduced as the order of median filter increases from 3, to 5, 7, 13, and 17 and finally removed for a M value of 27. However, higher M values require a much longer time to run the algorithm. Also, too large values of M may flatten the DTM by mistakenly removing all slopes. Hence, an optimum M

should be found for the required Δ, based on the available processing systems. With a regular desktop computer, for the study plot in this chapter, the optimum *M* value was 27. Finding this optimum *M* was of critical value for DTM generation. To find it, *AS* was calculated in DTM for a wide range of *M*, with a fixed Δ. For *M* values larger than 27, there is ignorable variation in *AS* (Figure 2.11). Figures 2.8, 2.11, 2.12, 2.13, and 2.14 show that the performance of the algorithm does not change in different seasons. The slight difference in 3D and 2D DTM between the profiles of summer and fall is because the scan stations were not exactly in the same position for summer and fall.

2.5 Conclusion

An algorithm based on median filtering and surface fitting was offered for effective automatic generation of DTM from ground-based LiDAR point cloud of a boreal forest. To assess the algorithm, qualitative and quantitative error analyses were carried out. The accuracy analysis of filtering results from the random sample datasets showed that only 0.07% errors were committed by the filter algorithm. Also, the errors associated with LiDAR classification on different data contexts, such as *point density*, *terrain slope*, *shadowing effect,* and *land cover type* of LiDAR data, were assessed. Furthermore, the performance of the proposed algorithm was tested for various design parameters such as the order of median filter and mesh grid size. The algorithm worked very well in the low complexity of land features such as smooth slopes, light vegetation and high density of visible ground points. In conclusion, to complement the results shown in this study, it would be useful to devote future research on the analysis of the error distribution in DTM generation, as this error can be transmitted consequently into derived products including Canopy Height Models (CHMs), hydrological indices, vegetation biomass, Leaf Area Index (LAI), and carbon storage (Fisher and Tate, 2006; Pirotti and Tarolli, 2010, Farid et al. 2008; Gonzalez et al. 2010). Also, for modeling of LiDAR data, development of more accurate algorithms and methods is still necessary.

Tables Legends

Table 2.1 Overview of some algorithms to generate DTM

Table 2.2 Leica Scan Station C10 Specifications.

Table 2.3 Quantitative comparisons of filters for type II and type I errors.

Table 2.4 Results of co-registration for four stations.

Table 2.5 Effect of point density, land cover, and terrain slope on filter performance.

Figures Legends

Figure 2.1 (a) Research site and field survey map location (b) terrestrial LiDAR observation at summer and (c) fall season.

Figure 2.2 Schematic of field setup in the study area in Peace River.

Figure 2.3 Reference target for co-registering of scanning data; (a) in field implementation (b) reference target after scanning (c) the coordinate of the central point of reference target is recognizable in the point cloud.

Figure 2.4 Removal of noise points for DTM model; (a) Tower (b) Sun beams in the field (c) Box and other devices in the field.

Figure 2.5 Summary of the processing and analysis steps of the proposed approach to generate DTM using LiDAR data.

Figure 2.6 Point cloud data schematic; (a) by perspective view (b) with elevation information (interval: 1m) (c) with intensity information (d) with color information from the scanner.

Figure 2.7 Schematic view of the DTM without median filtering; (a) 2D view (b) 3D view of unfiltered DTM.

Figure 2.8 2D view of DTM by applying a median filter of different orders; (a) fall season for M = 3, 5, 7, and 27 (b) summer season for M = 3, 13, 17, and 27.

Figure 2.9 2D view of DTM acquired for Δ = 0.2 m and Δ = 0.5 of constant M = 7 for the test area.

Figure 2.10 3D view of the DTM for the test area of 41×41 m^2 in fall season for resolution of (a) 0.2 m and M = 7 (b) 0.5 m and M = 7.

Figure 2.11 Relationship between the order of the median filter (*M*) and *Angle Score* (*AS)* to find the optimum median number in; (a) fall season (b) summer season.

Figure 2.12 2D view of DTM without filtering and by applying a median filter of different orders; (a) fall season for $M = 27$, 29, 31, and 33 (b) summer season for $M = 27$, 29, and 31.

Figure 2.13 2D view of Unfiltered DTM and DTM with applying a median filter of $M = 27$ for $\Delta = 0.2$ m in; (a) fall season (b) summer season.

Figure 2.14 3D view of DTM by applying a median filter of $M = 27$ for $\Delta = 0.2$ m in; (a) fall season (b) summer season.

Figure 2.15 Qualitative evaluation for separating ground points by the proposed algorithm; (a) raw data with high density in a sample set (b) ground points (yellow dots) and non-ground points (c) separated ground points.

Figure 2.16 Commission errors in; (a) high (b) medium (c) low density in 3 sample sets. The red circles in this figure indicate some of the commission errors.

Table 2.1 Overview of some algorithms to generate DTM

Algorithm description	**Authors**
Linear Prediction	Kraus and Mikhail, 1972
Hierarchical Robust Interpolation	Sithole and Vosselman, 2004
Maximum Local Slope (MLS) Filter	Zhang and Whitman, 2005
Skewness Balancing	Bartels et al. 2006
Elevation Threshold with Expanding Window (ETEW) Filter	Whitman et al. 2003
Iterative Progressive Morphological Filter (PM)	Zhang et al. 2003
Spline Interpolation	Brovelli et al. 2002
Hierarchical Modified Block Minimum	Wack and Wimmer, 2002
Progressive TIN densification	Sohn and Dowman, 2002

Table 2.2 Leica Scan Station C10 Specifications.

Scan Station C10	Specifications
General	
Instrument type	Compact, pulsed, dual-axis compensated, very high-speed laser scanner
Camera	Auto-adjusting integrated high-resolution digital camera with zoom video
System Performance	
Accuracy of single measurement	Position* 6 mm Distance* 4 mm Angle (horizontal/vertical) 60 µrad / 60 µrad (12" / 12")
Laser Scanning System	
Type	Pulsed; proprietary microchip
Color	Green, wavelength = 532 nm visible
Laser Class	3R (IEC 60825-1)
Range	300 m @ 90%; 134 m @ 18% albedo (minimum range 0.1 m)
Scan rate	Up to 50,000 points/sec, maximum instantaneous rate
Scan resolution **Spot size**	From 0 – 50 m: 4.5 mm (FWHH-based); 7 mm (Gaussian-based)
Point spacing	Fully selectable horizontal and vertical; <1 mm minimum spacing, through full range; single point dwell capacity
Field-of-View **Horizontal** **Vertical**	 360° (maximum) 270° (maximum)
Environmental	
Operating temp.	0° C to 40° C / 32° F to 104° F
Storage temp.	-25° C to +65° C / -13° F to 149° F
Lighting	Fully operational between bright sunlight and complete darkness
Physical	
Scanner **Dimensions (D x W x H)** **Weight**	 238 mm x 358 mm x 395 mm / 9.4" x 14.1" x 15.6" 13 kg / 28.7 lbs, nominal (w/o batteries)

* At 1 m – 50 m range, one sigma

Table 2.3 Quantitative comparisons of filters for type II and type I errors.

Participant, Year	**Elmqvist** (2002)	**Sohn** (2002)	**Roggero** (2001)	**Brovelli** (2002)	**Wack** (2002)	**Sithole** (2004)	**Pfeifer** (2008)
type II error %	2	12	1	2	2	1	3
type I error %	21	6	33	31	10	29	8

Table 2.4 Results of co-registration for four stations.

Constraint ID	Scan World number	Scan World number	Error
T2	Station 1	Station 3	0.003 m
T4	Station 1	Station 3	0.002 m
T1	Station 1	Station 4	0.002 m
T2	Station 1	Station 4	0.002 m
T2	Station 2	Station 3	0.002 m
T1	Station 1	Station 3	0.002 m
T2	Station 1	Station 2	0.002 m
T4	Station 1	Station 2	0.001 m
T2	Station 2	Station 4	0.001 m
T1	Station 1	Station 2	0.001 m
T4	Station 2	Station 3	0.001 m
T1	Station 2	Station 4	0.001 m
T1	Station 2	Station 3	0.001 m
T3	Station 1	Station 2	0.001 m
T3	Station 1	Station 4	0.001 m
T3	Station 2	Station 3	0.001 m
T3	Station 1	Station 3	0.001 m
T1	Station 3	Station 4	0.001 m
T3	Station 2	Station 4	0.001 m
T2	Station 3	Station 4	0.001 m
T3	Station 3	Station 4	0.000 m

Table 2.5 Effect of point density, land cover, and terrain slope on filter performance.

Sample Groups	Level of Point Density	Land Cover	Terrain Slope	Commission Error %
Set 1	High	Dense understory	Smooth slope	0.009
Set 2	Medium	Grass and open area	Flat	0.028
Set 3	Low	Single trees and open area	Steep slope	0. 171

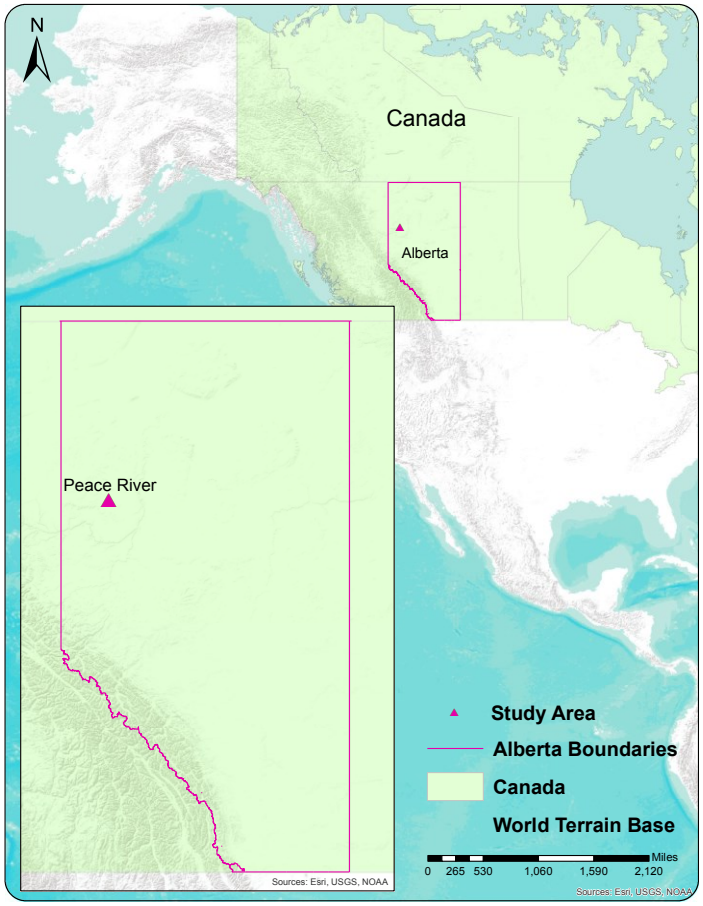

(a)

(b)

(c)

Figure 2.1 (a) Research site and field survey map location (b) terrestrial LiDAR observation at summer and (c) fall season.

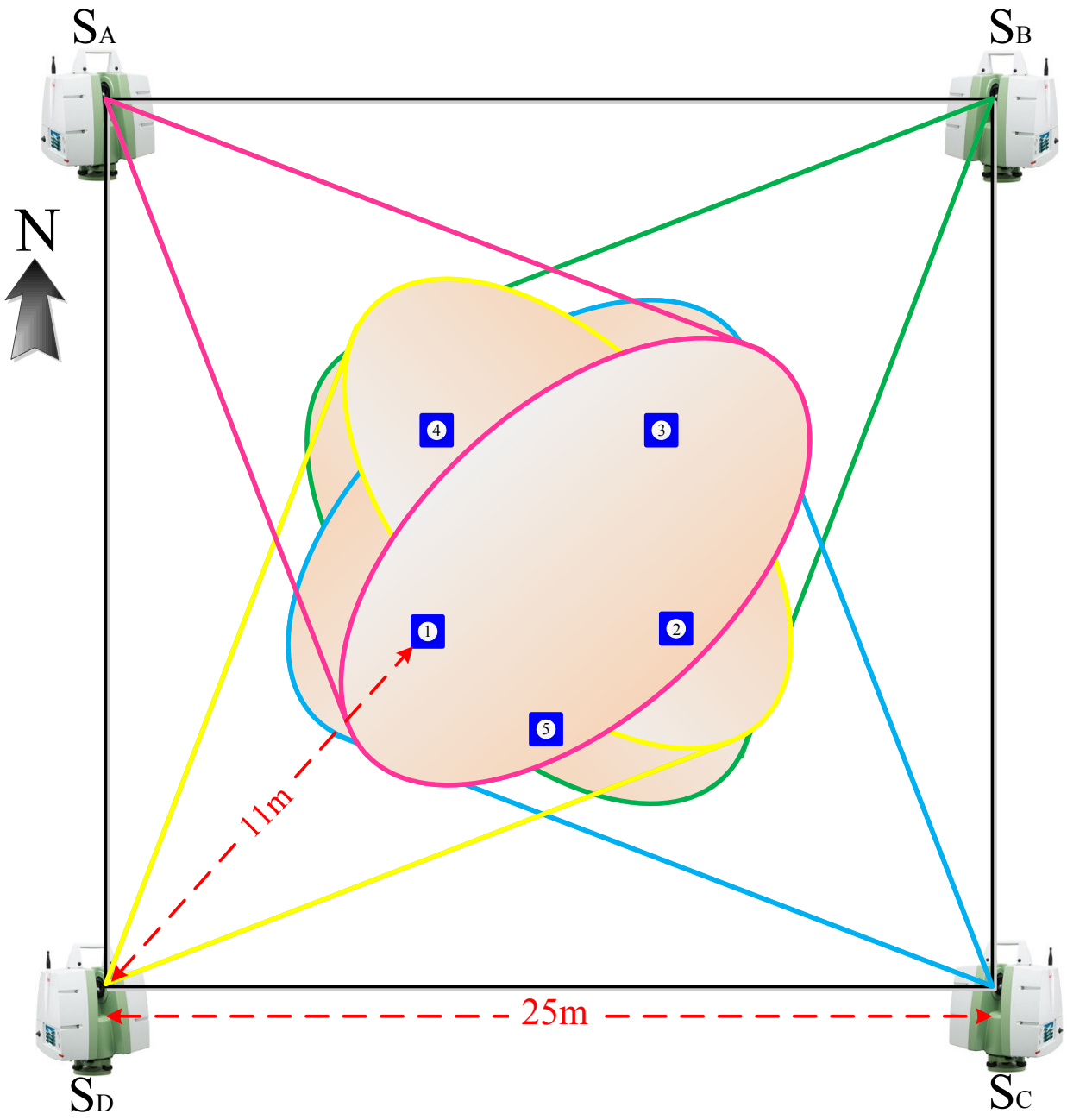

Figure 2.2 Schematic of field setup in the study area in Peace River.

(a) (b) (c)

Figure 2.3 Reference target for co-registering of scanning data; (a) in field implementation (b) reference target after scanning (c) the coordinate of the central point of reference target is recognizable in the point cloud.

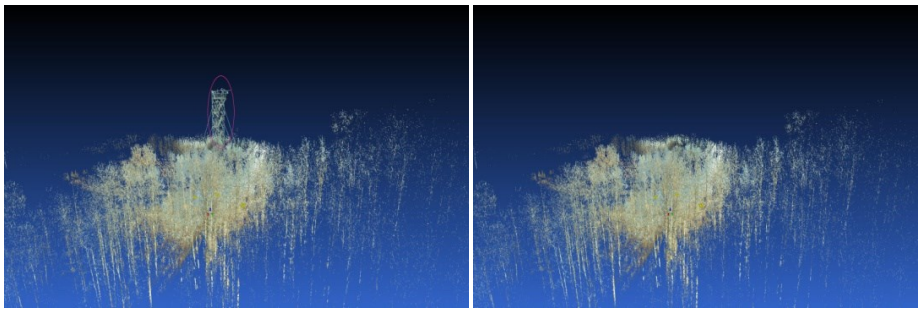

(a)

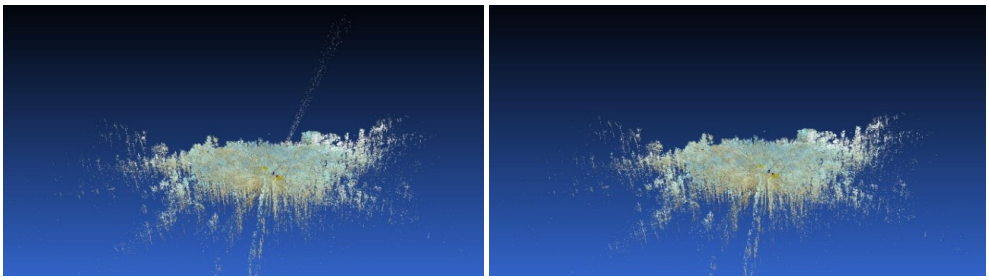

(b)

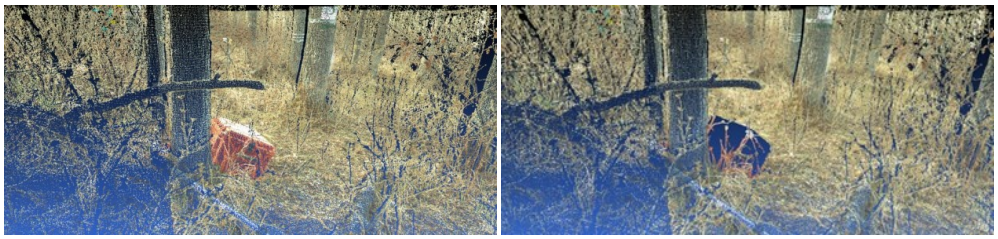

(c)

Figure 2.4 Removal of noise points for DTM model; (a) Tower (b) Sun beams in the field (c) Box and other devices in the field.

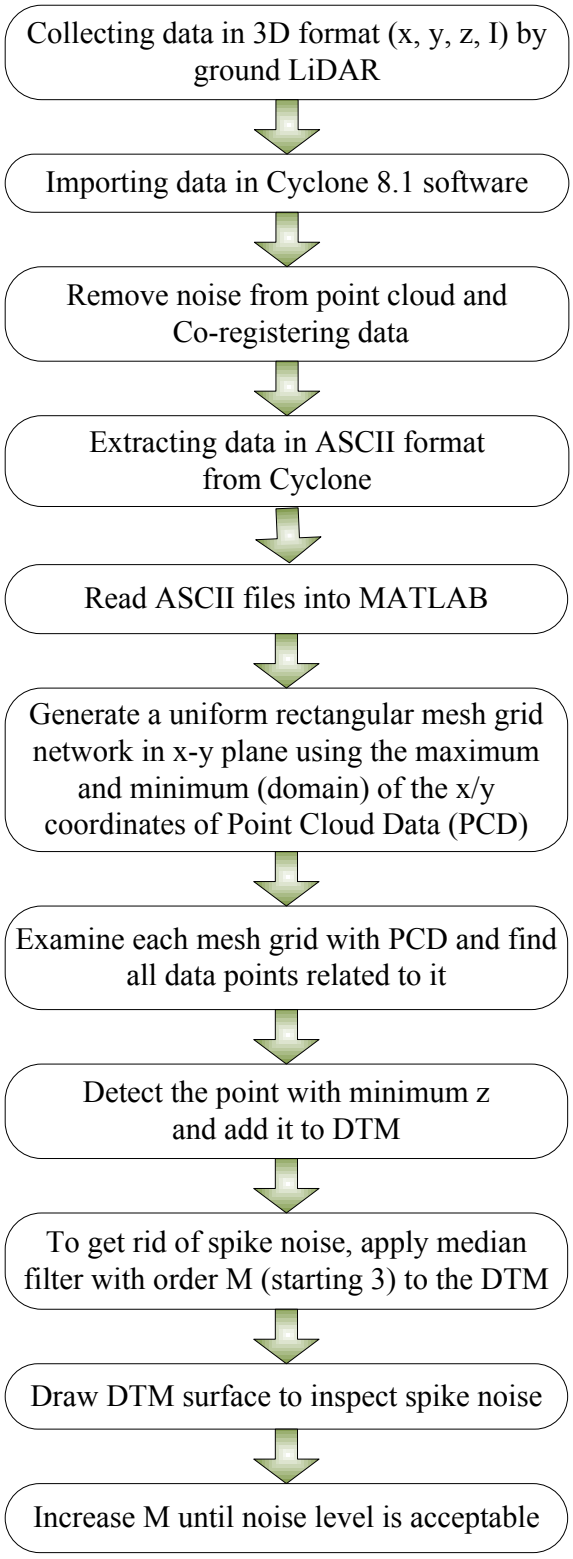

Figure 2.5 Summary of the processing and analysis steps of the proposed approach to generate DTM using LiDAR data.

(a)

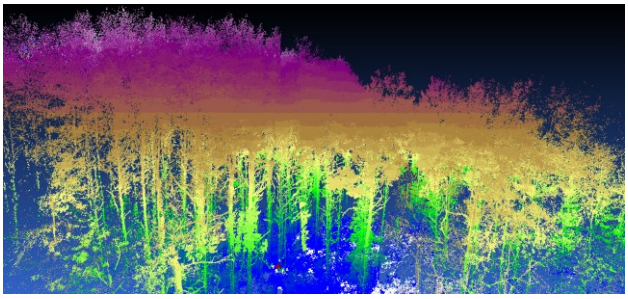

(b)

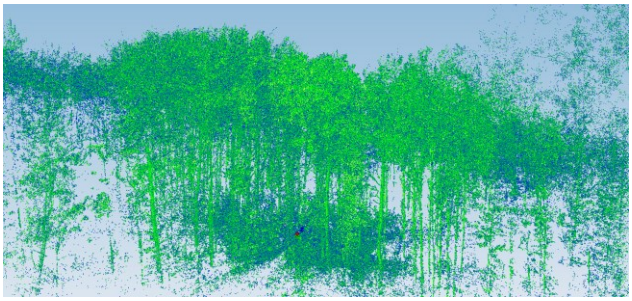

(c)

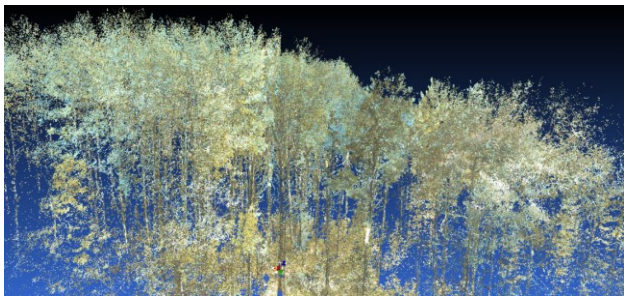

(d)

Figure 2.6 Point cloud data schematic; (a) by perspective view (b) with elevation information (interval: 1m) (c) with intensity information (d) with color information from the scanner.

(a)

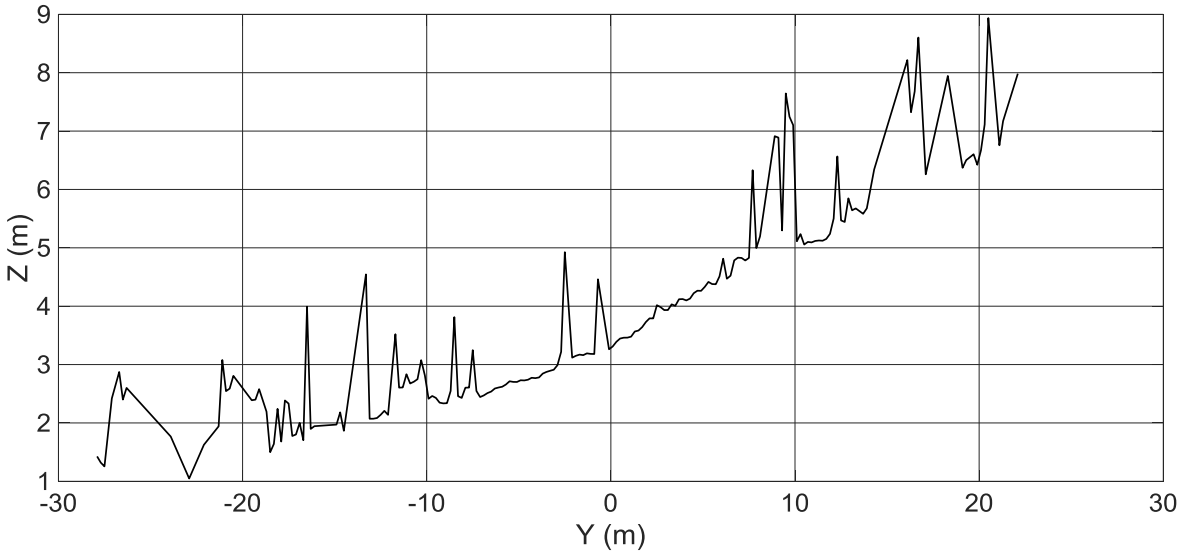

(b)

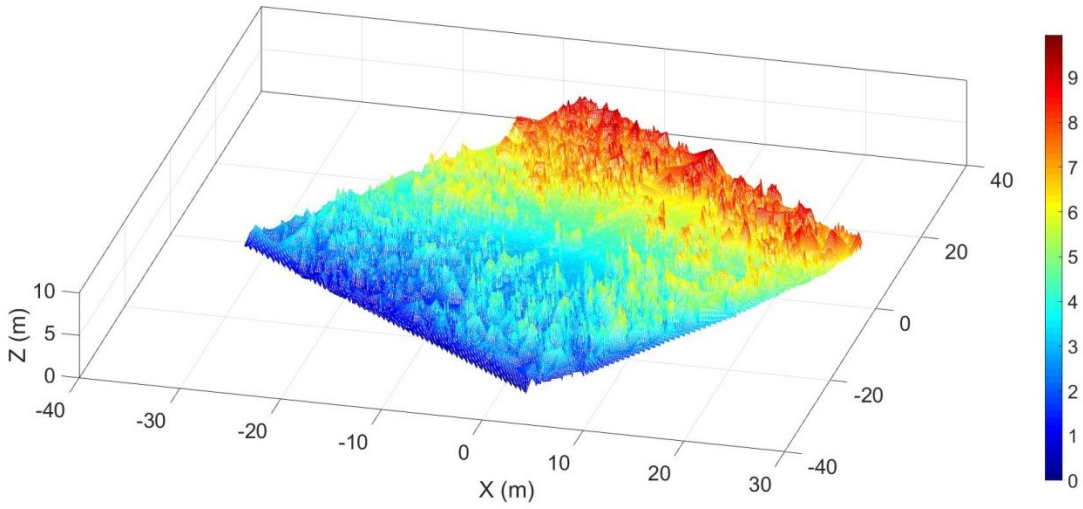

Figure 2.7 Schematic view of the DTM without median filtering; (a) 2D view (b) 3D view of unfiltered DTM.

(a)

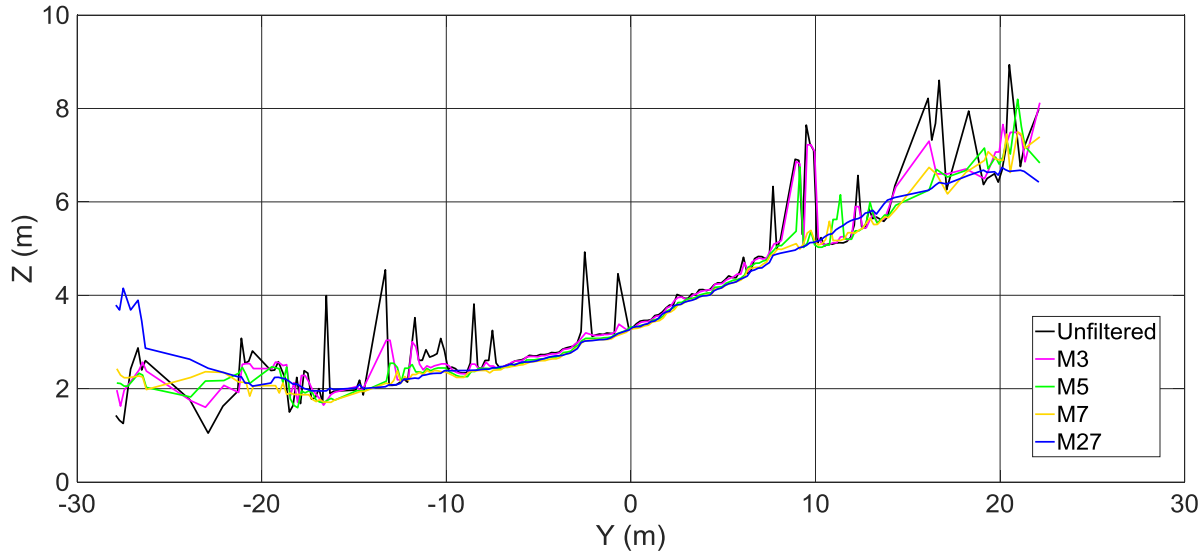

(b)

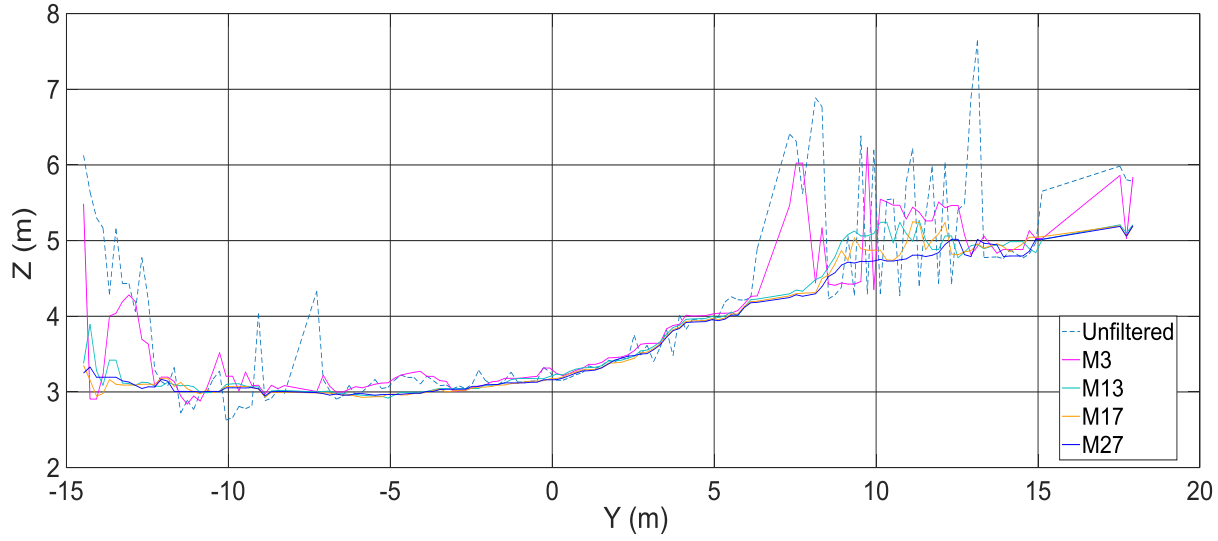

Figure 2.8 2D view of DTM by applying a median filter of different orders; (a) fall season for *M* = 3, 5, 7, and 27 (b) summer season for *M* = 3, 13, 17, and 27.

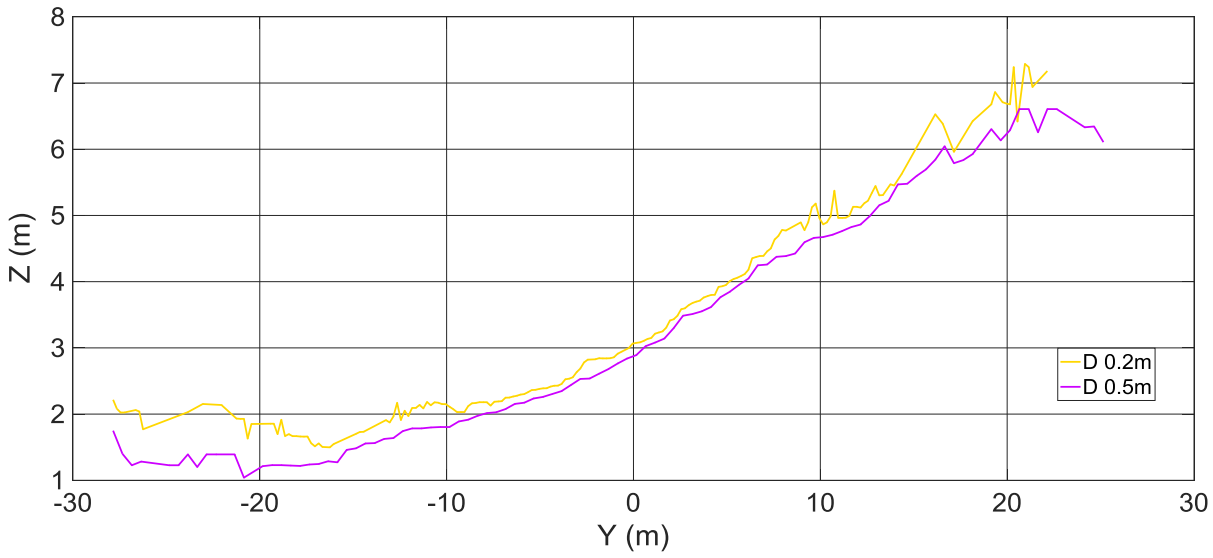

Figure 2.9 2D view of DTM acquired for $\Delta = 0.2$ m and $\Delta = 0.5$ of constant $M = 7$ for the test area.

(a)

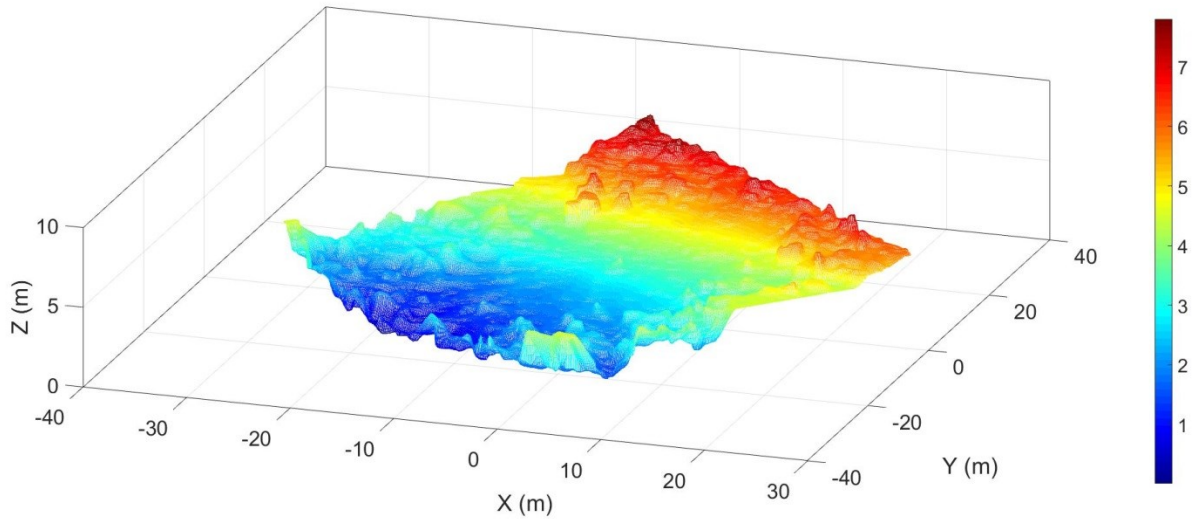

(b)

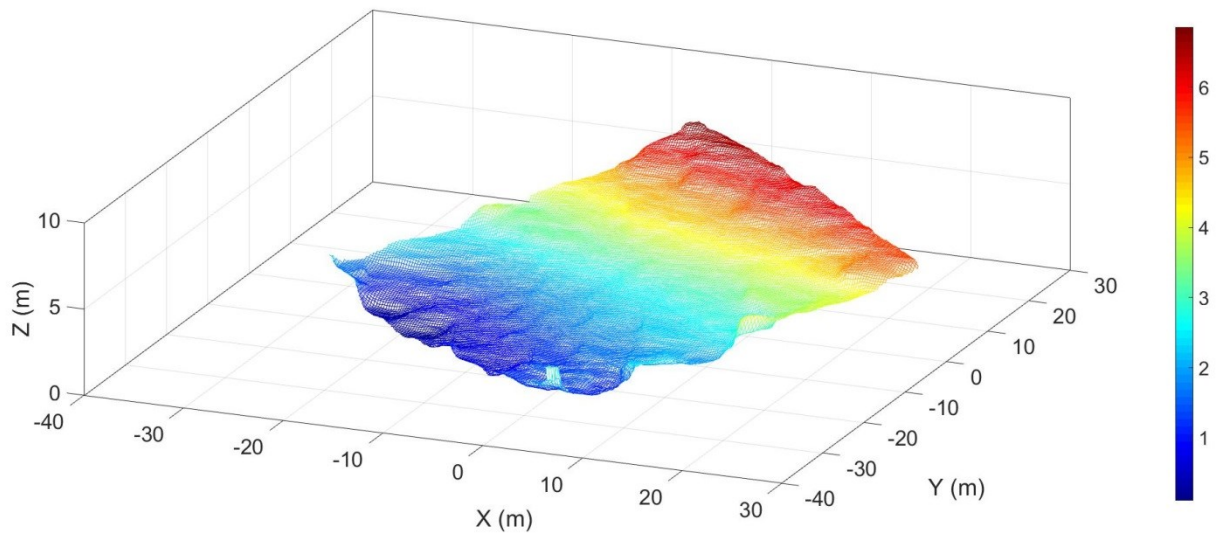

Figure 2.10 3D view of the DTM for the test area of 41×41 m^2 in fall season for resolution of (a) 0.2 m and $M = 7$ (b) 0.5 m and $M = 7$.

(a)

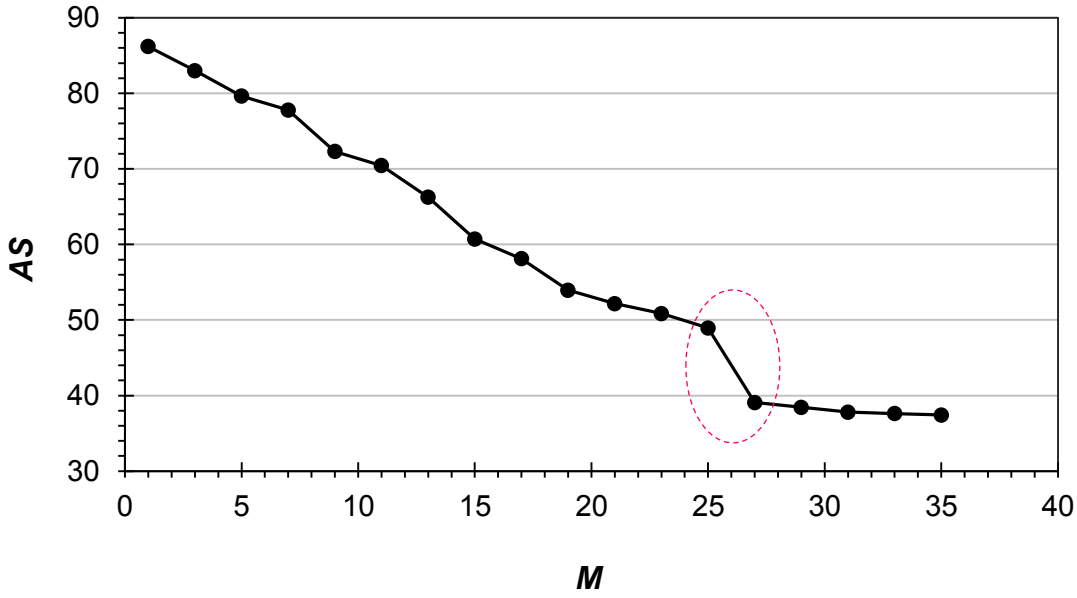

(b)

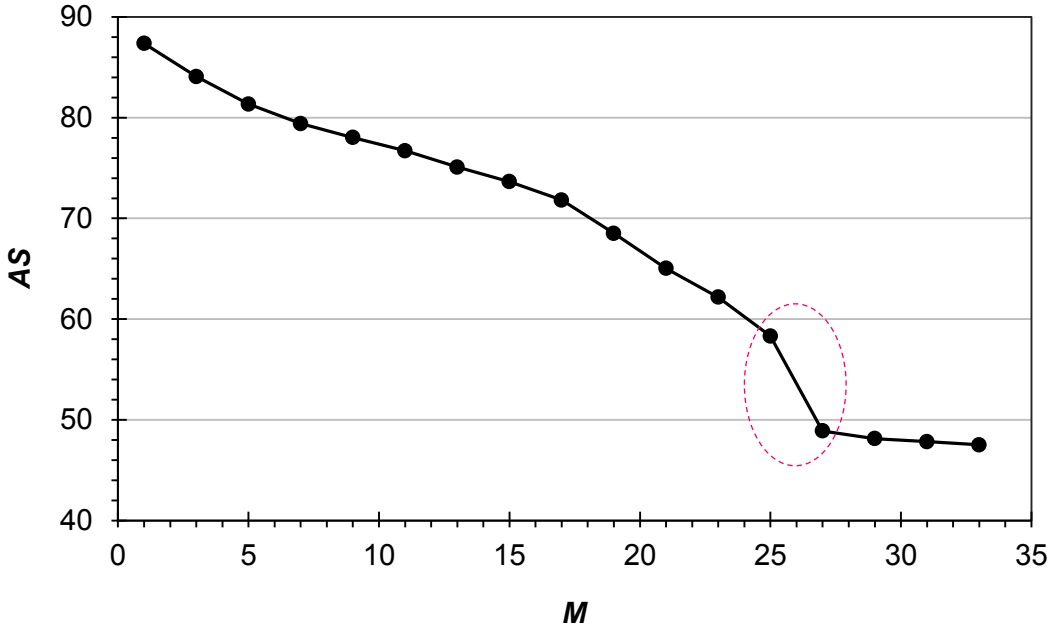

Figure 2.11 Relationship between the order of the median filter (*M*) and *Angle Score* (*AS*) to find the optimum median number in; (a) fall season (b) summer season.

(a)

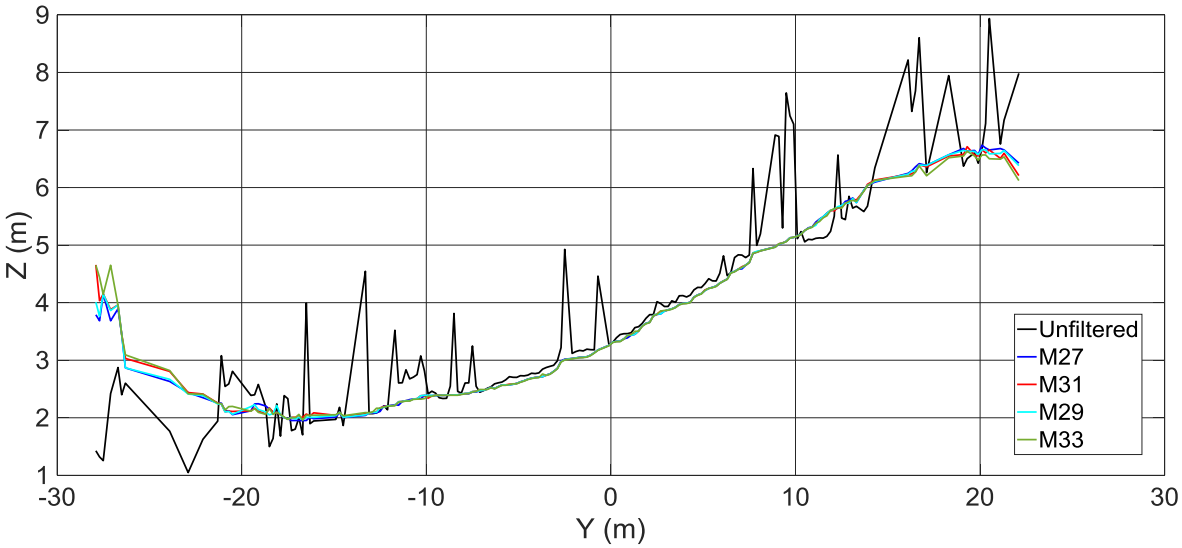

(b)

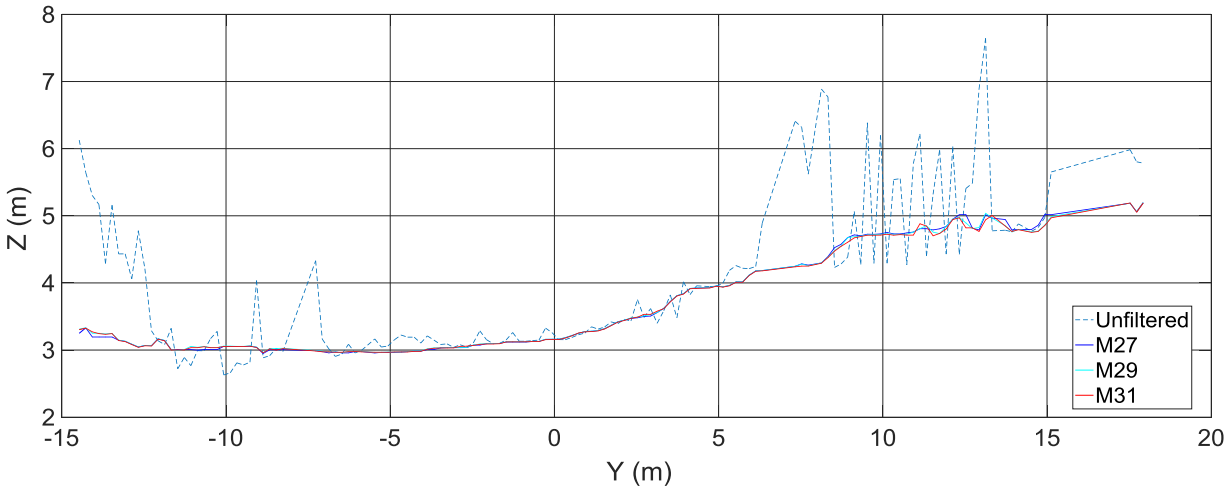

Figure 2.12 2D view of DTM without filtering and by applying a median filter of different orders; (a) fall season for $M = 27$, 29, 31, and 33 (b) summer season for $M = 27$, 29, and 31.

(a)

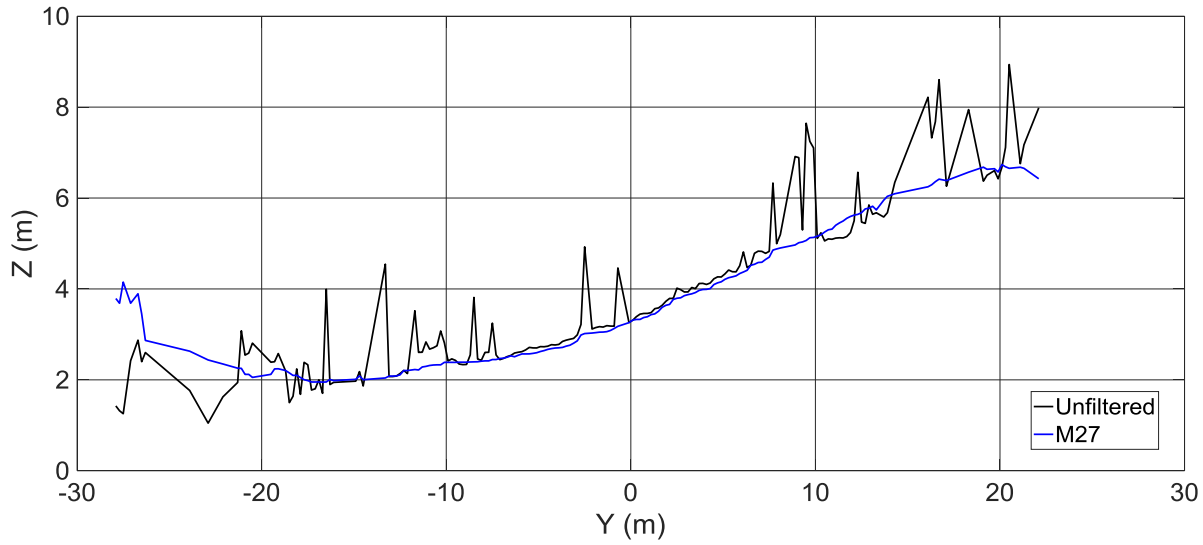

(b)

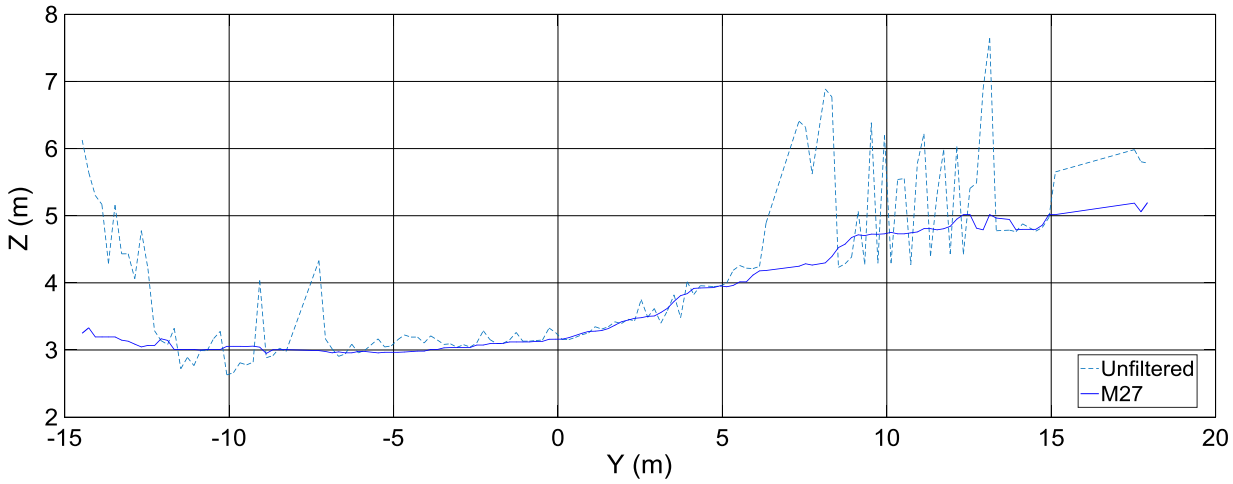

Figure 2.13 2D view of Unfiltered DTM and DTM with applying a median filter of $M = 27$ for $\Delta = 0.2$ m in; (a) fall season (b) summer season.

(a)

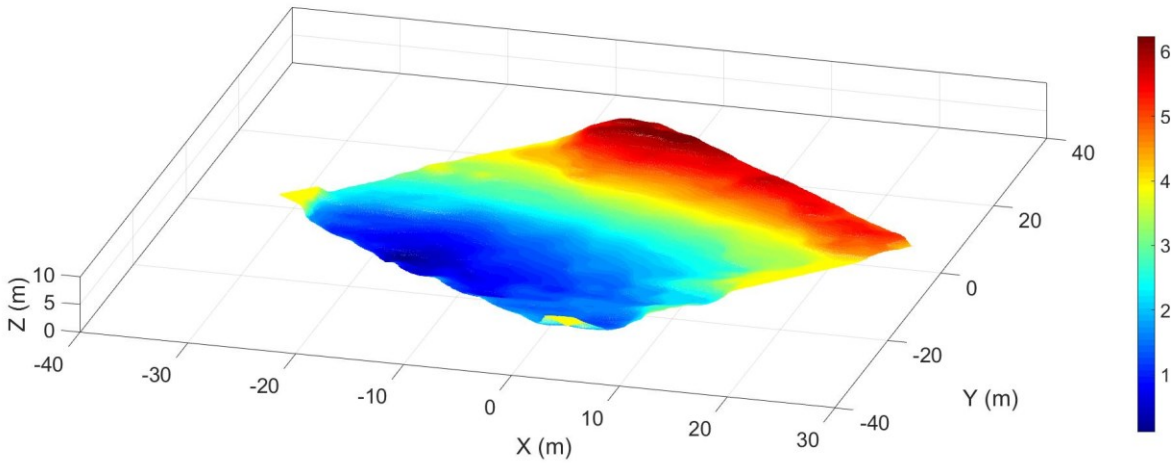

(b)

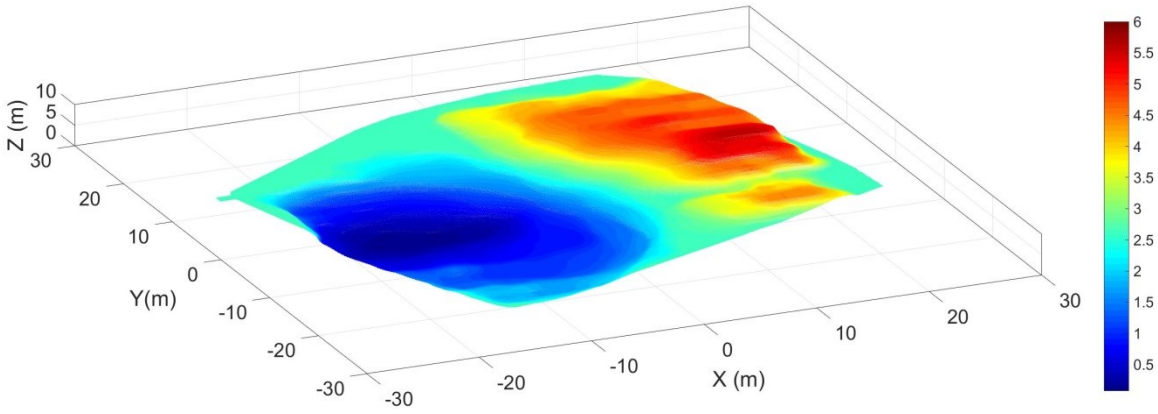

Figure 2.14 3D view of DTM by applying a median filter of $M = 27$ for $\Delta = 0.2$ m in; (a) fall season (b) summer season.

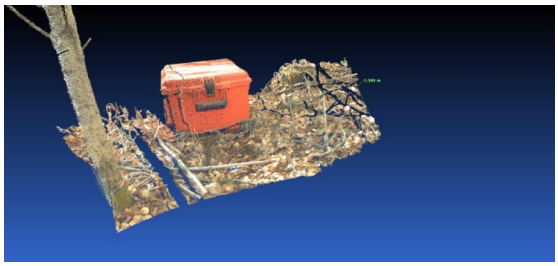

(a)

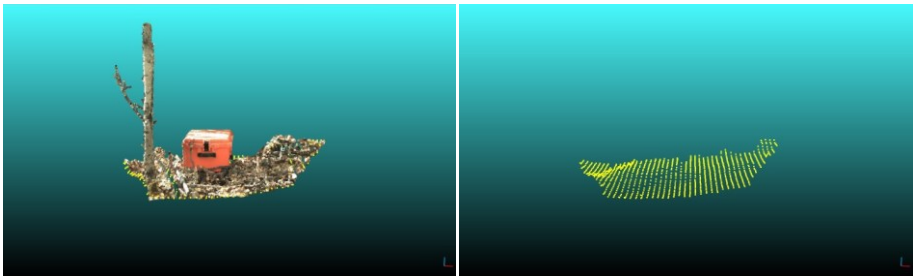

(b) (c)

Figure 2.15 Qualitative evaluation for separating ground points by the proposed algorithm; (a) raw data with high density in a sample set (b) ground points (yellow dots) and non-ground points (c) separated ground points.

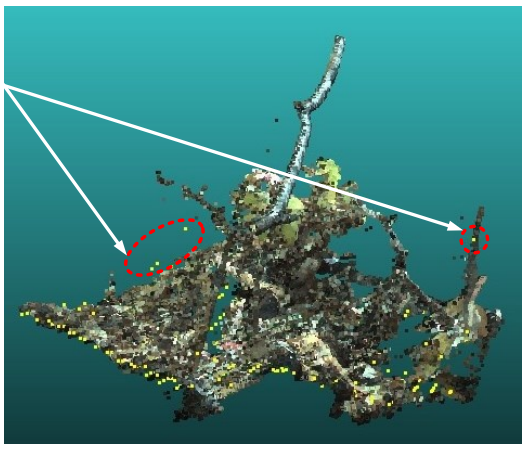

(a)

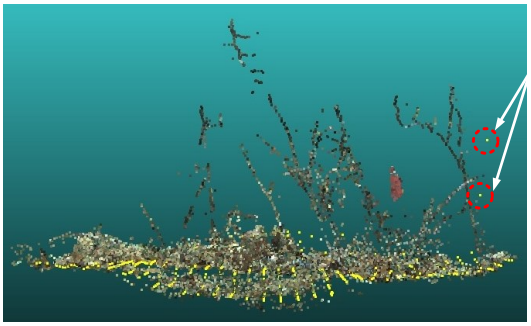

(b)

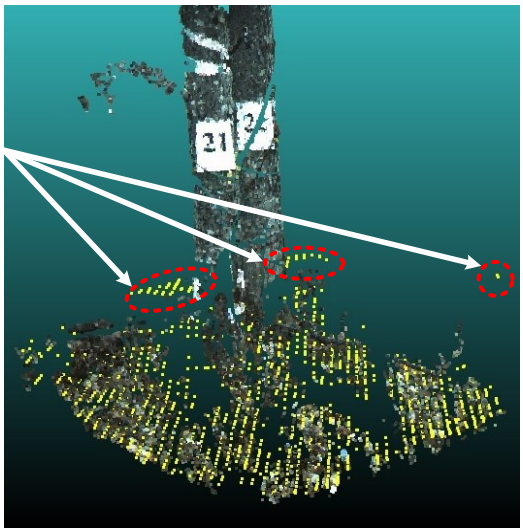

(c)

Figure 2.16 Commission errors in; (a) high (b) medium (c) low density in 3 sample sets. The red circles in this figure indicate some of the commission errors.

References

Abellán, A., Oppikofer, T., Jaboyedoff, M. Rosser, N.J., Lim, M., and Lato, M.J. 2014. Terrestrial laser scanning of rock slope instabilities. *Earth Surface Processes and Landforms*, 39, 80-97.

Arnold, N., Rees, W., Devereux, B., and Amable, G. 2006. Evaluating the potential of high-resolution airborne LIDAR data in glaciology. *International Journal of Remote Sensing*, 27, 1233-1251.

Axelsson, P. 1999. Processing of laser scanner data algorithms and applications. *ISPRS Journal of Photogrammetry and Remote Sensing*, 54 (2–3), 138-147.

Axelsson, P. 2000. DEM Generation from Laser Scanner Data Using Adaptive TIN Models. *International Archive of Photogrammetry, Remote Sensing and Spatial Information Sciences (ISPRS)*, 33 (B4), 110-117.

Bamber, J.L., and Rivera, A. 2007. A review of remote sensing methods for glacier mass balance determination. *Global Planet Change*, 59, 138-148.

Bartels, M., and Wei, H. 2010. Threshold-free object and ground point separation in LiDAR data. *Pattern Recognition Letters*, 31 (10), 1089-1099.

Bartels, M., Wei, H., and Mason, D. C. 2006. DTM Generation from LIDAR Data using Skewness Balancing. *Proceedings of the 18th International Conference on Pattern Recognition (ICPR'06)* 0-7695-2521-0/06. IEEE.

Bauwens, S., Bartholomeus, H., Calders, K., and Lejeune, P. (2016). Forest Inventory with Terrestrial LiDAR: A Comparison of Static and Hand-Held Mobile Laser Scanning. *Forests*, 7 (127), 1-17.

Beaumier, C., and Idrissa, M. 2016. Digital terrain models derived from digital surface model uniform regions in urban areas. *International Journal of Remote Sensing*, 37 (15), 3477-3493. http://dx.doi.org/10.1080/01431161.2016.1182666.

Brovelli, M.A., Cannata, M., and Longoni, U.M. 2002. Managing and processing LIDAR data within GRASS. *Proceedings of the Open source GIS* - GRASS users conference, Trento, Italy.

Chehata, N., Guo, L., and Mallet, C. 2009. Airborne LIDAR feature selection for urban classification using random forests. *International Archive of Photogrammetry, Remote Sensing and Spatial Information Sciences*, 38, 207-212.

Chen, Q. 2007. Airborne LIDAR data processing and information extraction. *Photogrammetric Engineering and Remote Sensing*, 73, 109–112.

Chen, Z., Xu, B., and Gao, B. 2016. An Image-Segmentation-Based Urban DTM Generation Method Using Airborne LiDAR Data. *IEEE, journal of selected topics in applied earth observations and remote sensing*, 9 (1), 496-506.

Cleveland, W.S., and Loader, C.L. 1996. Smoothing by local regression: Principles and methods. In *Statistical Theory and Computational Aspects of Smoothing*. New York, NY, USA: Springer-Verlag, 10-49.

Cothrun C. The Technical Side: Dual Axis Compensators. Available online: http://www.krcmar.ca/sites/default/files/1995_Spring_Dual%20Axis%20Compensators_1.pdf (accessed on 18 December 2016).

Elmqvist, M. 2002. Ground Surface Estimation from Airborne Laser Scanner Data Using Active Shape Models. *International Archives of the Photogrammetry, Remote Sensing and Spatial Information Sciences*, 34 (3A), Commission III, 09–13, Graz, Austria, 115-118.

El-Sheimy, N., Valeo, C., and Habib, A. 2005. *Digital Terrain Modeling*. Artech House, Boston, Mass. pp. 266.

Entwistle, J., McCaffrey, K., and Abrahams, P. 2009. Three-dimensional (3D) visualisation: The application of terrestrial laser scanning in the investigation of historical Scottish farming townships. *Journal of Archaeological Science*, 36, 860–866.

Ergun, B. 2010. A novel 3D geometric object filtering function for application in indoor area with terrestrial laser scanning data. *Optics and Laser Technology*, 42, 799–804.

Evans, J.S., and Hudak, A.T. 2007. A multiscale curvature algorithm for classifying discrete return LiDAR in forested environments. *IEEE Transactions on Geoscience and Remote Sensing*, 45 (4), 1029-1038.

Farid, A., Goodrich, D.C., Bryant, R., and Sorooshian, S. 2008. Using airborne lidar to predict leaf area index in cottonwood trees and refine riparian water-use estimates. *Journal of Arid Environments*, 72, 1-15.

Filin, S., and Pfeifer, N. 2006. Segmentation of airborne laser scanning data using a slope adaptive neighborhood. *ISPRS International Archives of the Photogrammetry, Remote Sensing and Spatial Information Sciences*, 60, 71–80.

Fisher, P.F., and Tate, N.J. 2006. Causes and consequences of error in digital elevation models. *Progress in Physical Geography*, 30, 467-489.

Gonzalez, P., Asner, G.P., Battles, J.J., Lefsky, M.A., Waring, K.M., and Palace, M. 2010. Forest carbon densities and uncertainties from lidar, QuickBird, and field measurements in California. *Remote Sensing of Environment*, 114, 1561-1575.

GSA BIM Guide for 3D Imaging. 2009. Available online: https://www.gsa.gov/portal/mediaId%20/226819/fileName/GSA_BIM_Guide_Series_03.action (accessed 18 December 2016).

Haralick, R., and Shapiro, L. 1992. *Computer and Robot Vision*. Addison Wesley, Reading, Mass.

Haugerud, R.A., and Harding D.J. 2001. Some Algorithms for Virtual Deforestation (VDF) of LiDAR Topographic Survey Data. Proceedings of the ISPRS workshop on Land Surface Mapping and Characterization Using Laser Altimetry. Annapolis, Maryland, *International Archives of the Photogrammetry, Remote Sensing and Spatial Information Sciences*, 34 (3/W4), Commission III, 203-209.

Herzfeld, U.C., Lingle, C.S. and Lee, L.H. 1993. Geostatistical evaluation of satellite radar altimetry for high-resolution mapping of Lambert Glacier, Antarctica. *Annals of Glaciology*, 17(1), 77-85.

Hollaus, M., Wagner, W., Eberhofer, C., and Karel, W. 2006. Accuracy of large-scale canopy heights derived from LiDAR data under operational constraints in a complex alpine environment. *ISPRS Journal of Photogrammetry and Remote Sensing*, 60 (5), 323-338.

Hong, S.H., Cho, H.S., Kim, N.H., and Sohn, H.G. 2015. 3D indoor modeling based on terrestrial laser scanning. *Journal of the Korean Society of Civil Engineers*, 35, 525-531.

Jaboyedoff, M., Oppikofer, T., Abellán, A., Derron, M. H., Loye, A., Metzger, R., and Pedrazzini, A. 2012. Use of LIDAR in landslide investigations: A review. *Natural Hazards*, 61, 5-28.

Jacobsen, K., and Lohmann, P. 2003. Segmented filtering of laser scanner DSMs. *International Archives of Photogrammetry and Remote Sensing*, 34 (3/W13).

Jaw, J.J., and Chuang, T.Y. 2008. Registration of ground-based LIDAR point clouds by means of 3D line features. *Journal of the Chinese Institute of Engineers*, 31, 1031-1045.

Jones, L. 2006. Monitoring landslides in hazardous terrain using terrestrial LIDAR: An example from Montserrat. *Quarterly Journal of Engineering Geology and Hydrogeology*, 39, 371-373.

Kilian, J., N. Haala, and M. English, 1996. Capture and Evaluation of Airborne Laser Scanner Data. *International Archives of Photogrammetry and Remote Sensing*, 31 (B3), Vienna, 383-388.

Kraus, K., and Mikhail, E.M., 1972. Linear least squares interpolation. 1016–1029.

Kraus, K., and Pfeifer, N. 1998. Determination of terrain models in wooded areas with airborne laser scanner data. *ISPRS International Archives of the Photogrammetry, Remote Sensing and Spatial Information Sciences*, 53, (4), 193-203.

Kraus, K., Karel, W., Briese, C. and Mandlburger, G. 2006. Local accuracy measures for digital terrain models. *The Photogrammetric Record*, 21 (116), 342-354.

Lee, H.S., and Younan, N. 2003. DTM extraction of LiDAR returns via adaptive processing. *IEEE Transactions on Geoscience and Remote Sensing*, 41 (9), 2063-2069.

Liu, X. 2008. Airborne LIDAR for DEM generation: Some critical issues. *Progress in Physical Geography*, 32, 31-49.

Lohmann, P., Koch, A., and Schaeffer, M. 2000. Approaches to the filtering of laser scanner data. *International Archives of Photogrammetry and Remote Sensing*, 33(B3/1), 534-541.

Maguya, A. S., Junttila, V. and Kauranne, T. 2014. Algorithm for Extracting Digital Terrain Models under Forest Canopy from Airborne LiDAR Data. *Remote Sensing*, 6, 6524-6548.

MATLAB R2016b, the MathWorks lnc., Natick, Massachusetts, United States, 2016.

Meng, X., Currit, N., and Zhao, K. 2010. Ground filtering algorithms for airborne LiDAR data: A review of critical issues. *Remote Sensing*, 2 (3), 833-860.

Miller, C. and LaFelamme, R.A. 1958. The digital terrain model theory and applications. *Photogrammetric Engineering*, 24 (3), 433-442.

Moholdt, G., Nuth, C., Hagen, J.O., and Kohler, J. 2010. Recent elevation changes of Svalbard glaciers derived from ICES at laser altimetry. *Remote Sensing of Environment*, 114, 2756-2767.

Mongus, D., and Zalik, B. 2012. Parameter-free ground filtering of LiDAR data for automatic DTM generation. *ISPRS Journal of Photogrammetry and Remote Sensing*, 67, 1-12.

Montealegre, A.L., Lamelas, M.T., and de la Riva, J. 2015. A Comparison of Open-Source LiDAR Filtering Algorithms in a Mediterranean Forest Environment. *IEEE Journal of Selected Topics in Applied Earth Observations and Remote Sensing*, 8(8), 4072-4085.

Morsdorf, F., Nichol, C., Malthus T., and Woodhouse, I.H..2009. Assessing forest structural and physiological information content of multi-spectral LiDAR waveforms by radiative transfer modelling. *Remote Sensing of Environment*,113, 2152-2163.

Nardinocci, C., Forlani, G., and Zingaretti, P. 2003. Classification and filtering of laser data. *International Archives of Photogrammetry and Remote Sensing*, 34.3/W13.

Nilsson, M. 1996. Estimation of tree heights and stand volume using an airborne LIDAR system. *Remote Sensing of Environment*, 56, 1-7.

Nurunnabi, A., West, G., and Belton, D. 2016. Robust Locally Weighted Regression Techniques for Ground Surface Points Filtering in Mobile Laser Scanning Three Dimensional Point Cloud Data. *IEEE, transactions on geoscience and remote sensing*, 54 (4), 2181-2193.

Petrie, G. and Kennie T.J.M. 1987. Terrain Modeling in surveying and Civil Engineering. *Computer-Aided Design*, 19 (4), 171-187.

Pfeifer, N. and Mandlburger, G. 2009. LiDAR data filtering and DTM generation. *Topographic Laser Ranging and Scanning*, 307–334.

Pfeifer, N., Reiter, T., Briese, C., and Rieger, W. 1999. Interpolation of high quality ground models from laser scanner data in forested areas. *International Archives of Photogrammetry and Remote Sensing*, 32 (3/W14), 31-36.

Pirotti, F., and Tarolli, P. 2010. Suitability of LiDAR point density and derived landform curvature maps for channel network extraction. *Hydrological Processes*, 24, 1187-1197.

Pope, A., Willis, I., Rees, W., Arnold, N., and Pálsson, F. 2013. Combining airborne LIDAR and landsat ETM+ data with photoclinometry to produce a digital elevation model for Langjökull, Iceland. *International Journal of Remote Sensing*, 34, 1005-1025.

Popescu, S.C., Wynne, R.H., and Nelson, R.F. 2003. Measuring individual tree crown diameter with LIDAR and assessing its influence on estimating forest volume and biomass. *Canadian Journal of Remote Sensing*, 29, 564-577.

Prokop, A. 2008. Assessing the applicability of terrestrial laser scanning for spatial snow depth measurements. *Cold Regions Science and Technology*, 54, 155-163.

Raber, G.T., Jensen, J.R. Schill, S.R. and Schuckman, K. 2002. Creation of Digital Terrain Models Using an Adaptive LiDAR Vegetation Point Removal Process. *Photogrammetric Engineering and Remote Sensing*, 68 (12), 1307-1316.

Reutebuch, S.E., McGaughey, R. J., Andersen, H. E., and Carson, W.W. 2003. Accuracy of a high-resolution LiDAR terrain model under a conifer forest canopy. *Canadian Journal of Remote Sensing*, 29 (5), 527-535.

Roering, J.J., Stimely, L.L., Mackey, B.H., and Schmidt, D.A. 2009. Using DInSAR, airborne LIDAR, and archival air photos to quantify landsliding and sediment transport. *Geophysical Research Letters*, 36, 1-5.

Roggero, M. 2001. Airborne laser scanning: clustering in raw data. *International Archives of the Photogrammetry, Remote Sensing and Spatial Information Sciences,* 34 (3/W4), 227- 232.

Roncella, R., Saletti, R., and Terreni, P. 1991. A novel bit-level systolic array median filter. In Solid-State Circuits Conference, ESSCIRC'91. Proceedings-Seventeenth European. *IEEE*. 1, 97-100.

Serifoglu, C., Gungor, O., and Yilmaz V. 2016. Performance evaluation of different ground filtering algorithms for UAV-based point clouds. *The International Archives of the Photogrammetry, Remote Sensing and Spatial Information Sciences*, 41.

Shan, J. and Sampath, A. 2005. Urban DEM generation from raw LiDAR data: A labelling algorithm and its performance. *Photogrammetric Engineering and Remote Sensing*, 71(2), 217-226.

Sheng, Y., Gong, P., and Biging, G.S. 2003. Orthoimage production for forested areas from large-scale aerial photographs. *Photogrammetric Engineering and Remote Sensing*, 69, 259-66.

Sithole, G. 2001. Filtering of Laser Altimetry Data Using a Slope Adaptive Filter. *International Archives of Photogrammetry Remote Sensing and Spatial Information Sciences*, 34(3/W4), 203-210.

Sithole, G. 2005. Segmentation and classification of airborne laser scanner data.

Sithole, G. and Vosselman, G. 2004. Experimental comparison of filter algorithms for bare earth extraction from airborne laser scanning point clouds. *ISPRS Journal of Photogrammetry and Remote Sensing*, 59, 85-101.

Slob, S., Hack, R. 2004. 3D terrestrial laser scanning as a new field measurement and monitoring technique. *Engineering geology for infrastructure planning in Europe*, 179-189.

Sohn, G., and Dowman, I. 2002. Terrain surface reconstruction by the use of tetrahedron model with the MDL criterion. *International Archives of the Photogrammetry, Remote Sensing and Spatial Information Sciences*, 34 (3A), 336-344.

Streutker, D., and Glenn, N. 2006. LiDAR measurement of sagebrush steppe vegetation heights. *Remote Sensing of Environment*, 102 (1–2), 135-145.

Tóvári, D. and Pfeifer, N., 2005. Segmentation based robust interpolation-a new approach to laser data filtering. *International Archives of Photogrammetry, Remote Sensing and Spatial Information Sciences*, 36(3/19), 79-84.

Tyagur, N. and Hollaus, M. 2016. Digital terrain models from mobile laser scanning data in Moravian Karst. *International Archives of the Photogrammetry, Remote Sensing and Spatial Information Sciences*, 41.

Vosselman, G. 2000. Slope based filtering of laser altimetry data. *International Archives of the Photogrammetry, Remote Sensing and Spatial Information Sciences*, 33 (B3), 935-942.

Vosselman, G., and Maas, H. G. 2010. *Airborne and Terrestrial Laser Scanning*. CRC Press, 2010.

Vosselman, G., and Mass, H. 2001. Adjustment and Filtering of Raw Laser Altimetry Data. In *Proceedings of OEEPE Workshop on Airborne Laserscanning and Interferometric SAR for Detailed Digital Terrain Models, Stockholm, Sweden*.

Wack, R., and Wimmer, A. 2002. Digital terrain models from airborne laser scanner data- a grid based approach. *International Archives of the Photogrammetry, Remote Sensing and Spatial Information Sciences*, 34 (3B), 293-296.

Wang, Y., Mercer, B., Tao, C., Sharma, J., and Crawford, S. 2001. Automatic Generation of Bald Earth Digital Elevation Models from Digital Surface Models Created Using Airborne IFSAR. In *Proceedings of 2001 ASPRS Annual Conference* (23-27).

Wang, Z., Li, H., and Wu, L. 2010. Geodesics-based topographical feature extraction from airborne LIDAR data for disaster management. In *Geoinformatics, 2010 18th International Conference on* (pp. 1-5). IEEE.

White, S.A., and Wang, Y. 2003. Utilizing dems derived from LiDAR data to analyze morphologic change in the North Carolina coastline. *Remote Sensing of Environment*, 85 (1), 39-47.

Whitman, D., Zhang, K., Leatherman, S.P., and Robertson, W. 2003. Airborne laser topographic mapping: application to hurricane storm surge hazards. *Earth Science in the City: A Reader*, 363-376.

Woolard, J.W., and Colby, J.D. 2002. Spatial characterization, resolution, and volumetric change of coastal dunes using airborne LIDAR: Cape Hatteras, North Carolina. *Geomorphology*, 48, 269-287.

Yu, B., Liu, H., Wu, J., Hu, Y., and Zhang, L. 2010. Automated derivation of urban building density information using airborne LIDAR data and object-based method. *Landscape and Urban Planning*, 98, 210-219.

Zak˘sek, K. and Pfeifer, N. 2006. An improved morphological filter for selecting relief points from a LIDAR point cloud in steep areas with dense vegetation. *Luubljana, Slovenia and Innsbruck, Austria: Institute of Anthropological and Spatial Studies, Scientific Research Centre of the Slovenian Academy of Sciences and Arts, and Institute of Geography, Innsbruck University.*

Zhang, C. 2003. A progressive morphological filter for removing nonground measurements from airborne LIDAR data. *IEEE Transactions on Geoscience and Remote Sensing*, 41(4), 872-882.

Zhang, J., and Lin, X. 2013. Filtering airborne LiDAR data by embedding smoothness-constrained segmentation in progressive TIN densification. *ISPRS International Archives of the Photogrammetry, Remote Sensing and Spatial Information Sciences*, 81, 44-59.

Zhang, K., Chen, S., Whitman, D., Shyu, M., Yan, J., and Zhang, C. 2003. A progressive morphological filter for removing nonground measurements from airborne LIDAR data. *IEEE Transactions on Geoscience and Remote Sensing*, 41(4), 872–882.

Zhang, K., Whitman, D. 2005. Comparison of three algorithms for filtering airborne LiDAR data. *Photogrammetric Engineering and Remote Sensing*, 71 (3), 313–324.

CHAPTER 3

Automatic Separation of Photosynthetic and Non-Photosynthetic Components in a Point Cloud Data from a Boreal Forest Canopy

3.1 Introduction

Accurate assessment of the canopy structure is required for sustainable forest management, modeling of ecosystem functions, global level ecosystem interactions, and the interactions between the land surface and the atmosphere (Sellers et al. 1997; Béland et al. 2011). Among the canopy structure parameters, the green biomass and the leaf area index (LAI) are two important parameters which define the effective received sunlight and the photosynthesis process. Hence, both parameters depend on the configuration and the quantity of the leaves (Parker, 1995).

Remote sensing technologies offer a powerful tool for analysis of the canopy structure and calculation of its parameters. Among various remote sensing systems, Light Detection and Ranging (LiDAR) offers an advanced high-resolution platform which provides a 3D Point Cloud Data (PCD). The LiDAR PCD is an inhomogeneous mixture of all forest features including wood and foliage which has been widely used for extraction of green leaves (Omasa et al. 2007; Hosoi and Omasa, 2006, 2009; Hopkinson et al. 2013; Greaves et al. 2015; Lin and Herold, 2016; Lovell et al. 2003; Morsdorf et al. 2006; Zheng et al. 2013, 2016; Ma et al. 2016a, b). For this purpose, the points belonging to the leaves have to be identified from the whole PCD, initially. This is a challenging task since a single tree may include millions of points representing foliage and wood which are irregularly scattered and intermixed. Some of the studies avoid the complexity associated with separation of foliage points and calculate the Plant Area Index (PAI) which includes both the leaf area and the wood area, instead of pure LAI (Takeda et al. 2008; Olivas et al. 2013; Pueschel et al. 2014). Also, some of the studies calculate the total biomass instead of green biomass (Askne et al. 2017; Margolis et al. 2015).

There are three techniques for separation of photosynthetic and non-photosynthetic materials in a tree PCD. In the first technique, the points are imported into a 3D demonstration software, and the PCD features are separated manually by the operator using visual color-based

recognition and based on geometrical distribution of points (Watt et al. 2005; Hosoi et al. 2010; Holopainen et al. 2011; Hauglin et al. 2013). This method is time-consuming and prone to user error since one needs to deal with millions of scattered points forming various geometries. This method has made the woody materials to be a key error source in estimating LAI (Whitford et al. 1995; Chen et al. 1997; Liu and Jin, 2017). Hosoi and Omasa (2007) showed that woody materials could contribute to LAI estimation errors from 4.2% to 32.7% depending on tree canopies. Clawges et al. (2007) found that the ratio of wooden material of a tree to the whole tree area ranged from 24% to 58%. Moorthy et al. (2008) demonstrated that considering woody material results in an improvement of initial PAI estimation with a root mean square error (RMSE) of 1.13 to LAI retrievals with a RMSE of 0.68; hence, the accuracy of LAI assessment could be highly improved if the woody material could be separated completely from the foliage.

Hence, other techniques are developed to perform this task automatically. The second technique utilizes statistical tools such as eigenvalues, conditional probability functions and Gaussian mixture models for the identification of leaf geometry (Hebert and Vandapel 2003; Vandapel et al. 2004; Lalonde et al. 2006; Ma et al. 2016). The leaf geometry technique is only based on geometry identification which is different for wood and leaf features. As a simple intuitive alternative, the third technique based on "intensity" parameter has recently been proposed (Eitel et al. 2009, 2010, 2011, 2014, Donoghue et al. 2007; Beland et al. 2011, 2014). Intensity parameter is provided by LiDAR for every point in PCD along with its Cartesian coordinates (*x, y, z*).

The intensity of the reflected laser beam which is received at the LiDAR depends on several factors including (*i*) the *constituent materials* of the hit point, (*ii*) *laser wavelength*, (*iii*) *incidence angle* at the hit point, and (*iv*) the *distance* between laser scanner and the hit point (Pozar, 2006). The effect of each mentioned factor needs to be studied. (*i*) *Constituent materials*: Since leaves have higher chlorophyll and water content compared to woody material, their absorption of the laser beam energy is totally different (Gao, 1996; Sims and Gamon, 2003; Sims and Gamon, 2003; Lim et al. 2003; Pfennigbauer and Ullrich, 2010; Béland et al. 2011; Wu et al. 2013; Beland et al. 2014; Ma et al. 2016); (*ii*) *Laser wavelength*: The wavelength is governed by the laser transceiver. Various LiDAR products may apply a single or multiple wavelengths (Li et al., 2013). Multiple-wavelength LiDAR offers more information about hit point features which is of benefit for separation of wood and leaf, at the expense of the higher cost of apparatus. The

apparatus used in the present dissertation is a Leica C10 which supports a single wavelength 532 nm laser (green light). Usually, each study dedicated to the separation of wood and foliage offers instructions, equations, and curves which are specific to its laser device wavelength; (*iii*) *Incidence angle*: The incidence angle of a laser beam depends on the relative orientation of the beam with the leaf or wood extent. Since the PCD from Leica C10 scanner doesn't provide any information about the surface vectors of leaf or wood, this factor is ignored in the present study. This factor is also ignored in the current state of the art, under the assumption of Lambertian scattering; (*iv*) *Distance*: The power of laser beam is inversely proportional to the squared distance between the source and the hit point (Pozar, 2006). Hence, each LiDAR instrument supports a limited range of distance depending on the sensitivity of its receiver which is mentioned in its datasheet (Horaud et al. 2016). For the Leica C10, the maximum distance is 300 m according to its data sheets.

Current state of the art on separation of leaf from wood based on laser intensity parameter take advantage of the raw intensity parameter returned by LiDAR (Béland et al. 2011; Beland et al. 2014). These studies don't distinguish the effects of constituent materials and distance which are two independent factors. Since the different points forming a tree PCD are at different distances from the scan station, the raw intensity isn't an appropriate scale for separation of leaf from wood.

This chapter proposes an algorithm for automatic separation of leaves from wood in terrestrial LiDAR PCD by discriminating the factors of distance and constituent materials. Initially, the physical process of reflection of laser beam over tree features is studied and a model is developed. Then, the effect of distance is compensated in the raw LiDAR intensity using square law to calculate the absorption intensity. The absorption intensity is demonstrated to be a suitable scale for separation of leaf from wood. The proposed simple intuitive algorithm doesn't need the leaf-off PCD or calibration of intensity by distance sweeping of spectral white panels (Béland et al. 2011; Beland et al. 2014). The rest of this chapter is organized as follows; Section 2 presents the study area and methodology. The result and discussion are described in sections 3 and 4, respectively. Finally, Section 5 concludes the chapter.

3.2 Materials and Methods

3.2.1 Study Area and Site Characteristics

A rectangular study plot with the size of 50m × 50m was set up in the Peace River Environmental Monitoring Super Site (PR-EMSS), which is forest stand of Trembling Aspen (*Populus tremuloides*) with a broad leaf deciduous canopy. This plot was surveyed between August 2014, and Oct 2014. The area is a hilly terrain, located at latitude 56° 44' 39" North and longitude -118° 20' 40" West, at an altitude of 871 m.

In the study plot, the PCD was collected using a Leica Scan Station C10 at four stations. Tree height and Diameter at Breast Height (DBH) were also collected for all trees using TruPulse 200 laser Rangefinder and a measuring tape.

3.2.2 Instrument and in Situ Measurements Description

The ground-based LiDAR, also known as Terrestrial Laser Scanning (TLS), was the Leica Scan Station C10 (Leica Geosystems AG, Heerbrugg, Switzerland). The Leica is emitting laser beam pulses at 532 nm (green laser) within a $360^{\circ} \times 270^{\circ}$ field of the view window. Leica is a discrete return LiDAR **(**only first return points are used to characterize the object at a given location). The information that is provided by Leica includes coordinates data *(x, y, z)*, and intensity. It uses the beam's travel time to compute the distance to the targets. For a 90% albedo target, the instrument can detect a return signal from 300 m away, and at 18% albedo, it can detect a return signal at 134 m. The Leica C10 can also be used for short range targets up to a minimum distance of about 0.1 m. The trees in this study were scanned from six locations to minimize the occlusion effect. The scans were performed in leaf-on (summer 2014) and leaf-off (fall 2014) seasons. At the medium resolution, each scan took about 10–15 min to complete. For all scans, the Leica C10 was placed on a leveled survey tripod about 1.5 m above ground to avoid the covering effect of the dense understory. After scanning, any pair of scans was aligned to common reference targets using the Cyclone 8.1 software. All processing of the LiDAR PCD were performed in MATLAB Software (R2016b).

The average tree density computed in the study area was 675 trees ha^{-1}, the large majority of which are mature trees with a DBH more than 5 cm. For this study, a set of Trembling Aspen trees were selected within a plot of 50 m × 50 m in the study area to carry out the LiDAR measurements as well as field measurements. In this study, the proposed method was applied on 21 trees.

3.2.3 Algorithm Steps

An algorithm for the automatic separation of photosynthetic from non-photosynthetic components in LiDAR PCD is developed in this study. The algorithm doesn't require any information on temporal characteristics such as seasonal data, laser wavelength, or tree distance. The algorithm steps are summarized in Figure 3.1 and elaborated as follows.

I. The tree PCD in the leaf-on season (containing leaf and wood) is loaded into the algorithm. PCD includes the point coordinates along with point intensity (*x, y, z, I*) which forms the 4th column of PCD matrix. *I* is a Real number in the range of (-2047, +2048).

II. The range of *I* is changed from (-2047, +2048) to (0, +1) scale using a simple linear equation (1):

$$I_{norm} = \frac{I}{4095} + \frac{2048}{4095} \qquad (1)$$

III. The intensity of the received laser beam from the hit point depends on the total power loss that it undergoes in its two-way travel from the laser source to hit point and also in the return path from hit point to the laser source and the target. The laser beam power loss originates in *path loss* and *absorption loss* (Figure 3.2). The *path loss* is proportional to squared distance (R^2) which is known for every point in PCD (Pozar, 2006). In Figure 3.2, the *path loss* is demonstrated by two red arrows extending from LiDAR to the hit spot on the leaf and from hit spot to the LiDAR. However, the *absorption loss* depends on water and the surface physical properties such scattering characterization and pigment. Since the leaf and wood tend to have different ranges of water, pigment, and scattering characterization, *absorption loss* can be used to identify leaf from wood (Pozar, 2006). In

Figure 3.2, this is demonstrated by the orange bouncing arrow over the leaf. In order to separate wood from the leaf, the absorption loss should be distinguished from the path loss. To achieve the intensity only due to absorption loss ($I_{absorption}$), I_{norm} should be multiplied by squared distance as equation (2):

$$I_{absorption} = I_{norm}.R^2 \qquad (2)$$

The distance can be simply calculated for each specific point based on its recorded Cartesian coordinate (*x, y, z*) which is presented by LiDAR, as in equation (3):

$$R = \sqrt{x^2 + y^2 + z^2} \qquad (3)$$

Hence:

$$I_{absorption} = I_{norm} \,.\, (x^2 + y^2 + z^2) \qquad (4)$$

IV. To separate wood from leaf, the threshold intensity (I_{th}) should be found. For $I > I_{th}$, either leaf or wood is separated. There are two ways to meet this purpose:

***A. Beland Threshold*:** Beland et al. (2011) developed a method for finding a threshold value for separating leaf from wood (Figure 3.3). Their method is based on the raw LiDAR intensity (*I*) and needs the PCD in both leaf-off (PCD_{dry}: leaf-off) and leaf-on season (PCD_{wet}: leaf-on). They draw the graph of the number of laser returns for each recorded intensity in both seasons. Finally, the threshold intensity for separation is found by balancing two areas representing leaf returns classified as wood (LW) and wood returns classified as leaves (WL). This is shown in Figure 3.3a. The steps are elaborated as follows:

i. The abundance graph of intensity is drawn for both PCD_{wet} and PCD_{dry} (Figure 3.3a). In this graph, the horizontal axis is *I* and the vertical axis is the number of points (N). This results in two different curves of $N_{wet}(I)\ and\ N_{dry}(I)$ for leaf-on

and leaf-off season, respectively. Since I is not continuous, the values should be discretized to smaller ranges. As an example, to divide I range into 100 steps, the step width should be calculated as in equation (5):

$$I_{step} = \frac{I_{max} - I_{min}}{100} \quad (5)$$

ii. Using the abundance equations, two summation curves should be drawn and compared. The summation functions (σ) are defined as in equation (6) and (7):

$$\sigma_{dry}(I_n) = \sum_{I_{min}}^{I_n} N_{dry}(I_n) \quad (6)$$

$$\sigma_{diff}(I_n) = \sum_{I_n}^{I_{max}} \{N_{wet}(I_n) - N_{dry}(I_n)\} \quad (7)$$

I_{th} is the intersection of σ_{dry} and σ_{diff} curves (Figure 3.3b). This reference does not present any justification for their method.

***B. Fine Tuning*:** As an alternative to Beland's method (2011), I_{th} can be simply found by fine tuning; The first step is to use an initial guess for I_{th} which might be the median value of $I_{absorption}$ as in equation (8):

$$I_{median} = \frac{I_{max} + I_{min}}{2} \quad (8)$$

Then, the points with $I_{absorption} < I_{th}$ are separated.

3.2.4 Accuracy Assessment

To evaluate the performance of the separation method, both qualitative and quantitative analyses were employed. The qualitative method can be implemented using 3D point cloud demonstration softwares such as CloudCompare. In the software, two PCDs are loaded simultaneously and with different colors: the whole PCD and the separated points. This allows

for visual comparison of the separated point (Zhang and Whitman 2005; Serifoglu et al. 2016). For quantitative assessment, the Sithole and Vosselman (2004) method is used. In this method, error type I (omission error) and error type II (commission error) are calculated as in equation (9):

$$\text{Error type I} = \frac{a}{GP}$$
$$\text{Error type II} = \frac{b}{NGP} \quad (9)$$

where a is the number of green points separated as non-green, b is the number of non-green points classified as green, GP is the total number of green points, and NGP is the total number of non-green points (Montealegre et al. 2015). 3D point cloud demonstration softwares such as CloudCompare can be used for counting different classes of points and finding the above-mentioned parameters. Zooming and fencing functions in the software allows for the required modifications in the original raw PCD and manual separation of the leaves. The high scan resolution of LiDAR preserves the actual geometry of leaf and wood features.

3.3 Results

In this section, the proposed algorithm is run on tree PCDs in the summer season, to examine its efficacy in the separation of leaf from wood. For these trees, the *absorption loss* ranges from 0 to 500 (mostly below 300). Initially, the optimal threshold of $I_{absorption}$ is found by fine-tuning. A wide range of intensity thresholds including 250, 200, 90, 86, 70, 50, and 20 was applied. This is depicted in Figure 3.4 with a gradual transition from a small subset of leaves to the whole tree PCD. Leaves belong to the higher values of intensity and wood belong to the lower values of intensity. Next, the Optimum Intensity Threshold (OIT) has to be determined by minimizing both commission and omission errors. To do this, the proposed algorithm was run over 21 trees to find the errors. Figure 3.5 shows the commission and omission errors for three sample trees (*i, r, b*) in study plot. As an example, for tree *i,* the omission error ranges from 2.4% to 99% and the commission error ranges from 0.0008% to 82.8% (Figure 3.5a). The minimum

omission error of 2.4% corresponds to a low commission error of 0.82% and also the OIT of 80 (Figure 3.4e). For tree *r* and tree *b,* the OIT value is 90 and 75, respectively (Figure 3.5 b,c).

For a visual demonstration of the efficacy of OIT = 80, in Figure 3.6 the separated green-colored points are compared and overlaid on the whole PCD of the tree (the background PCD in the RGB color in two dimensions). This Figure shows the overlaying from the top view. Figure 3.7 shows the overlaying from the side view. A section of the tree crown is selected in Figure 3.7a. The separated green points are depicted in Figure 3.7b. For comparison, the separated green points are overlaid on the background PCD (RGB color) in Figure 3.7c. It can be visually assessed that the algorithm has been successful in its task. As can be seen in Figure 3.6 and 3.7, the trunk and small branches in the crown are completely removed.

For comparison, Beland`s method (2011) is applied over normalized intensity which is in the range of (0, 1). Figure 3.8 shows the graphs for determining the intensity threshold for the same sample single tree. According to Beland`s method, the intersection of leaf-on and leaf-off intensity curves indicates the OIT for separating leaf from wood which is 0.19. In Figure 3.9, different normalized intensity threshold values are applied on the sample tree PCD to separate leaf from wood. As can be seen, all of the threshold values ranging from 0.6 to 0.1 have resulted in the separation of a mixture of wood and leaf including a portion of the trunk and also a portion of the crown. Even applying OIT value of 0.19 does not separate leaf and wood effectively. Figure 3.10 compares separation based on fine-tuning of absorption intensity with OIT value of 80 and Beland's method on normalized intensity with OIT value of 0.19.

To have a comprehensive analysis of Beland`s method, it is also applied to *absorption intensity* which ranges from 0-500 (Figure 3.11). Both leaf-on and leaf-off PCD`s of the tree were available for this purpose. In Figure 3.11, the intersection of leaf-on and leaf-off curves result in OIT value of 38 which is far off the OIT of 80, found by fine-tuning and error analysis. Figure 3.12 demonstrates the optimal threshold calculated based on minimum commission and omission errors for 21 trees in the stand level. It can be observed that the OIT value varies for different individual trees. But it is in the range of 75-92 for all trees.

3.4 Discussion

The objective of this study was to develop an effective method for separating photosynthetic from non-photosynthetic components using the intensity information of laser points in ground-based LiDAR PCD. The core contribution of this method was the introduction of a parameter which is calculated solely based on the information collected by LiDAR. This parameter is *absorption intensity* which is different from the raw point intensity provided by LiDAR for each point in PCD. The *absorption intensity* was shown to be a suitable scale for separation of foliage from wood and it is calculated by considering the effect of distance on the laser beam (Eitel et al. 2009; Thoren and Schmidhalter, 2009). This is also shown in Figure 3.4 where the points are arranged and separated.

The proposed method differs from existing methods, such as the visual color-based and geometrical distribution of points recognition (Watt et al. 2005; Hosoi et al. 2010; Holopainen et al. 2011; Hauglin et al. 2013), and the statistical methods (Hebert and Vandapel 2003; Vandapel et al. 2004; Lalonde et al. 2006; Ma et al. 2016). The proposed method is also different from other methods using LiDAR intensity parameter such as Beland et al. (2011). In this chapter, Beland's method was comprehensively elaborated. For comparison, the tree PCD were classified using both Beland`s method (2011) and the proposed algorithm (see Figure 3.10). Beland's method was applied to two different intensity scales including *normalized intensity* and *absorption intensity* which both were unsuccessful in separation (Figure 3.9 and Figure 3.11). It can be seen from Figure 3.8 that the intersection of leaf-on and leaf-off graphs with *normalized intensity* gives a threshold of 0.19 which is not suitable for separation of leaf from wood (see Figure 3.9g) where most of the separated green points belong to the tree trunk. As Figure 3.11 shows, the intersection of leaf-on and leaf-off curves with *absorption intensity* result in OIT value of 38 based on Beland`s method while in Figure 3.10d, with a threshold value of 38, the trunk PCD are included in separated green points.

Beland's method involves several theoretical and practical limitations. For example, it requires data collection in both leaf-on and leaf-off season which is costly and labor-intensive especially for remote forests. On the other hand, Beland's threshold depends on the number of

laser returns for every intensity value. This is not a suitable criterion for separating wood from leaf. Also, Beland (2011) presents graphs and equations that relate the raw point intensity (*I*) recorded by LiDAR to the intensity due to absorption loss at different distances. To carry out this task, they had to put several spectral panels with different absorption losses (very low/ low/ medium/ high/ very high) as reference target at different distance range of 5 to 30 m. Hence, the preparation of their mathematical model is a cumbersome, challenging and labor intensive task. Despite all the mentioned drawbacks, Beland's study is a significant part of the literature on separation.

The commission and omission error of the proposed algorithm were calculated for the 21 trees in the study plot. As an example, the commission and omission errors are shown in Figure 3.5 for three sample trees. The minimum omission error of 2.4% corresponds to a low commission error of 0.82% for tree i. However, in Beland`s method, there are many instances of commission errors in separated green points in trunk and branches. Comparison of the two methods indicates that much more non-photosynthetic points in Beland`s method are incorrectly classified as photosynthetic components (Figure 3.9 and Figure 3.10 c). Figure 3.12 shows that OIT is in range of 75-92 for the study area.

In this study, the data was collected in the summer and fall seasons in August and October for comparison of methods and it is a single time observation. Hence, there may be temporal variation in different months during growing season. The application of the proposed algorithm in different months will be helpful for the further development of this method. This method was applied successfully in the study plot in a boreal forest for broad leaf trees, to separate leaf from wood components. Further work is needed to explore the response of other broad leaf species or needle leaf tree species.

3.5 Conclusion

The LiDAR intensity parameter which is provided by terrestrial LiDAR can be used as an effective parameter for separation of wood and foliage in PCD. To carry out this task, the effect of propagation and absorption of the laser beam has to be studied comprehensively and distinguished. The laser intensity related to *absorption loss* has to be extracted from raw point

intensity provided by LiDAR using the effect of *path loss*. This method separates wood from foliage based on a new intensity scale. The threshold intensity can then be found by fine-tuning the absorption intensity. Based on this method, an algorithm was developed and implemented in MATLAB. The algorithm was run for separation of leaf and wood in PCD of a single tree with very low commission and omission error.

Figures Legends

Figure 3.1 Procedures used to separate photosynthetic of non-photosynthetic material from LiDAR Point Cloud Data (PCD).

Figure 3.2 Schematic of the path loss and the absorption loss. (R) is the distance between the scanner and the hit point.

Figure 3.3 Histogram-based approach for separating leaf from wood from leaf-on and leaf-off TLS point cloud; (a) In the leaf-on season histogram, there are two distinguishable areas, one (L) represents the leaf reflectance and (WL) refers to wood returns categorized as leaves. In the leaf-off season histogram, (W) represents the wood returns while the (LW) area shows leaf returns classified as a wood return (b) To identify the threshold value between the leaf and wood materials in the histogram, the regression value of WL and LW areas must be in balance.

Figure 3.4 Photosynthetic components separated by proposed algorithm representation, using Terrestrial Laser Scanner (TLS) data with different intensity thresholds. Raw point cloud for; (a) a single tree, and photosynthetic components point cloud separated with (b) threshold 250 (c) threshold 200 (d) threshold 90 (e) threshold 80 (f) threshold 70 (g) threshold 50 and (h) threshold 20.

Figure 3.5 Accuracy assessment (commission and omission errors) of the point cloud classification versus intensity threshold for; (a) tree i (b) tree r (c) tree b, at Peace River, EMSS.

Figure 3.6 Results of the separation between wood and foliage based on the Optimum Intensity Threshold (OIT) from the top view; (a) The whole PCD of the tree (black and brown dots) (b) the separated leaf points (green dots) and (c) overlaying the separated leaf points on the whole tree PCD.

Figure 3.7 Results of the separation between wood and foliage based on the Optimum Intensity Threshold (OIT) from a side view; (a) The whole PCD of the branch (black and brown dots) (b)

the separated leaf points (green dots) and (c) overlaying the separated leaf points on the whole branch PCD.

Figure 3.8 Illustration of intensity laser return within the range of (0-1); (a) regression analysis (b) intensity profile.

Figure 3.9 Photosynthetic components separated by Beland`s method (2011), using Terrestrial Laser Scanner (TLS) data with different normalized intensity thresholds; (a) Raw point cloud for a single tree and photosynthetic components point cloud separated with (b) threshold 0.6 (c) threshold 0.5 (d) threshold 0.4 (e) threshold 0.3 (f) threshold 0.25 (g) threshold 0.19 and (h) threshold 0.1.

Figure 3.10 Comparison of Beland`s method and fine-tuning performance for separation leaf and wood; (a) The whole tree PCD (b) separated points based on fine-tuning of absorption intensity with OIT value of 80 (c) Beland`s method on normalized intensity with OIT value of 0.19 (d) Beland`s method on absorption intensity with OIT value of 38.

Figure 3.11 Illustration of absorption intensity for leaf-on and leaf-off seasons for a single tree; (a) regression analysis (b) intensity profile, the intersection of leaf-on and leaf-off curves result in OIT value based on Beland`s method. The blue dashed line shows the OIT value of 38 by Beland`s method and the red dashed line shows the OIT value of 86 by fine-tuning method.

Figure 3.12 The optimal intensity threshold (OIT) for 21 trees in the stand level.

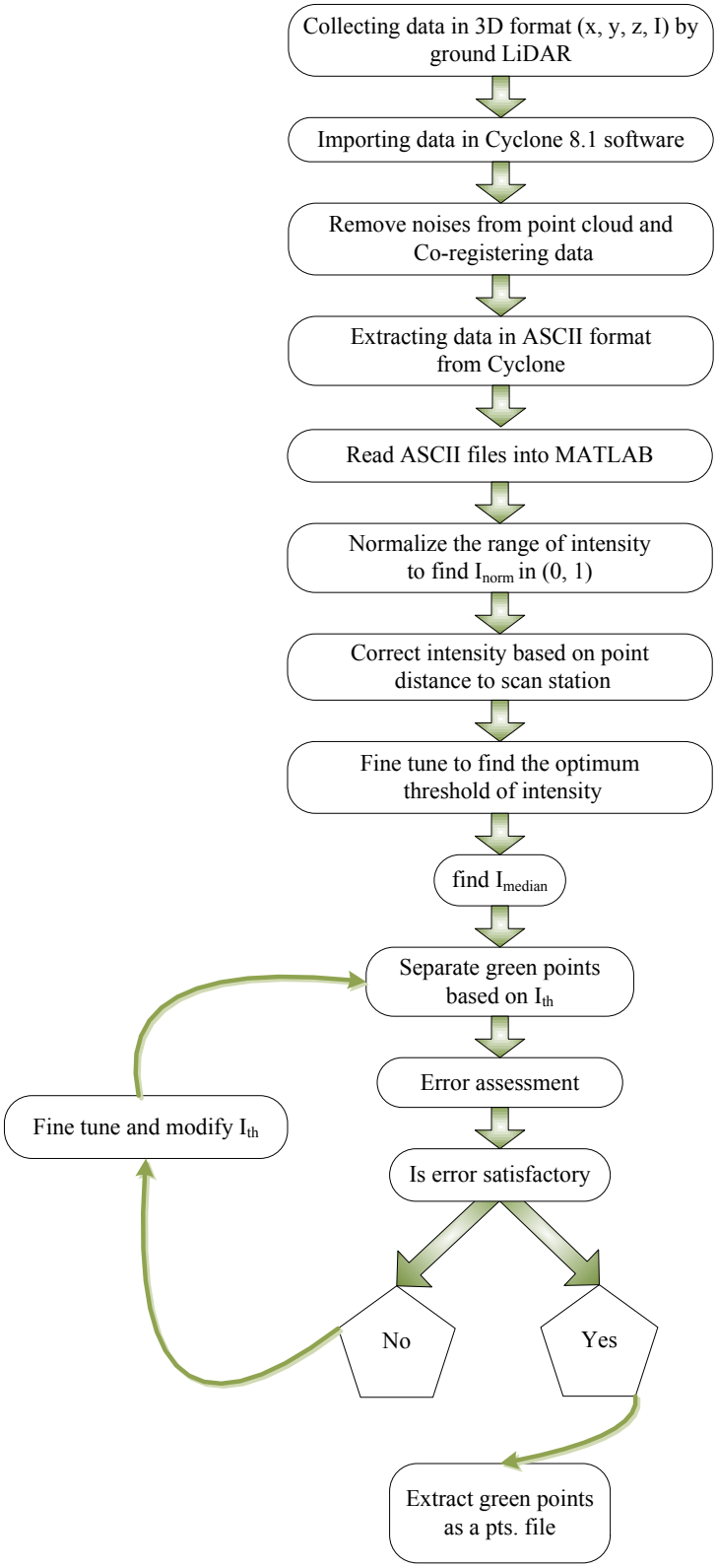

Figure 3.1 Procedures used to separate photosynthetic of non-photosynthetic material from LiDAR Point Cloud Data (PCD).

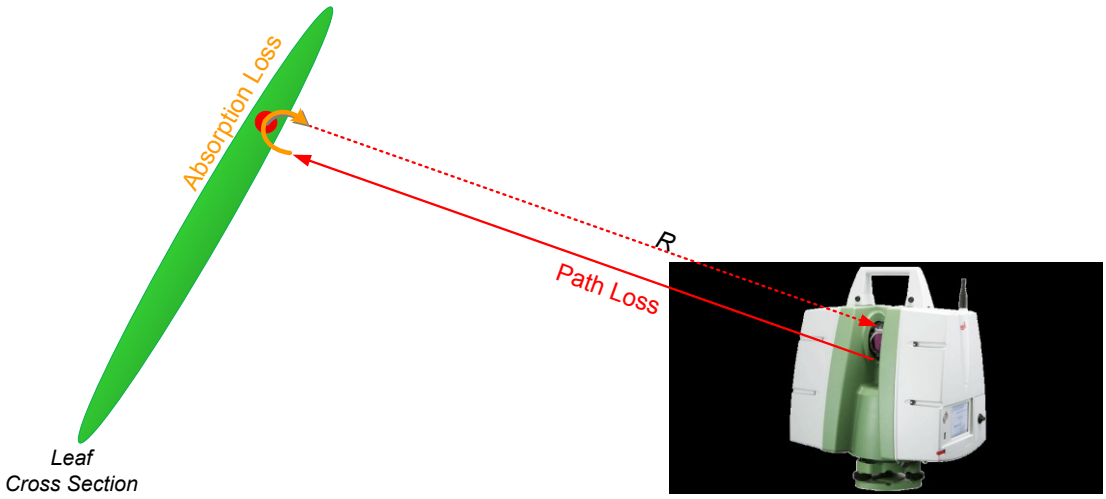

Figure 3.2 Schematic of the path loss and the absorption loss. (R) is the distance between the scanner and the hit point.

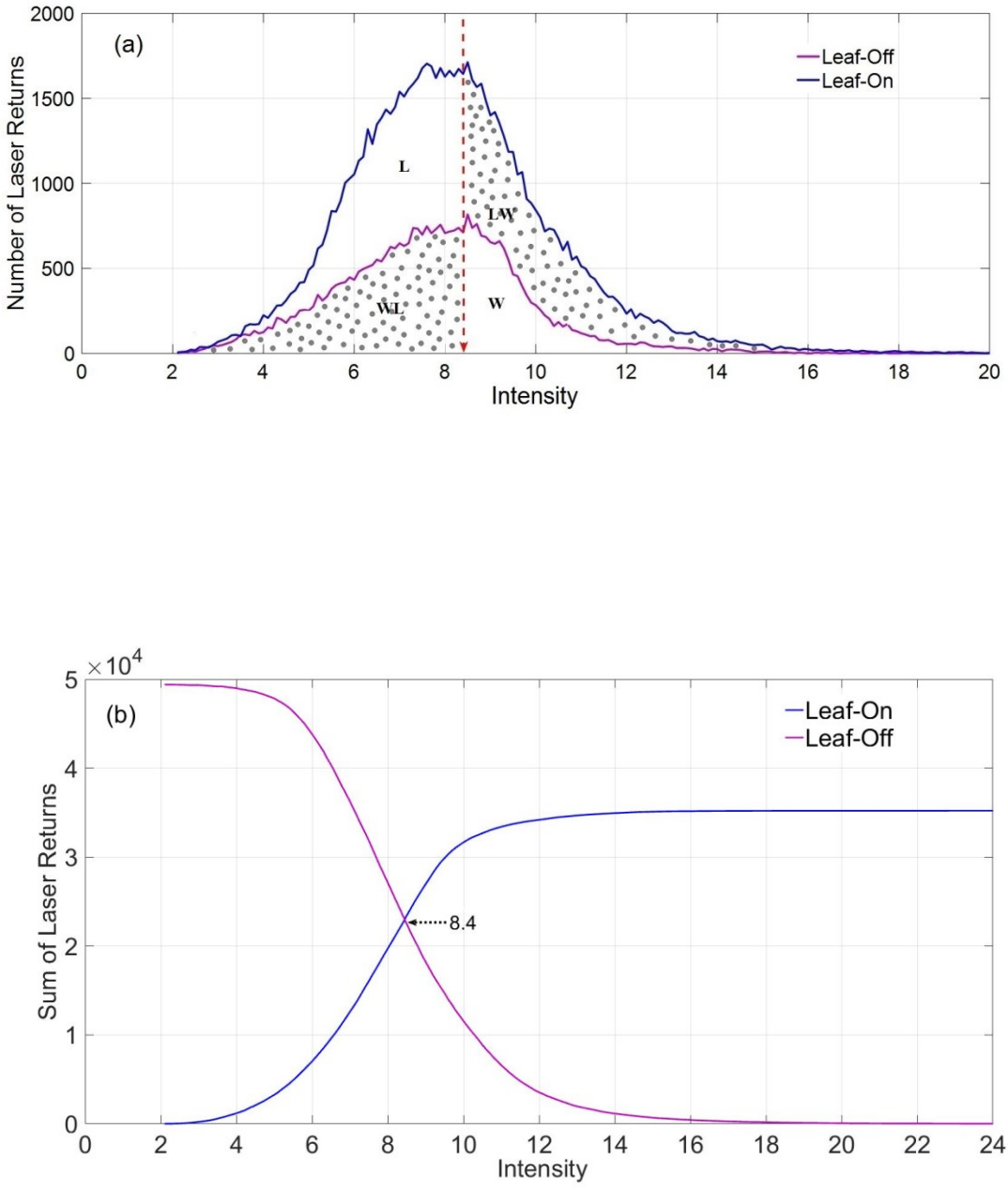

Figure 3.3 Histogram-based approach for separating leaf from wood from leaf-on and leaf-off TLS point cloud; (a) In the leaf-on season histogram, there are two distinguishable areas, one (L) represents the leaf reflectance and (WL) refers to wood returns categorized as leaves. In the leaf-off season histogram, (W) represents the wood returns while the (LW) area shows leaf returns classified as a wood return (b) To identify the threshold value between the leaf and wood materials in the histogram, the regression value of WL and LW areas must be in balance.

Figure 3.4 Photosynthetic components separated by proposed algorithm representation, using Terrestrial Laser Scanner (TLS) data with different intensity thresholds. Raw point cloud for; (a) a single tree, and photosynthetic components point cloud separated with (b) threshold 250 (c) threshold 200 (d) threshold 90 (e) threshold 80 (f) threshold 70 (g) threshold 50 and (h) threshold 20.

(a)

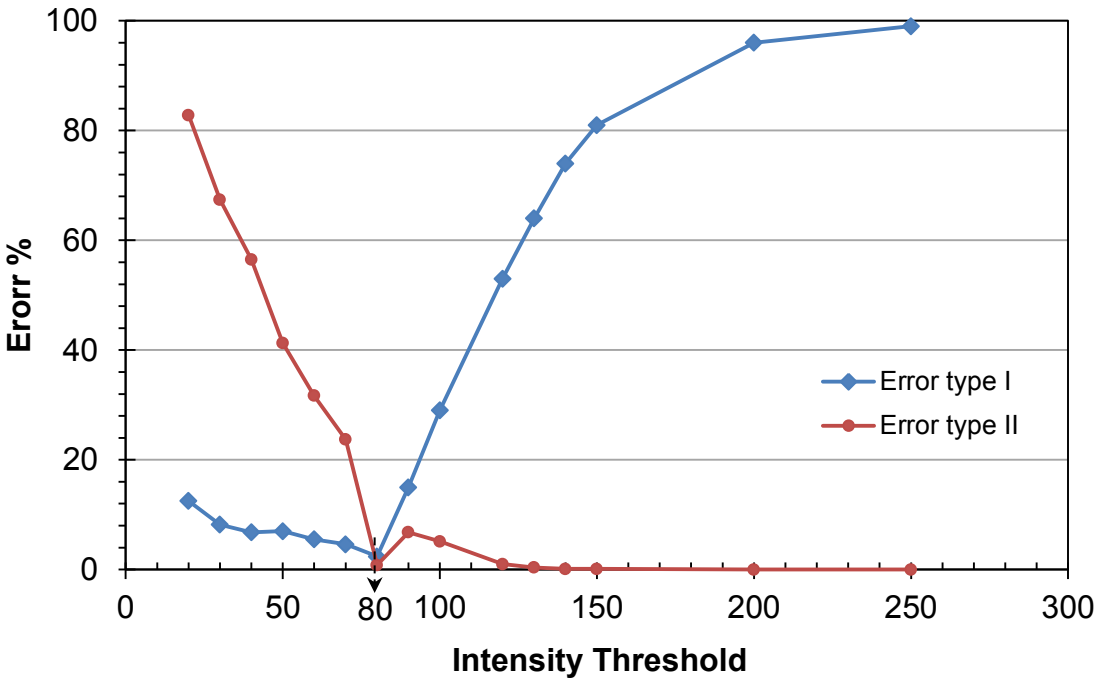

Figure 3.5 Accuracy assessment (commission and omission errors) of the point cloud classification versus intensity threshold for; (a) tree i, at Peace River, EMSS.

(b)

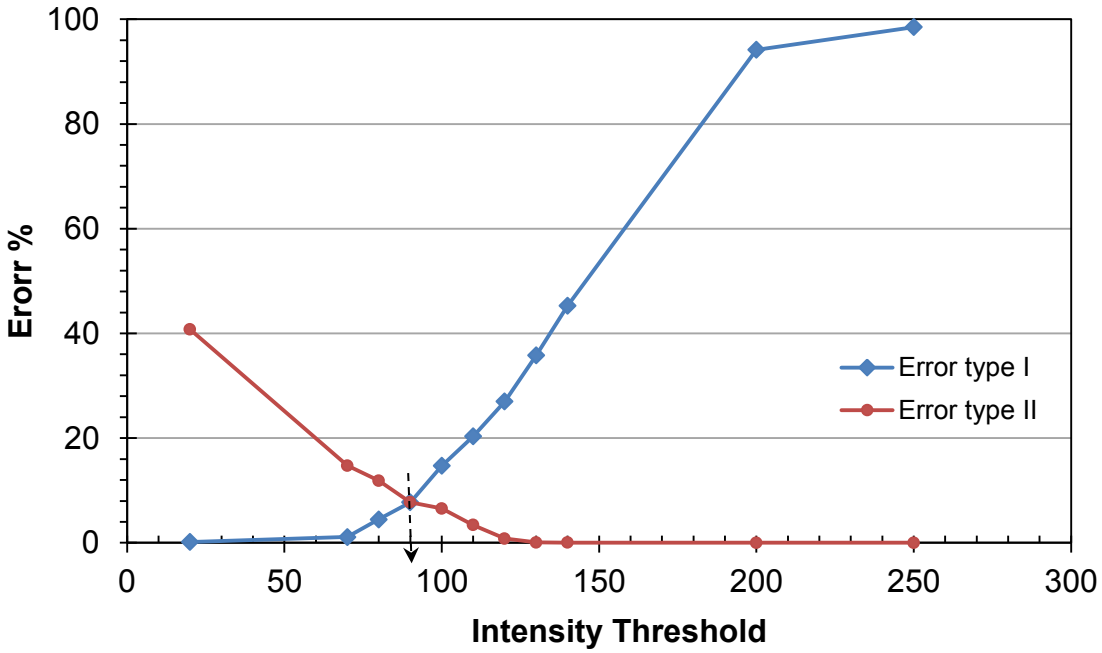

Figure 3.5 Accuracy assessment (commission and omission errors) of the point cloud classification versus intensity threshold for; (b) tree r, at Peace River, EMSS.

(c)

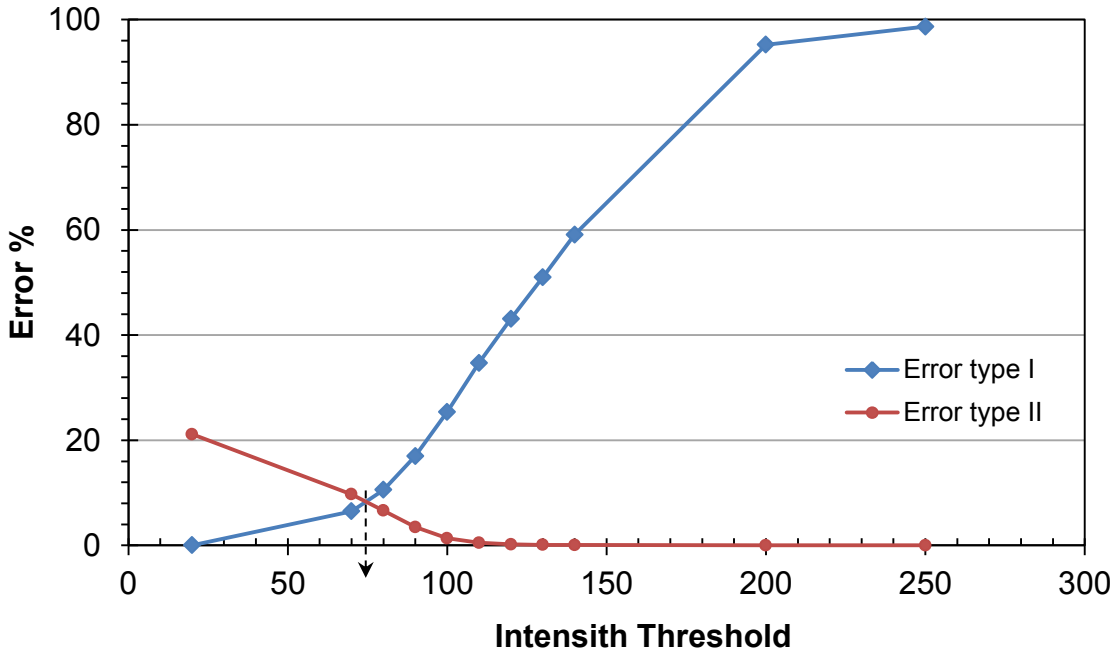

Figure 3.5 Accuracy assessment (commission and omission errors) of the point cloud classification versus intensity threshold for; (c) tree b, at Peace River, EMSS.

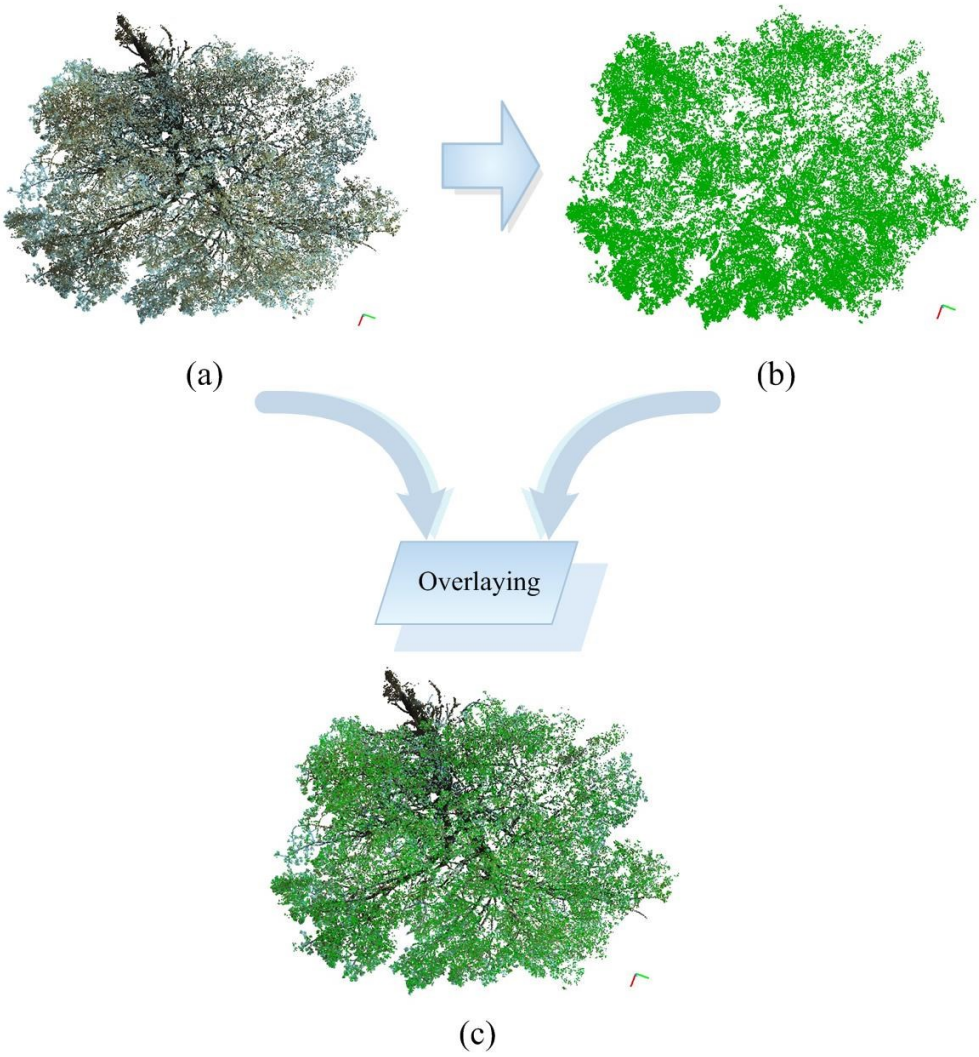

Figure 3.6 Results of the separation between wood and foliage based on the Optimum Intensity Threshold (OIT) from the top view; (a) The whole PCD of the tree (black and brown dots) (b) the separated leaf points (green dots) and (c) overlaying the separated leaf points on the whole tree PCD.

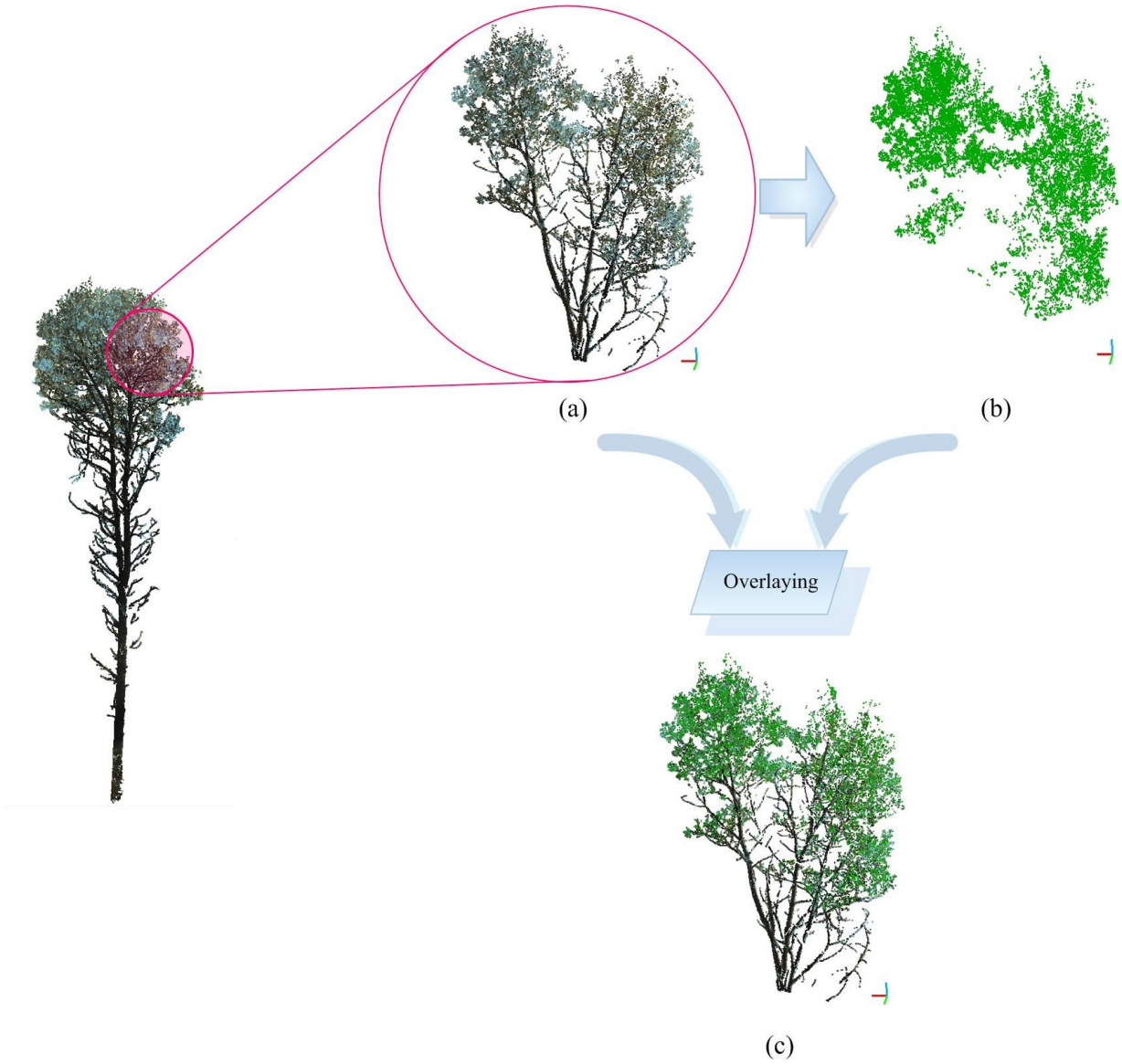

Figure 3.7 Results of the separation between wood and foliage based on the Optimum Intensity Threshold (OIT) from a side view; (a) The whole PCD of the branch (black and brown dots) (b) the separated leaf points (green dots) and (c) overlaying the separated leaf points on the whole branch PCD.

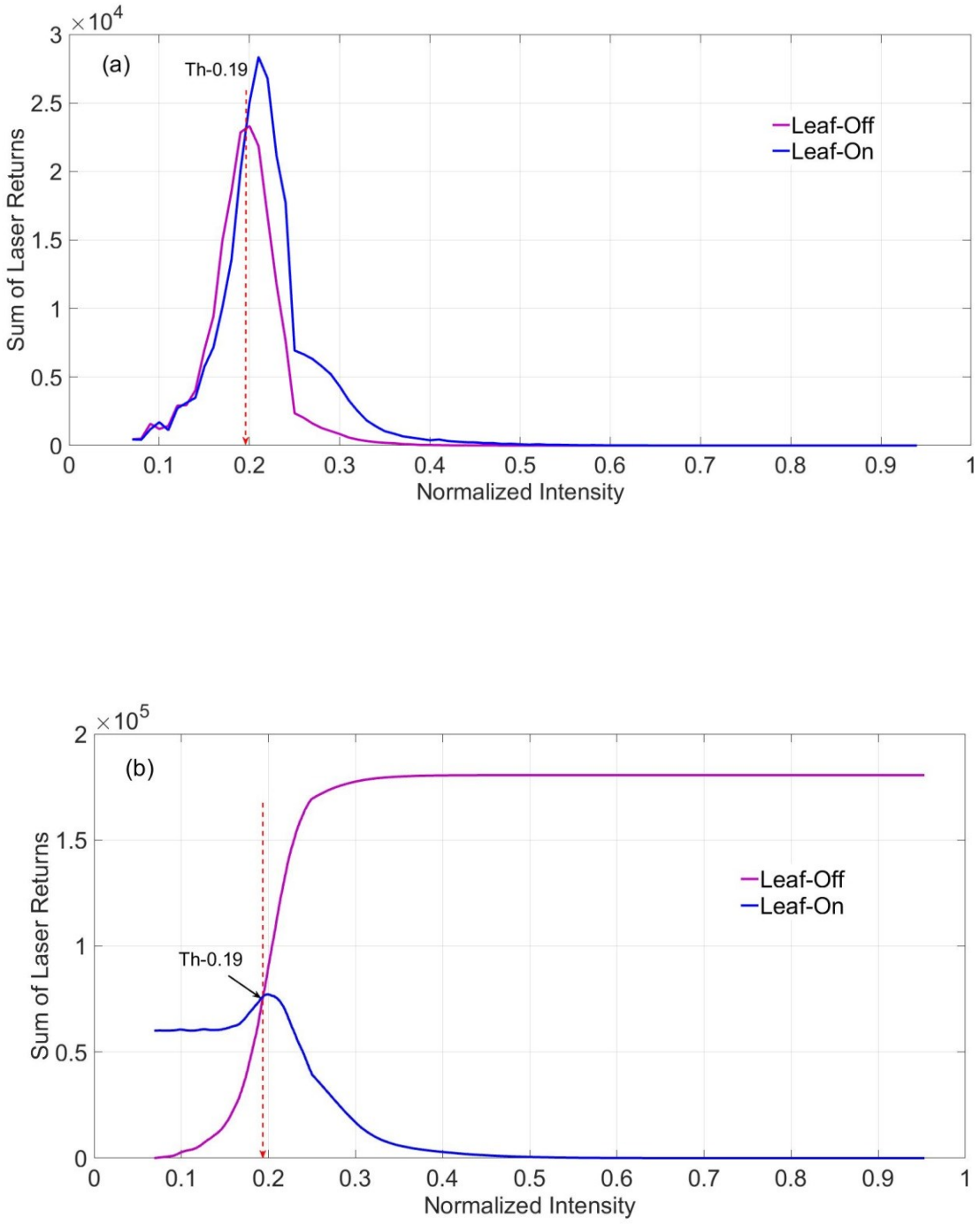

Figure 3.8 Illustration of intensity laser return within the range of (0-1); (a) regression analysis (b) intensity profile.

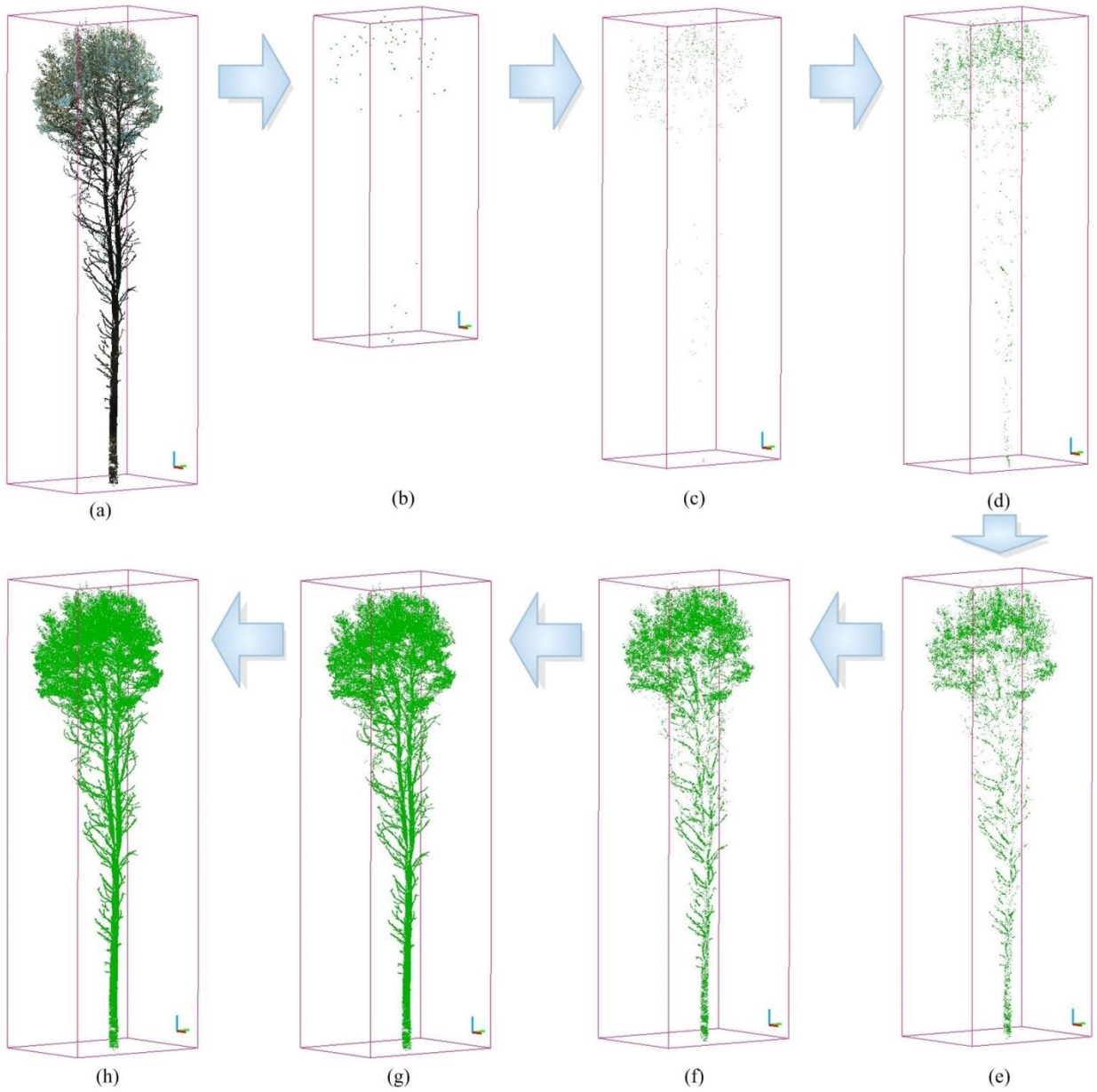

Figure 3.9 Photosynthetic components separated by Beland`s method (2011), using Terrestrial Laser Scanner (TLS) data with different normalized intensity thresholds; (a) Raw point cloud for a single tree and photosynthetic components point cloud separated with (b) threshold 0.6 (c) threshold 0.5 (d) threshold 0.4 (e) threshold 0.3 (f) threshold 0.25 (g) threshold 0.19 and (h) threshold 0.1.

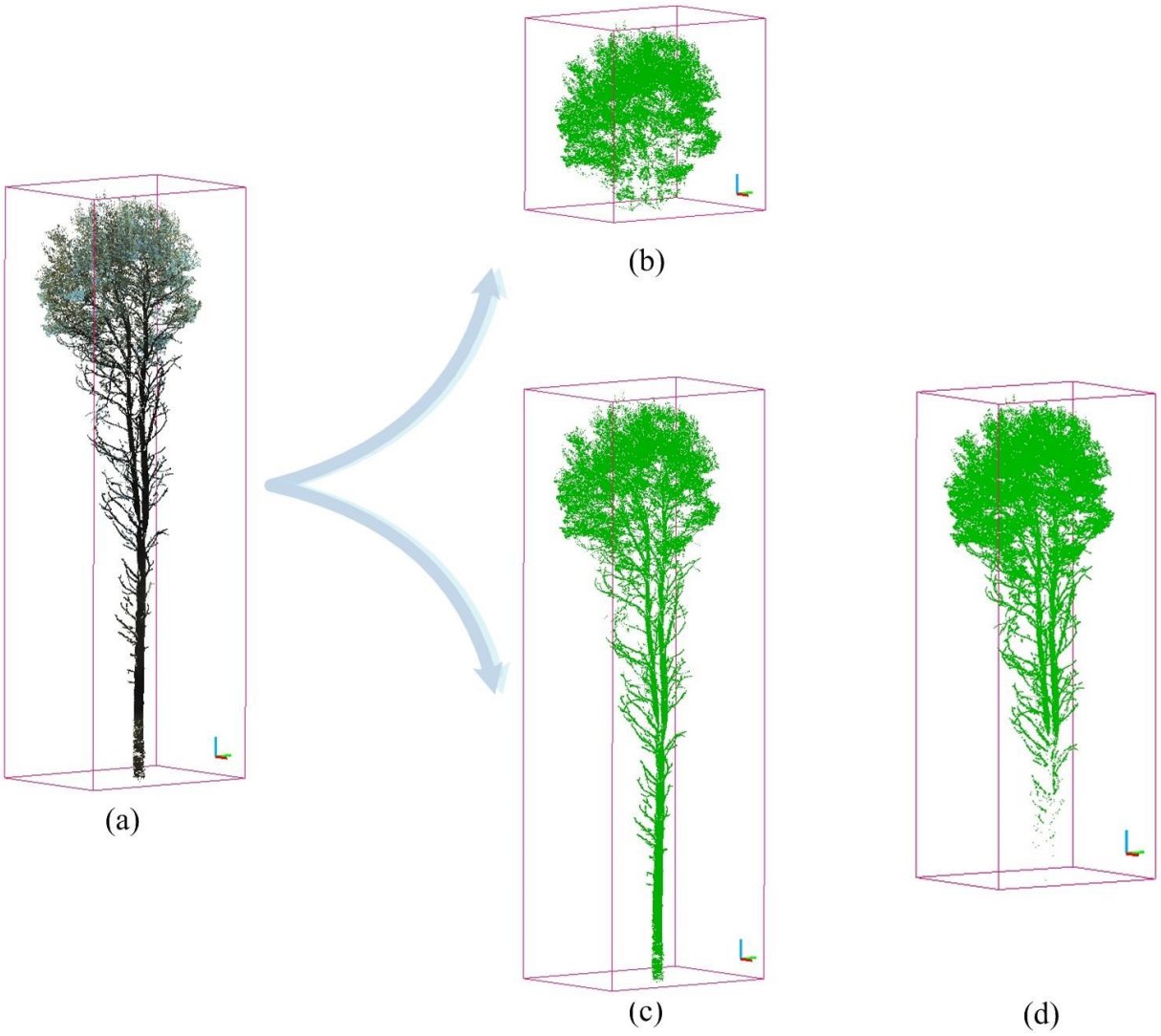

Figure 3.10 Comparison of Beland`s method and fine-tuning performance for separation leaf and wood; (a) The whole tree PCD (b) separated points based on fine-tuning of absorption intensity with OIT value of 80 (c) Beland`s method on normalized intensity with OIT value of 0.19 (d) Beland`s method on absorption intensity with OIT value of 38.

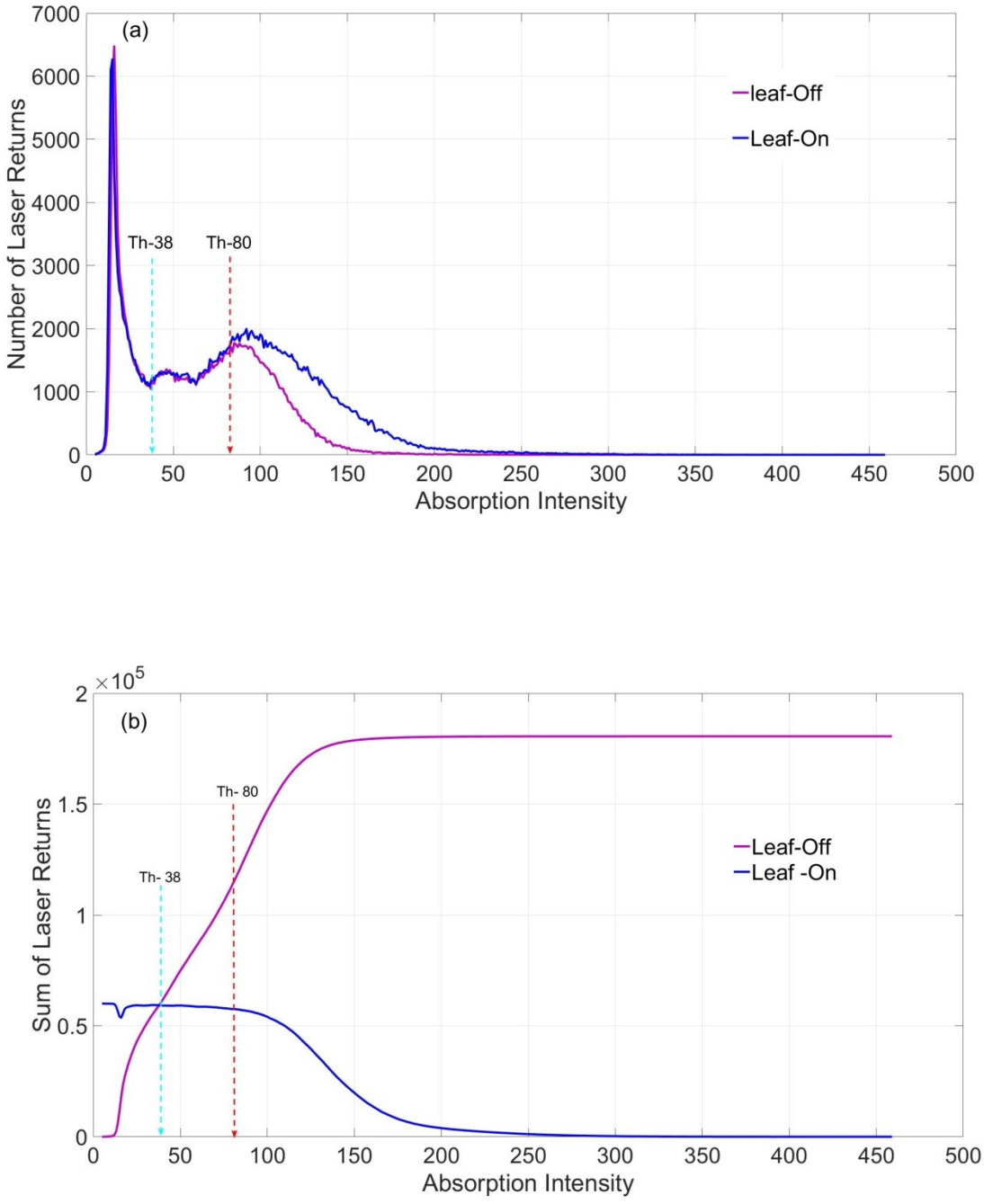

Figure 3.11 Illustration of absorption intensity for leaf-on and leaf-off seasons for a single tree; (a) regression analysis (b) intensity profile, the intersection of leaf-on and leaf-off curves result in OIT value based on Beland`s method. The blue dashed line shows the OIT value of 38 by Beland`s method and the red dashed line shows the OIT value of 86 by fine-tuning method.

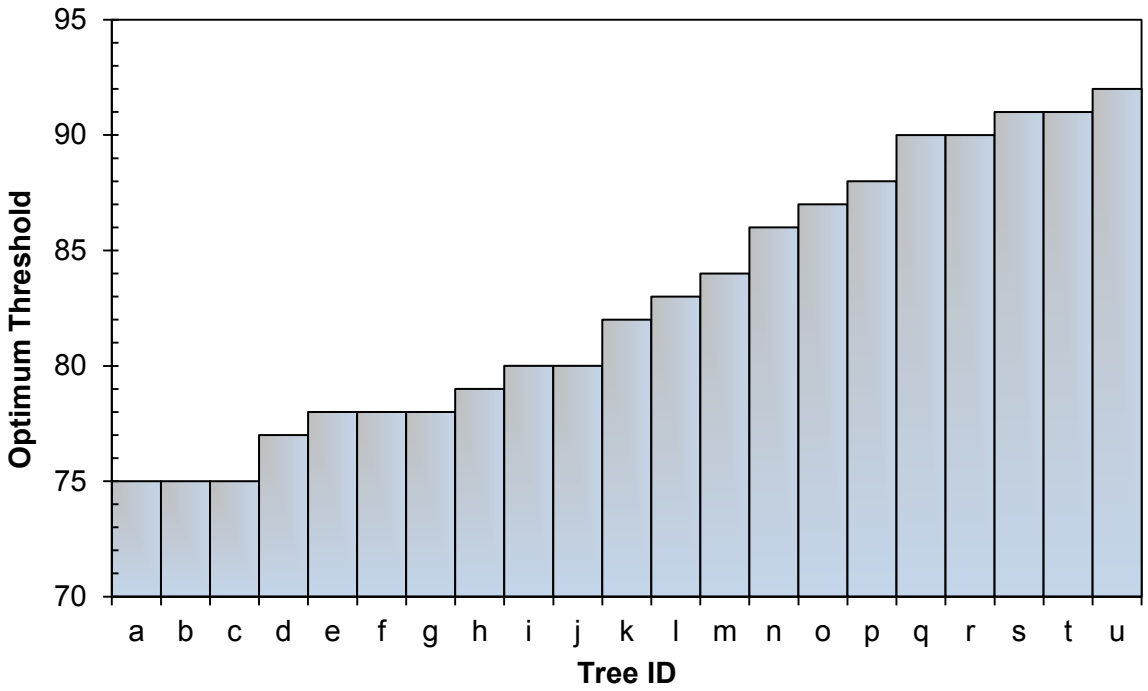

Figure 3.12 The optimal intensity threshold (OIT) for 21 trees in the stand level.

References

Askne, J.I.H., Soja, M.J., and Ulander, L.M.H. 2017. Biomass estimation in a boreal forest from TanDEM-X data, lidar DTM, and the interferometric water cloud model. *Remote Sensing of Environment*, 196, 265-278.

Beland, M., Baldocchi, D.D., Widlowski, J.L., Fournier, R.A., and Verstraete, M.M. 2014. On seeing the wood from the leaves and the role of voxel size in determining leaf area distribution of forests with terrestrial Lidar. *Agricultural and Forest Meteorology*, 184, 82-97.

Beland, M., Widlowski, J.L., Fournier, R.A., Côté, J. F., and Verstraete, M.M. 2011. Estimating leaf area distribution in savanna trees from terrestrial LiDAR measurements. *Agricultural and Forest Meteorology*, 151, 1252-1266.

BreÂda, N.J.J. 2003. Ground-based measurements of leaf area index: a review of methods, instruments and current controversies. *Journal of Experimental Botany*, 54 (392), 2403-2417.

Chen, J. M., Rich, P. M., Gower, S. T., Norman, J. M., and Plummer, S. 1997. Leaf area index of boreal forests: Theory, techniques, and measurements. *Geophysical Research Atmospheres*, 102 (D24), 29429-29443.

Clawges, R., Vierling, L., Calhoon, M., and Toomey, M. 2007. Use of a ground based scanning lidar for estimation of biophysical properties of western larch (*Larix occidentalis*). *International Journal of Remote Sensing*, 28 (19), 4331-4344.

Danson, F.M., and Curran, P.J. 1993. Factors affecting the remotely sensed response of coniferous forest plantations. *Remote Sensing of Environment*, 43, 55-65.

Danson, F.M., Hetherington, D., Morsdorf, F., Koetz, B., and Allgower, B. 2007. Forest canopy gap fraction from terrestrial laser scanning. *IEEE Geoscience and Remote Sensing Letter*, 4, 157-160.

Donoghue, D.N.M., Watt, P.J., Cox, N.J., and Wilson, J. 2007. Remote sensing of species mixtures in conifer plantations using LiDAR height and intensity data. *Remote Sensing of Environment*, 110, 509-522.

Drake, J.B., Dubayah, R.O., Clark, D.B., Knox, R.G., Blair, J.B., Hofton, M.A., and Prince, S. 2002. Estimation of tropical forest structural characteristics using large footprint lidar. *Remote Sensing of Environment*, 79 (2), 305-319.

Ducey, M.J., Astrup, R., Seifert, S., Pretzsch, H., Larson, B.C., and Coates, K.D. 2013. Comparison of forest attributes derived from two terrestrial Lidar systems. *Photogrammetric Engineering and Remote Sensing*, 79 (3):245-257.

Eitel, J.U.H., Long, D.S., Gessler, P.E., Hunt, E.R., and Brown, D.J. 2009. Sensitivity of ground-based remote sensing estimates of wheat chlorophyll content to variation in soil reflectance. *Soil Science Society of America Journal*, 73, 1715-1723.

Eitel, J.U.H., Vierling, L.A., and Long, D.S. 2010. Simultaneous measurements of plant structure and chlorophyll content in broadleaf saplings with a terrestrial laser scanner. Remote Sensing of Environment, 114, 2229-2237.

Eitel, J.U.H., Magney, T.S., Vierling, L. A., and Dittmar, G. 2014. Assessment of crop foliar nitrogen using a novel dual-wavelength laser system and implications for conducting laser-based plant physiology. *ISPRS Journal of Photogrammetry and Remote Sensing*, 97, 229-240.

Fournier, R.A., Mailly, D., Walter, J.M.N. and Soudani, K. 2003. Indirect measurement of forest canopy structure from in situ optical sensors. *Remote sensing of forest environments,* 77-113, Springer US.

Franklin, J. 1986. Thematic mapper analysis of coniferous forest structure and composition. *International Journal of Remote Sensing*, 7, 1287-1301.

Gao, B. 1996. NDWI- A normalized difference water index for remote sensing of vegetation liquid water from space. *Remote Sensing of Environment*, 58 (3), 257-266.

Gemmell, F.M. 1995. Effects of forest cover, terrain and scale on timber volume estimation with thematic mapper data in a Rocky Mountain site. *Remote Sensing of Environment*, 51, 291-305.

Greaves, H.E., Vierling, L.A., Eitel, J.U.H., Boelman, N.T., Magney, T.S., Prager, C.M., and Griffin, K.L. 2015. Estimating aboveground biomass and leaf area of low-stature arctic shrubs with terrestrial lidar. *Remote Sensing of Environment*, 164, 26-35.

Hauglin, M., Astrup, R., Gobakken, T., and Næsset, E. 2013. Estimating single-tree branch biomass of Norway spruce with terrestrial laser scanning using voxel-based and crown dimension features. *Scandinavian Journal of Forest Research*, 28 (5), 1-14.

Hebert, M., and Vandapel, N. 2003. Terrain classification techniques from ladar data for autonomous navigation. *Robotics Institute*, 411.

Holopainen, M., Vastaranta, M., Kankare, V., Räty, M., Vaaja, M., Liang, X., Yu, X., Hyyppä, J., Hyyppä, H., Viitala, R. and Kaasalainen, S., 2011. Biomass estimation of individual trees using stem and crown diameter TLS measurements. *ISPRS-International Archives of the Photogrammetry, Remote Sensing and Spatial Information Sciences*, 38(12), 91-95.

Hopkinson, C., Lovell, J., Chasmer, L., Jupp, D., Kljun, N. and van Gorsel, E. 2013. Integrating terrestrial and airborne lidar to calibrate a 3D canopy model of effective leaf area index. *Remote Sensing of Environment*, 136, 301-314.

Horaud, R., Hansard, M., Evangelidis, G. and Ménier, C. 2016. An overview of depth cameras and range scanners based on time-of-flight technologies. *Machine Vision and Applications*, 27(7), 1005-1020.

Hosoi, F., and Omasa, K. 2006. Voxel-based 3-D modeling of individual trees for estimating leaf area density using high-resolution portable scanning lidar. *IEEE transactions on geoscience and remote sensing*, 44(12), 3610-3618.

Hosoi, F., and Omasa, K. 2007. Factors contributing to accuracy in the estimation of the woody canopy leaf area density profile using 3D portable lidar imaging. *Journal of Experimental Botany*, 58(12), 3463-3473.

Hosoi, F., and Omasa, K. 2009. Estimating vertical plant area density profile and growth parameters of a wheat canopy at different growth stages using three-dimensional portable lidar imaging. *ISPRS Journal of Photogrammetry and Remote Sensing*, 64(2), 151-158.

Hosoi, F., Nakai, Y., and Omasa, K. 2010. Estimation and error analysis of woody canopy leaf area density profiles using 3-D airborne and ground-based scanning lidar remote-sensing techniques. *IEEE Transactions on Geoscience and Remote Sensing*, 48(5), 2215-2223.

Huang, P., and Pretzsch, H. 2010. Using terrestrial laser scanner for estimating leaf areas of individual trees in a conifer forest. *Trees*, 24 (4), 609-619.

Jupp, D.L.B., Culvenor, D.S., Lovell, J.L., Newnham, G.J., Strahler, A.H., and Woodcock, C.E. 2009. Estimating forest LAI profiles and structural parameters using a ground based laser called 'Echidna (R)'. *Tree Physiology*, 29 (2), 171-181.

Kato, A., Moskal, L.M., Schiess, P., Swanson, M.E., Calhoun, D., and Stuetzle, W. 2009. Capturing tree crown formation through implicit surface reconstruction using airborne lidar data. *Remote Sensing of Environment*, 113 (6), 1148-1162.

Kelbe, D., Romanczyk, P., van Aardt, J. and Cawse-Nicholson, K. 2013. Reconstruction of 3D tree stem models from low-cost terrestrial laser scanner data. *SPIE Defense, Security, and Sensing*, 873106-873106.

Koetz, B., Morsdorf, F., Sun, G., Ranson, K.J., Itten, K., and Allgower, B. 2006. Inversion of a lidar waveform model for forest biophysical parameter estimation. *IEEE Geoscience and Remote Sensing Letter,* 3 (1), 49-53.

Lalonde, J.F., Vandapel, N., Huber, D. F., and Hebert, M. 2006. Natural terrain classification using three-dimensional lidar data for ground robot mobility. *Journal of Field Robotics*, 23(10), 839-861.

Lefsky, M., and McHale, M. 2008. Volume estimates of trees with complex architecture from terrestrial laser scanning. *Journal of Applied Remote Sensing*, 2(1), 023521-023521.

Li, Z., Douglas, E., Strahler, A., Schaaf, C., Yang, X., Wang, Z., Yao, T., Zhao, F., Saenz, E. J., Paynter, I., and Woodcock C.E. 2013. Separating leaves from trunks and branches with Dual_Wavelenght Terrestrial Lidar Scanning. *In Geoscience and Remote Sensing Symposium (IGARSS) IEEE,* 3383- 3386.

Liang, X.L., Litkey, P., Hyyppa, J., Kaartinen, H., Vastaranta, M., and Holopainen, M. 2012. Automatic stem mapping using single-scan terrestrial laser scanning. *IEEE Transactions on Geoscience and Remote Sensing*, 50(2), 661-670.

Lin, Y., and Herold, M. 2016. Tree species classification based on explicit tree structure feature parameters derived from static terrestrial laser scanning data. *Agricultural and Forest Meteorology*, 216, 105-114.

Lin, Y., and West, G. 2016. Retrieval of effective leaf area index (LAIe) and leaf area density (LAD) profile at individual tree level using high density multi-return airborne LiDAR. *International Journal of Applied Earth Observation and Geoinformation*, 50, 150-158.

Liu, Z., and Jin, G. 2017. Importance of woody materials for seasonal variation in leaf area index from optical methods in a deciduous needle leaf forest. *Scandinavian Journal of Forest Research*, 1-11.

Loudermilk, E.L., Hiers, J.K., O'Brien, J.J., Mitchell, R.J., Singhania, A., Fernandez, J.C., and Slatton, K.C. 2009. Ground-based LIDAR: a novel approach to quantify fine scale fuel bed characteristics. *International Journal Wildland Fire*, 18 (6), 676-685.

Lovell, J.L., Jupp, D.L.B., Culvenor, D.S., and Coops, N.C. 2003. Using airborne and ground-based ranging lidar to measure canopy structure in Australian forests. *Canadian Journal of Remote Sensing*, 29, 607-622.

Ma, L., Zheng, G., Eitel, J. U. H., Moskal, M., He, W., and Huang, H. 2016. Improved Salient Feature-Based Approach for Automatically Separating Photosynthetic and Nonphotosynthetic Components Within Terrestrial Lidar Point Cloud Data of Forest Canopies. *IEEE Transaction on Geoscience and Remote Sensing*, 54(2), 679-696.

Ma, L., Zheng, G., Eitel, J.U., Magney, T.S. and Moskal, L.M. 2016a. Determining woody-to-total area ratio using terrestrial laser scanning (TLS). *Agricultural and Forest Meteorology*, 228, 217-228.

Ma, L., Zheng, G., Eitel, J.U., Moskal, L.M., He, W. and Huang, H. 2016b. Improved salient feature-based approach for automatically separating photosynthetic and nonphotosynthetic components within terrestrial LiDAR point cloud data of forest canopies. *IEEE Transactions on Geoscience and Remote Sensing*, 54(2), 679-696.

Maas, H-G., Bienert, A., Scheller, S., and Keane, E. 2008. Automatic forest inventory parameter determination from terrestrial laser scanner data. *International Journal of Remote Sensing*, 29(5), 1579-1593.

Margolis, H.A., Nelson, R.F., Montesano, P.M., Beaudoin, A., Sun, G., Andersen, H.E. and Wulder, M.A. 2015. Combining satellite lidar, airborne lidar, and ground plots to estimate the amount and distribution of aboveground biomass in the boreal forest of North America. *Canadian Journal of Forest Research*, 45(7), 838-855.

Martínez, B., García-Haro, F.J. and Camacho-de Coca, F. 2009. Derivation of high-resolution leaf area index maps in support of validation activities: Application to the cropland Barrax site. *Agricultural and forest meteorology*, 149(1), 130-145.

MATLAB R2016b, the MathWorks lnc., Natick, Massachusetts, United States, 2016.

Monsi, M., and Saeki, T. 2005. On the factor light in plant communities and its importance for matter production. *Annals of Botany*, 95 (3), 549-567.

Moorthy, I., Miller, J.R., Hu, B.X., Chen, J., and Li, Q.M. 2008. Retrieving crown leaf area index from an individual tree using ground-based LiDAR data. *Canadian Journal of Remote Sensing*, 34 (3), 320-332.

Morsdorf, F., Kotz, B., Meier, E., Itten, K., Allgower, B., 2006. Estimation of LAI and fractional cover from small footprint airborne laser scanning data based on gap fraction. *Remote Sensing of Environment*, 104, 50-61.

Olivas, P.C., Oberbauer, S.F., Clark, D.B., Clark, D.A., Ryan, M.G., O'Brien, J.J. and Ordonez, H. 2013. Comparison of direct and indirect methods for assessing leaf area index across a tropical rain forest landscape. *Agricultural and forest meteorology*, 177, 110-116.

Olsoy, P.J., Glenn, N.F., and Clark, P.E. 2014b. Estimating sagebrush biomass using terrestrial laser scanning (TLS). *Rangeland Ecology and Management*, 67(2), 224-228.

Omasa, K., Hosoi, F., and Konishi, A. 2007. 3D lidar imaging for detecting and understanding plant responses and canopy structure. *Journal of Experimental Botany*, 58 (4), 881-898.

Parker, G.G. 1995. Structure and microclimate of forest canopies. In: Lowman, M., Madkarni, N. (Eds.), Forest Canopies. *Academic Press, California, USA*, 73-106.

Pfennigbauer, M., and A. Ullrich, 2010. Improving quality of laser scanning data acquisition through calibrated amplitude and pulse deviation measurement. *Proceedings of SPIE*, 7684.

Pozar, D.M., 2006. Microwave engineering. *Publishing House of Electronics Industry*.

Pueschel, P., Newnham, G., and Hill, J. 2014. Retrieval of Gap Fraction and Effective Plant Area Index from Phase-Shift Terrestrial Laser Scans. *Remote Sensing*, 6, 2601-2627.

Radtke, P.J., and Bolstad, P.V. 2001. Laser point-quadrat sampling for estimating foliage-height profiles in broad-leaved forests. *Canadian Journal of Forest Research*, 31 (3), 410-418.

Schilling, A., Schmidt, A., and Maas, H.G. 2012. Tree topology representation from TLS point clouds using depth-first search in voxel space. *Photogrammetric Engineering and Remote Sensing*, 78(4), 383-392.

Scholes, R.J., Frost, P.G.H., and Tian, Y. 2004. Canopy structure in savannas along a moisture gradient on Kalahari sands. *Global Change Biology*, 10, 292-302.

Sellers, P.J., Dickinson, R.E., Randall, D.A., Betts, A.K., Hall, F.G., Berry, J.A., Collatz, G.J., Denning, A.S., Mooney, H.A., Nobre, C.A. and Sato, N. 1997. Modeling the exchanges of energy, water, and carbon between continents and the atmosphere. *Science*, 275(5299), pp.502-509.

Serifoglu, C., Gungor, O., and Yilmaz V. 2016. Performance evaluation of different ground filtering algorithms for UAV-based point clouds. *The International Archives of the Photogrammetry, Remote Sensing and Spatial Information Sciences*, 41.

Simonse, M., Aschoff, T., Spiecker, H. and Thies, M. 2003. Automatic determination of forest inventory parameters using terrestrial laser scanning. *In Proceedings of the scandlaser scientific workshop on airborne laser scanning of forests,* 252-258.

Sims, D.A., and Gamon, J.A. 2003. Estimation of vegetation water content and photosynthetic tissue area from spectral reflectance: a comparison of indices based on liquid water and chlorophyll absorption features. *Remote Sensing of Environment*, 84 (4), 526-537.

Song, Y., Maki, M., Imanishi, J. and Morimoto, Y. 2011. Voxel-based estimation of plant area density from airborne laser scanner data. *In Proceedings of the ISPRS Workshop Laser Scanning, Calgary, Canada,* 38, (5/W12), 209-212.

Stoker, J. 2009. Visualization of multiple-return lidar data: using voxels. *Photogrammetric Engineering and Remote Sensing*, 75 (2), 109-112.

Strahler, A.H., Jupp, D.L., Woodcock, C.E., Schaaf, C.B., Yao, T., Zhao, F., Yang, X., Lovell, J., Culvenor, D., Newnham, G. and Ni-Miester, W. 2008. Retrieval of forest structural parameters using a ground-based lidar instrument (Echidna®). *Canadian Journal of Remote Sensing*, 34(S2), 426-440.

Takeda, T., Oguma, H., Sano, T., Yone, Y., and Fujinuma, Y. 2008. Estimating the plant area density of a Japanese larch (Larix kaempferi Sarg.) plantation using a ground-based laser scanner. *Agriculture and Forest Meteorology*, 148 (3), 428-438.

Thoren, D., and Schmidhalter, U. 2009. Nitrogen status and biomass determination of oilseed rape by laser-induced chlorophyll fluorescence. *European Journal of Agronomy*, 30, 238-242.

Vandapel, N., Huber, D.F., Kapuria, A., and Hebert, M. 2004.Natural terrain classification using 3-D lidar data. *in Proc. IEEE ICRA, New York, NY, USA*, 1–5, 5117-5122.

Warren Wilson, J. 1959. Analysis of the spatial distribution of foliage by two dimensional point quadrats. *New Phytologist*, 58 (1), 92-99.

Warren Wilson, J. 1960. Inclined point quadrats. *New Phytologist*, 59 (1), 1-8.

Warren Wilson, J., 1963. Errors resulting from thickness of point quadrats. *Australian Journal of Botany*, 11, 178-188.

Watt, P.J., and Donoghue, D.N.M. 2005. Measuring forest structure with terrestrial laser scanning. *International Journal of Remote Sensing*, 26 (7), 1437-1446.

Whitford, K., Colquhoun, I., Lang, A., and Harper, B. 1995. Measuring leaf area index in a sparse eucalypt forest: A comparison of estimates from direct measurement, hemispherical photography, sunlight transmittance and allometric regression. *Agricultural Forest Meteorology*, 74(3), 237–249.

Wu, J.Y., Cawse-Nicholson, K., and Aardt, J.V. 2013. 3D Tree reconstruction from simulated small footprint waveform lidar. *Photogrammetric Engineering and Remote Sensing*, 79 (12), 1147-1157.

Zhang, C. 2003. A progressive morphological filter for removing nonground measurements from airborne LIDAR data. *IEEE Transactions on Geoscience and Remote Sensing*, 41(4), 872-882.

Zhang, K., and Whitman, D. 2005. Comparison of three algorithms for filtering airborne LiDAR data. *Photogrammetric Engineering and Remote Sensing*, 71 (3), 313–324.

Zhao, F., Yang, X., Schull, M.A., Roman-Colon, M., Yao, T., and Wang, Z. 2011. Measuring effective leaf area index foliage profile, and stand height in New England forest stands using a full-waveform ground-based lidar. *Remote Sensing of Environment*, 115, 2954-2964.

Zheng, G., and Moskal, L.M. 2012. Spatial variability of terrestrial laser scanning based leaf area index. *International Journal of Applied Earth Observation and Geoinformation*, 19, 226-237.

Zheng, G., Ma, L., He, W., Eitel, J.U., Moskal, L.M. and Zhang, Z. 2016. Assessing the contribution of woody materials to forest angular gap fraction and effective leaf area index using terrestrial laser scanning data. *IEEE Transactions on Geoscience and Remote Sensing*, 54(3), 1475-1487.

Zheng, G., Moskal, L.M., and Kim, S.H. 2013. Retrieval of effective leaf area index in heterogeneous forest with terrestrial laser scanning. *IEEE Geoscience and Remote Sensing*, 51, 777-786.

CHAPTER 4

Calculation of Leaf Area Index in a Canadian Boreal Forest Using Ground-Based LiDAR

4.1 Introduction

Forests are important natural resources due to their benefits toward the economy and ecosystem services including climate control, wildlife protection, and pollution reduction (Law et al. 2001; Barr et al. 2004). Hence, forest assessment is of ultimate significance for resource management and sustainable development. Research into the 3D canopy structure is the key to the accurate quantitative assessment of forests (Martínez et al. 2009). Canopy structure is the vertical and horizontal distribution of all the foliage elements with a variety of shape, size, and orientation of different species groups above-ground in a forest stand (Norman and Campbell, 1989; McIntosh et al. 2009).

The distribution, orientation, and area of leaves are the most important biophysical properties of a canopy which determine the interaction of a given sunbeam with plant chlorophyll and hence the amount of intercepted light at a canopy (Barclay, 2001). Hence, a single assessment parameter is needed to represent the leaf area and configuration in order to quantify the interaction of plant with light. Leaf Area Index (LAI) is an important forest parameter which is based on the total effective single sided area (with the unit of m^2) of live photosynthetic leaf material in a tree per horizontal unit ground area (m^2), considering the overlap, shadowing and clumping effect among leaves (Watson, 1947; Chen and Black, 1992; Breda, 2003; Asner et al. 2003; Weiss et al. 2004; Schleppi et al. 2007; Nasahara et al. 2008; Hosoi and Omasa, 2009). LAI is dimensionless and it can be calculated for a single tree or the whole forest. In addition, LAI is an accurate indicator of forest dynamics and ecological processes such as balance of the global carbon exchange, energy cycle in photosynthesis, evapotranspiration mechanisms, precipitation interception, and water/nutrient cycling (Chen et al. 2005; Dufrene et al. 2005; Dietz et al. 2006; Duchemin et al. 2006; Cleugh et al. 2007; Zheng et al. 2007; Gobron, 2008 and Duursma et al. 2009; Yue et al. 2013; Sainte-Marie et al. 2014).

The current state of the art presents various direct and indirect techniques for calculation of LAI. Direct invasive methods include manual clipping, counting and measuring the size of leaves which is time-consuming and labor-intensive even for a single tree (Norman and Campbell, 1989; Hosoi and Omasa, 2009; Olsoy et al. 2014). Due to the huge quantity of vegetation material in the forests, direct measurement becomes impractical in large scale (Béland et al. 2011). Thus, as a preferred alternative, non-invasive indirect and remote sensing methods have been developed (Hosoi and Omasa, 2009; Olsoy et al. 2014).

Recently, remote sensing methods have become popular in forest assessment. These powerful techniques enable accurate, indirect, simple, low-cost, and nondestructive data collection from canopy structure for estimation of LAI in different spatial resolutions (Riano et al. 2004; Feng et al. 2006; Styers et al. 2014; Kim et al. 2015). Point quadrat is the first indirect method that was developed by Warren-Wilson in 1960. In this method, a probe with a sharp head is inserted into the vegetation and then the number of intersection of leaves or stems with the probe is counted. LAI can be estimated based on the measured contact frequency. This method is also labor-intensive and prone to an unavoidable error margin (Norman and Campbell, 1989). A more advanced indirect approach is the gap fraction method which is carried out by optical sensors such as the LICOR LAI-2200 Plant Canopy Analyzer and fish-eye lens cameras (Hosoi and Omasa, 2009). These commercial optical sensors are widely applied since they allow nondestructive, automatic and less laborious assessments. The calculations of the mentioned optical sensors are based on the assumption of random distribution of vegetation. The mentioned automatic techniques are associated with several limitations and drawbacks; first, the assumption of random distribution of vegetation is not completely true for all canopies and every section of a forest. This exposes these methods to a certain level of error (Hosoi and Omasa, 2009); second, their estimation is local and can't be extended spatially (Weiss et al. 2004; Gobron, 2008); third, they cannot separate non-photosynthetic materials such as trunks and branches from photosynthetic materials such as leaves. Hence, instead of accurate calculation of Leaf Area Index, Plant Area Index (PAI) is found. PAI is not an appropriate estimation of LAI since trunks and branches may have a considerable contribution to the total leaf area; fourth, these instruments cannot be effectively used for irregular canopies like savannas (Ryu et al. 2010).

Among different remote sensing instruments, Light Detection and Ranging (LiDAR) has been demonstrated to be the most effective tool for this purpose (Béland et al. 2011; Zheng et al,

2012b). LiDAR generates 3D Point Cloud Data (PCD) representing every feature in the forest with an extremely high resolution (Hosoi and Omasa, 2009). The first attempt to retrieve LAI from LiDAR data was conduct with airborne LiDAR (Lefsky et al. 1999; Lovell et al. 2003; Lim et al. 2003; Riano et al. 2004; Houldcroft et al. 2005; Morsdorf et al. 2006). However, the airborne LiDAR systems can't offer a comprehensive PCD due to the aircraft speed and the resulting low sample density. Hence, ground-based LiDAR is preferred for this purpose (Lovell et al., 2003).

Many methods are proposed for processing the PCD from ground-based LiDAR for extraction of LAI (Zheng et al. 2013, 2016; Ma et al. 2016a, b). The two building blocks of these methods are the voxelization of PCD and the algorithm for automatic calculation (Leblanc et al. 2014). To voxelize, the PCD is confined within a large box and divided to an array of equi-size smaller boxes which are called 3D voxels (Hosoi et al. 2013). Then, a radiative transfer model is used to calculate several intermediate parameters such as extinction coefficient and gap fraction and finally calculate LAI from the intermediate parameters (Chen and Black, 1991; Eriksson et al. 2005; Widlowski et al. 2014; Fang et al. 2014; Beland et al. 2014a).

The current state of the art on the extraction of LAI based on voxelization of LiDAR PCD is prone to many sources of error. First, it ignores the laser spatial sampling resolution. Standard LiDAR datasheets mention a sampling resolution at a specific distance. However, the sampling resolution is not only an effective parameter; it varies as a function of the distance between the station and the hit spot. This effect is emphasized for taller trees and longer distances. This causes the inter-distance of samples to be larger for remote spots. In the present methods, the sampling resolution is assumed to be constant and the voxel size is defined as a constant value. However, the voxel size has to be a function of sampling resolution and hence the distance of each voxel from the scan station. Second, the large confining box around the whole PCD doesn't conform to the tree crown shape (Hosoi et al, 2007). This generates a huge number of redundant voxels which are assumed and counted as empty voxels and directly result in miscalculations. Third, the auxiliary models such as the radiative transfer model are approximate since they are based on the assumption of randomly distributed points in the PCD. However, this assumption is not true since the probability of the existence of leaves is much higher around branches and stems. Besides, the configuration of branches follows a specific pattern for each species. Hence,

this assumption in radiative transfer models exposes LAI calculations to an extra level of error (Olivas et al, 2013).

The main motivation of the present chapter is to address these drawbacks and offer an improved voxelization scheme along with a dedicated algorithm for the calculation of LAI. First, a mathematical model is offered to analyze and calculate the LiDAR spatial sampling resolution as a function of distance and to define the voxel size based on it. *For the first time*, the proposed method refrains from using voxels of fixed size for all of the trees of any distance from the scan station and all the features at various heights in a tree. Instead, the PCD of an individual tree is divided into *adaptive* voxels which gradually vary in lateral size from the bottom of the trunk to the top of crown. Second, the proposed voxelization scheme doesn't need a large outer confining box. Instead, the PCD is vertically sliced and then divided to an array of pixels. Also, the redundant voxels are minimized and the number of empty voxels doesn't affect the calculations. Third, LAI is calculated directly from each voxel. Hence, the errors associated with radiative transfer model, gap fraction, and extinction factor are avoided.

The proposed method is applied to the field measurement data from a Canadian boreal forest and the results are comprehensively analyzed. This chapter is organized as follows: Section 2 discusses the material and methods, Section 3 presents the results. The numerical results and instructions are extensively discussed in Section 4. Finally, a conclusion is drawn in Section 5.

4.2 Materials and Methods

4.2.1 Site Characteristics and LiDAR Measurements

The study area in this research is located in northwestern Alberta, Canada at the Peace River Environmental Monitoring Super Site (PR-EMSS) which is part of an industry-research forestry region for Ecosystem Management Emulating Natural Disturbance (EMEND) project. The study area generally is boreal mixed wood plains, located at a latitude of 56.744223◦ N and a longitude of -118.344673◦ W. The PR-EMSS study area lies within stand of Trembling Aspen (*Populus tremuloides*) with a broad leaf deciduous canopy.

The Trembling Aspen tree leaves are lozenge in shape and relatively flat. A sample of tree leaf is shown in Figure 4.1. In this study, 21 trees were randomly selected within an area of 50 m × 50 m to carry out the LiDAR measurements as well as direct measurements. Terrestrial LiDAR measurements were acquired in both leaf-on and leaf-off conditions in the summer and fall 2014-2016. In order to explore the effect of the number of scan stations on LAI estimation and the reduction of occlusion effect a combination of six scans was used. The number of points for each scan was counted and related LAI for each scan permutation was calculated. The approximate tree height of this stand is 25.84 m (standard deviation, S.D. = 1.36 m) and the average elevation of this stand is 871 m. The collection, registration, and processing of PCD were performed in the Cyclone 8.1 software and MATLAB R2016.

4.2.2 Theory and Method

LAI is a significant parameter in the assessment of forest canopy structure. This subsection discusses the issues associated with the LAI calculation methods and explains how they are addressed in our proposed method.

4.2.2.1 Auxiliary Models

The process starts with confining the PCD inside a box. Then, it is divided into a multitude of horizontal slices (as depicted in Figure 4.2 a,b), and each slice is voxelized in order to simplify the handling of raw data. Next, for each slice, the gap fraction (*P*) and extinction coefficient (*G*) are calculated. *P*, *G,* and LAI are inter-related by radiation transfer model equation (1), as

$$LAI(z) = -\frac{cos(\theta)}{G(\theta)} log(P(\theta, z)) \qquad (1)$$

where z is the slice height and θ is the zenith angle showing the direction of solar beams. For perpendicular direct sun light beam (parallel to *z-axis*) θ, is set to 0 and the equations are further simplified. In this study, only $\theta = 0$ situation is considered. The case of oblique incidence can be analyzed based on present simplified model without loss of generality. It shall be the topic of

future work. Also, it should be noted that LAI can be calculated either in each slice as a function of z or for the whole canopy.

Using equation (1), LAI is indirectly calculated. Voxelization allows for the calculation of G and P at each slice. Voxel size is usually picked arbitrarily (Hosoi and Omasa, 2007; Song et al. 2011). Based on the above-mentioned method, some voxels shall be non-empty and include data points (ON). But, some are empty and without data points (OFF). P is calculated based on the number of empty voxels (nOFF) and non-empty voxels (nON) as equation (2):

$$P(z) = \frac{n_{OFF}}{n_{OFF}+n_{ON}} \qquad (2)$$

The main box fitted to PCD doesn't conform to the actual shape of the tree crown. This creates many empty voxels which are out of actual tree crown boundaries. Consequently, error in n_{OFF} directly affects the calculation of P. To demonstrate this, a sample horizontal cut is depicted from the top view and in 2D in Figure 4.2 c. Hence, an alternative to the box method should be sought to remove the extra OFF voxels or a technique should be used which does not rely on the ratio of n_{OFF} to n_{ON}.

G depends on the number, configuration, and coordinates of data points inside each voxel. To simplify calculations, G is assumed constant for a specific species in some studies (Zhao et al. 2015). However, some studies try to calculate G based on PCD. Two other auxiliary models are offered for this purpose. However, both add extra complexity to the analysis and their estimations contribute to the error in LAI (Beland et al. 2011). In the first model, G is described using an extra parameter χ as (Ross, 1981):

$$G(\theta;\chi) = \chi.\cos(\theta) + (1-\chi).\frac{2}{\pi}.\sin(\theta) \qquad (3)$$

where θ is the zenith angle. The second model uses Miller's formula:

$$\int_0^{\pi/2} G(\theta).\sin(\theta).d\theta = 0.5 \qquad (4)$$

which requires solving an inverse problem with complicated numerical integration over few selected discrete zenith annuluses to find G.

In the case of large areas of forests, canopy assessment using the auxiliary models requires a large volume of computations. To avoid that, in the proposed method, LAI can be simply and directly calculated from PCD using its straightforward definition as:

$$LAI = \frac{S_{leaf}}{S_{gnd}} \quad (5)$$

where S_{leaf} is the effective light receiving area of the leaves, and S_{gnd} is the ground surface area. To find S_{gnd}, PCD is projected on *xy-plane* and a 2D Convex Hull (CH) is drawn around it. The proposed algorithm in this study is designed for calculation of S_{leaf}.

4.2.2.2 LiDAR Spatial Sampling Resolution

The spatial sampling resolution (res_R) of the Leica C10 LiDAR scan station is 4 *mm* at 50 *m,* according to its datasheet. However, res_R depends on the distance (R) between the scan station and the hit spot. Despite its significance, none of the present methods in the literature have considered this factor in their LAI calculations. To consider this effect for LAI calculation, a mathematical model should be developed. Ground-based LiDAR scans the surrounding space with predetermined azimuth and zenith angle steps. As depicted in Figure 4.3, with an angular resolution of $\Delta\Psi$, the arc length (res_R) is calculated as equation (6):

$$res_R = R.\Delta\Psi \quad (6)$$

At close distances (~ several meters), the change in *res* is small and irrelevant in calculations. However, this parameter should be considered in calculations for forest trees. In the ideal case of having an error-free scanning system with infinitesimal beam diameter (light ray), using equation (6), *res* can be approximated. Considering $\Delta\Psi = 60\,\mu rad$ based on Leica C10 datasheet, $res_{R=30m} = 1.8\,mm$. However, the practical values of *res* are larger because of non-ideal scanner and randomly-oriented leaves. Hence, to have a better estimation of resolution, a PCD from forest scan is studied. In the PCD, 20 adjacent pairs of points in different distances from LiDAR (3 m < R < 50 m) are selected. The selected points are along both azimuth and zenith direction. The distance between points in each pair (*res*) is calculated. Then, the resolution

of the points belonging to each distance is averaged, and the graph of resolution versus distance is drawn. Using interpolation, this equation is extracted:

$$res(R) = \begin{cases} 0.47(R-3)+3 & 3 < R < 18 \\ 1.33(R-18)+10 & 18 < R < 50 \end{cases} \quad (7)$$

where *R* is in *m* and *res* is in *mm*. Hence, this equation can be used for the resolution in azimuth and elevation directions. According to equation (7), *res* can be as large as 5 cm which is comparable to the diameter of leaves. Considering the diamond-like shape of leaves and the fact that leaf diameter (*D*) is its largest dimension (Figure 4.4), a far leaf may merely be missed in a scan. Nevertheless, closer leaves might be represented by tens of points. This is ignored in previous studies and it can cause a major error in the calculation of *G* especially for voxels which carry 1 or 2 points. Hence, both *D* and *res* should be involved in the voxelization, slicing and also the calculation algorithm. To avoid these complexities, some studies use a value of 0.9 for *G* (Macfarlane et al. 2007). Zheng and Moskal (2012a) recommend the voxel size to be 1.5 times *res*. However, the variation of resolution is not studied and uniform voxels are usually applied.

The effect of sampling resolution becomes even more dramatic at far distances due to the divergence of the laser beam. For the Leica C10, the beam diameter (*d*) is 4.5 mm right at the output. At the focal distance which is 25 m, *d* decreases to 3 mm and then increases for farther distances. At 50 m, *d* shall be 4.5 mm again. Hence, *d* as a function of distance can be calculated using equation (8):

$$d = \begin{cases} 0.06(R-25)+3 & R > 25 \\ 0.06(25-R)+3 & R < 25 \end{cases} \quad (8)$$

where *d* is in *mm* and *R* is in *m*. Thus, *d* might be comparable with *res*. To consider all practical measurement aspects and minimize the resulting calculation errors, both *res* and *d* have to be involved in the algorithm.

4.2.3 Algorithm Steps

The following algorithm is designed for calculation of S_{leaf}.

Step I: To get the crown PCD (cPCD), the algorithm for separation of photosynthetic from non-photosynthetic features in the previous chapter is applied to the whole PCD. The tree crown starts at around a height of 18 m, for the species under study.

Step II: cPCD is horizontally sliced with a thickness equal to the average diagonal size of the leaf (*D*) which is around 5 cm in our study to find $cPCD_k$ (Figure 4.4). Index *k* denotes the slice number. Then, each $cPCD_k$ is projected over *xy-plane*.

Step III: The 2D $cPCD_k$ is pixelized for further analysis. The points are constrained inside a rectangular outer boundary which is constrained between (X_{min_k}, X_{max_k}) and (Y_{min_k}, Y_{max_k}). The pixel size has to depend on sampling resolution. However, since the slice data points are at different distances from the scan station, the middle point of that slice is picked ($\frac{X_{min_k}+X_{max_k}}{2}$, $\frac{Y_{min_k}+Y_{max_k}}{2}$, z_k) and its distance to the scan station is calculated. Then, the resolution is acquired using equation (7) and a pixel size ($u \times u$) of $10res_k \times 10res_k$ is selected. Each voxel is denoted by index of (i, j, k) where *i* and *j* shows its number along *x* and *y axes*.

Figure 4.5 shows the schematic pixelization with two select slices from lower and upper height in the crown which is pixelized with different sizes. At each slice, using equation (7) and (8), the conditions of $(u, D) \gg d$ should be controlled. If for a specific type of tree and distance, $D \gg d$ doesn't hold, the slice thickness should be increased to $10D$. Also, if $u \gg d$ doesn't hold, the lateral size of pixels is increased to $50res_k \times 50res_k$.

Step IV: The plant area of each pixel (S_{ijk}) is calculated based on the number (n_{ijk}) and configuration of points inside each pixel as:

a) $n_{ijk} = 0$: This pixel doesn't contribute to plant area.
b) $n_{ijk} = 1 : S_{ij} = 1 \times S_0$ where S_0 is the area of a single average leaf. To run the algorithm, the first step is defining parameter D for the study area which is the average diagonal size of leaves. For 27 leaf samples from different trees and various spots in the study area, D is 52 mm. This also determines the slice thickness of 52 mm and also the single leaf area which is $S_0 = 0.00081\ m^2$.

c) $n_{ijk} = 2$: The distance between the two points (L) should be measured. If $L >$ D, then $S_{ijk} = 2 \times S_0$, otherwise $S_{ij} = 1 \times S_0$.

d) $n_{ijk} \geq 3$: In case of 3 points, they are checked for collinearity. If they aren't collinear, 2D ConvexHull (CH) is used to find the area. Since the laser is single return, many of the leaves might be occluded behind the features at the front. Using CH can partially compensate for occlusion.

Step V: S_{leaf} is calculated by summing the individual plant area of all pixels in all slices as:

$$S_{leaf} = \sum_k \sum_{i,j} S_{ijk} \qquad (9)$$

Note that, in the proposed method, the number of OFF voxels/pixels doesn't affect the calculations, contrary to the common methods of calculation of P in radiative transfer models.

4.3 Results

In this Section, the proposed algorithm is applied to the PCD from field measurements and its different aspects are investigated and evaluated. Before running the algorithm, the PCD has to be processed to separate the photosynthetic features as elaborated in Chapter 3.

4.3.1 LAI Estimation for an Individual Tree

A typical individual tree is scanned from six stations (A-B-C-D-E-F) as illustrated in Figure 4.6. The tree PCD is shown in Figure 4.7 a,b from the side and top view. The points are color-coded for improved visual representation based on the height where warmer colors are assigned to lower heights and cooler colors indicate higher points. The visualization is carried out using Cyclone with the Color Map Elevation Map features in View tab. It is worth mentioning that Cyclone offers a wide variety of visual representation such as "Colors from Scanner", "Intensity Map", "Single Color", and "Image Texture Map", which should be selected based on the specific application and project. The imported PCD (Figure 4.7 b) includes both branches and leaves which look like an actual tree. This implies the validity of the LiDAR scans.

The results from Table 4.1 show that the LAI values increased from 1.91 to 3.24 as the number of scan stations increased from one to six, respectively. Table 4.1 demonstrates that at least four stations are required for a comprehensive scan. Increasing the number of stations to five and six does not change the number of points and LAI value significantly. Also, it can be visually verified that the tree point collection is complete and the point density is almost uniform over all sides of the tree. This is due to using four scan stations which offer a comprehensive data set of a tree and minimizes the occlusion effect. The PCD from single station usually lacks the part of tree features which are on the opposite side of scan station and results in lower point density at the opposite side. Figure 4.8 compares LAI calculated by TLS and other optical sensors such as LICOR LAI-2000 Plant Canopy Analyzer, Tracing Radiation and Architecture of Canopies (TRAC), and Digital Hemispherical Photography (DHP) (Gower et al. 1997; Chen et al. 1997a; Kucharik et al. 1997, 1998; Davidson et al. 2000; Barr et al. 2004; Bourque and Quazi, 2008; Ma et al. 2016a). The LAI value of 3.2 provided by four stations in this study is close to the value calculated using TLS by Ma et al. (2016a). This verifies the proposed algorithm.

Since the algorithm works based on vertical slicing, it is advantageous to inspect the point collections at the different slices before algorithm implementation. There are two ways to do this: MATLAB code and Cyclone fencing feature which should agree. The crown section of the selected individual tree is divided into 175 slices which are 52 mm thick. Here, slice number 81 ($k = 81$) is selected and the points enclosed in this section are separated and extracted by Cyclone and shown in Figure 4.7 c from the top view. It is noteworthy that the outer boundaries of Figure 4.7 c coincide with outer boundaries of Figure 4.7 b. This verifies the slicing procedure carried out in Cyclone since the points of slice 81 are a small subset of the large collection of points.

The first step to analyze PCD is the slice point density distribution graph which is depicted in Figure 4.9. The number of points in each slice is assigned to the horizontal axis while the slice number is shown on the vertical axis. The slice point density graph reveals the approximate shape of the tree crown on the vertical profile and varies between 1 and 6998 points. These minimum and maximum values directly depend on the slice thickness, scan properties, and tree species. The number of points for slices up to around 5 is small and almost uniform. However, for the higher slices, the number of points increases and reaches a maximum around slice 111. After that, the number of points decreases up to the top slice. This trend is generally true for most of the trees in our field area.

The next step is the lateral pixelization of each horizontal slice which is done independently for each slice. The z coordinate of the points in each slice is ignored and hence a 2-Dimensional collection of points is achieved which is easier to deal, than a 3Dimensional PCD. The lateral size of pixels ($u \times u$) in each slice is defined based on the scan resolution (res_k) of LiDAR which depends on both technical aspects and the distance of scan station to the tree stand. To perform this step, the middle spot of each slice is found and its distance to scan station (R) is calculated as in equation (12):

$$R = \sqrt{{X_{mid}}_k^{\,2} + {Y_{mid}}_k^{\,2} + {Z_{mid}}_k^{\,2}} \qquad (12)$$

The scan station is assumed to be at the center of coordinates (0, 0, 0). For an individual tree, res_k is drawn for all slices based on equation (12) in Figure 4.10. Hence, the average scan resolution for slices changes from 11.46 to 20.86 mm for the lowest to highest slices. This is equivalent to overall 9.4 mm change in scan resolution which shifts the pixel lateral size ($u \times u$) by 94 mm among slices and causes considerable change in calculated results. The proposed adaptive voxelization technique tunes the voxel volume over the PCD from bottom to top of the crown and increases it by 231%.

During the next step, the distribution of the points at each slice defines the leaf content and its effective leaf area. The algorithm is run on six different PCD's which complement each other including the data from a different combination of scan stations such as A, AC, ABC, ABCD, ABCDE, and ABCDEF. There are other possible combinations which are not included here due to brevity. LAI results and a total number of points for these six PCSs are summarized in Table 4.1. Increasing the number of stations provides a more comprehensive PCD from the tree with a higher number of points which allows better LAI assessment.

To find out the optimum lateral size of an adaptive voxel, the proposed algorithem was run for different lateral size ($u \times u$) of ($10res_R \times 10res_R$), ($20\text{res}_R \times 20res_R$), and ($30res_R \times 30res_R$) (Table 4.2). Optical estimates of LAI for trembeling aspen by DHP is 1.67, by TRAC is 2.4, by Plant Canopy Analyzer is 2.1, and TLS estimates of LAI for aspen is 3.32 (Ma et al. 2016a; Barr et al. 2004)). The results in Table 4.2 showed the optimum lateral size of each pixel is $u = 10res_R$ that gives the LAI value in the acceptable range based on literature for TLS (3.2). To find the

effect of fixed voxel size and comparing it with adaptive voxel, the proposed algorithm is modified and the results are shown in Table 4.3. By changing the fixed voxel size from $10\overline{res}$ to $20\overline{res}$ and 30 $\overline{res}$, the LAI value increases from 3.96, to 7.35 and 9.07, respectivaly. $u = 10\overline{res}$ results in the estimation error of 19.2% which is much higer than the case for $u = 10res_R$ which leads to an estimation error of 3.6%.

According to Table 4.1, the increase of scan stations from 1 to 6 increases the number of points from 180,608 to 581,791 which is 3 times. This verifies the significant effect of occlusion. However, the increase of scan stations from 1 to 6 increases LAI from 1.91 to 3.24 which is almost twice. This shows the robustness of the proposed adaptive voxelization method.

Usually, a fixed value is picked for voxel size which is kept independent of surrounding conditions. In this work, however, for the first time, an adaptive voxel size ($10res_k \times 10res_k \times D$) is proposed based on the engineering features of the scan station, the scan size and the tree leaf properties (Figure 4.11). To prove the effectiveness of present study and inspect the appropriateness of the proposed parameters, they are changed in the algorithm to inspect the results and compared with previous results. The sensitivity analysis is as follows:

a) *Efficacy of parameter $u = 10.res_k$*

To show that selecting 10 is the optimum coefficient of resolution for LAI results, it is changed to 20 and 30 in the algorithm (($20res_k \times 20res_k \times D$) and ($30res_k \times 30res_k \times D$)) and it is run over PCD from four scan stations. The results are summarized in Table 4.2. Using larger adaptive voxels increases the calculated LAI value and renders it out of valid ranges reported in the state of the art (Ma et al. 2016a; Barr et al. 2004). This proves that the 10-fold coefficient is appropriate for LAI calculations, although 20-fold and 30-fold coefficients make larger voxels and quicker voxelization.

b) Comparison of adaptive and constant voxeling

To show the efficacy of the adaptive method, voxels with constant sizes of ($10\overline{res} \times 10\overline{res} \times D$), ($20\overline{res} \times 20\overline{res} \times D$) and ($30\overline{res} \times 30\overline{res} \times D$) are applied over the PCD from four stations and the results are summarized in Table 4.3. All these LAI values are out of acceptable range for trembling aspen.

4.3.2 LAI Estimation for the Stand Level

Our study field includes many trees. In the PCD from six scan stations, 21 trees are separated and individually assessed. The height and DBH of those individual trees were measured, and the LAI was calculated using the proposed algorithm. These trees have a height of 25.85 ± 1.36 m (average ± standard deviation), a DBH of 31.79 ± 7.13 cm. The LAI for the mentioned stand is 3.13 ± 0.10. Figure 4.12 shows DBH versus tree height (R^2 = 0.66). Figure 4.13 illustrates the correlation between the LAI and DBH (R^2 = 0.82) Figure 4.14 shows the relationship between the LAI and tree heights. (R^2 = 0.84).

4.4 Discussion

To show the performance and the effectiveness of the proposed method for forest assessment, the sensitivity of LAI to the major parameters such as fixed and adaptive voxel size should be studied. Also, a comprehensive study requires investigation of the major sources of error in measurement and calculations.

The main enhancement in the proposed voxelization/algorithm compared to the state of the art is incorporating the effect of LiDAR sampling resolution and intuitive selection of voxel size (slice thickness and pixel lateral size) based on physical and geometrical specifications of the canopy under study. We have also avoided auxiliary models such as radiative transfer model which expose calculations to a high margin of approximation in order to be able to calculate forest parameters directly based on common straightforward textbook definitions. The proposed method takes advantage of some select instructions on clumping/occlusion effect or laser beam diameter in previous studies on LiDAR-based LAI by incorporating them in the algorithm (Beland et al. 2014b). For minimizing the clumping effect, the voxels are instructed in literature to be small enough to avoid large gaps between branches and crowns. This is considered in the present method by building voxels of size ($u \times u \times D$) with $u_k = 10.res_k$. This is an adaptive method since res_k is a function of the distance between the scanner and the hit point. res_k is calculated based on the analysis of the distances between sampled points inside the PCD. Hence, no further action is required to find res_k. Furthermore, the under-sampled leaves are recommended to be considered in leaf area calculations for minimizing the occlusion effect. This

is assured by rules in algorithm Step IV where a ConvexHull is used or even a single point can represent a single leaf. Besides, the voxel dimensions are instructed in the literature to be much larger than the laser beam diameter (d). This is controlled in the proposed algorithm by calculating the beam diameter at each step as a function of distance and imposing several logical conditions to control that $(u, D) \gg d$ at Step III. In all LiDAR studies in literature, the laser beam diameter is assumed constant and they have not considered its effect.

About the number of scan stations for data collection, current literature recommends 3 or 4 stations which result in more comprehensive PCD and a better representation of canopy (Zheng and Moskal, 2012). It is observed that the increase in the number of stations changes the total number of points in PCD and also the LAI. The algorithm is run on six different PCD's from different combinations of scan stations: A, AC, ABC, ABCD, ABCDE, and ABCDEF. There are other possible combinations which are not included here due to brevity.

At the stand level, 21 trees were analyzed. The coefficient of variability in DBH and height is 22% and 5.3%, respectively. The difference among DBH is caused by their age. The of the trees is almost similar which is expected for a forest stand. The coefficient of variability in LAI is 3.2%. This shows almost similar crown features and leaf configuration for the study plot. There is a strong correlation between LAI and DBH ($R^2 = 0.82$) and also between LAI and tree height ($R^2 = 0.84$). This means that the taller trees and the trees with thicker trunk are expected to have higher LAI.

4.4.1 Adopting the Algorithm for Other Sites

The proposed algorithm in this study is applied on trembling aspen in a boreal forest stand in north of Alberta. By adopting some of variables in the algorithm it can be applied on other PCD data in other species and other forest stand. For example, for other laser scanning systems based on the sampling resolution and beam diameter the lateral size should be obtained and equation 7 and 8 should be rewritten. Also for parameter D in this algorithm based on the shape of the leaves in any species equations 7 and 8 should be modified. Since LAI will change during the growing season, to have the annual average of LAI it is better to measure LAI several times during the growing season.

4.5 Conclusion

This study presented a general, intuitive, and simple technique based on adaptive voxelization to estimate LAI using the point cloud data from ground-based LiDAR. *For the first time*, the effect of laser spatial sampling resolution was studied theoretically and experimentally as a function of distance and incorporated into the voxelization/algorithm for processing the point cloud data based on adaptive voxels which vary in size based on their location. This technique directly calculates LAI without the need to auxiliary models such as radiative transfer which deals with intermediate parameters such as gap fraction and extinction factor. These results in simplification of calculations and removal of the error margin associated with auxiliary models to allow higher precision. Furthermore, the present technique calculates the laser beam diameter and incorporates it inside the algorithm.

This method was applied to a boreal forest for comprehensive analysis of canopy structure. The results show that one scanning station is not appropriate for delivering the spatial distribution of point density to estimate the LAI. We recommend using at least 4 scan stations to keep the LAI measurement and calculation error within minimum error while minimizing the occlusion effect. It verifies the previous findings for our proposed technique (Zheng and Moskal, 2012).

The application of the proposed method to a cross-section of forest from a single and multiple scan stations shall be the subject of a future work, where we shall compare the calculated canopy parameters of different individual trees with forest stands of various areas. In the present study, only perpendicular sunbeam radiation over canopy ($\theta = 0$) is studied and oblique sunbeam shall be the topic of a future research.

Tables Legends

Table 4.1 Leaf Area Index for multiple scan stations for an individual tree.

Table 4.2 Leaf Area Index for different *u.*

Table 4.3 Fixed size voxels for LAI calculation.

Figures Legends

Figure 4.1 Illustration of *Populus tremuloides* leaf in a boreal forest.

Figure 4.2 Conventional voxelization method; (a) Confining box boundary (b) Horizontal slices (c) ON and OFF voxels in a slice which includes many redundant OFF pixels. The slice boundary is shown in dashed gray line.

Figure 4.3 2D schematic of sampling resolution on a target leaf.

Figure 4.4 Sample leaf of *Populus tremuloides* and its sizes.

Figure 4.5 Side view of the tree crown pixelization schematic in proposed algorithm.

Figure 4.6 Schematic of an individual tree scanning from six stations (A-B-C-D-E-F) around it.

Figure 4.7 Illustrations of the LiDAR point clouds for a single tree in Cyclone; (a) Side view (b) Top view (c) Point cloud acquired from slice 81.

Figure 4.8 LAI calculations of six stations for a single tree and comparison with LAI values obtained by TLS and other optical sensors. The black dots represent the LAI measured in this study by LiDAR using one to six scan stations. The dashed red line shows the LAI value (3.32) from TLS, the dashed blue line is the LAI value (2.4) from TRAC, the dashed purple line shows the LAI value of 2.1 from the LAI-2000 Plant Canopy Analyzer, and the dashed green line is the LAI value (1.67) by DHP.

Figure 4.9 Point density profile along a single slice. The number of points processed at each slice.

Figure 4.10 Sampling resolution at the middle voxel in *mm* used for defining *u* in each slice.

Figure 4.11 Different voxelization techniques; (a) fixed size voxels (u × u × D) (b) voxels of adaptive size ($u_1 \times u_1 \times D$), ($u_2 \times u_2 \times D$), and ($u_3 \times u_3 \times D$) depending on their distance from scan station.

Figure 4.12 Diameter at Breast Height (DBH) versus Leaf Area Index (LAI) for the 21 sampled Trees derived from PCD data in summer season.

Figure 4.13 Scatter plot of LAI as a function of DBH with a linear regression line (21 trees) in summer season.

Figure 4.14 Scatter plot of LAI as a function of tree height with a linear regression line (21 trees) in summer season.

Table 4.1 Leaf Area Index for multiple scan stations for an individual tree.

Number of Scan stations	number of points	LAI
A	180608	1.91
AC	359662	2.52
ABC	412077	2.91
ABCD	534941	3.2
ABCDE	579992	3.23
ABCDEF	581791	3.24

Table 4.2 Leaf Area Index for different *u*.

u	**10 res_R**	**20 res_R**	**30 res_R**
LAI	3.2	5.81	7.92

Table 4.3 Fixed size voxels for LAI calculation.

u	**10** $\overline{res}$	**20** $\overline{res}$	**30** $\overline{res}$
LAI	3.96	7.35	9.07

Figure 4.1 Illustration of *Populus tremuloides* leaf in a boreal forest.

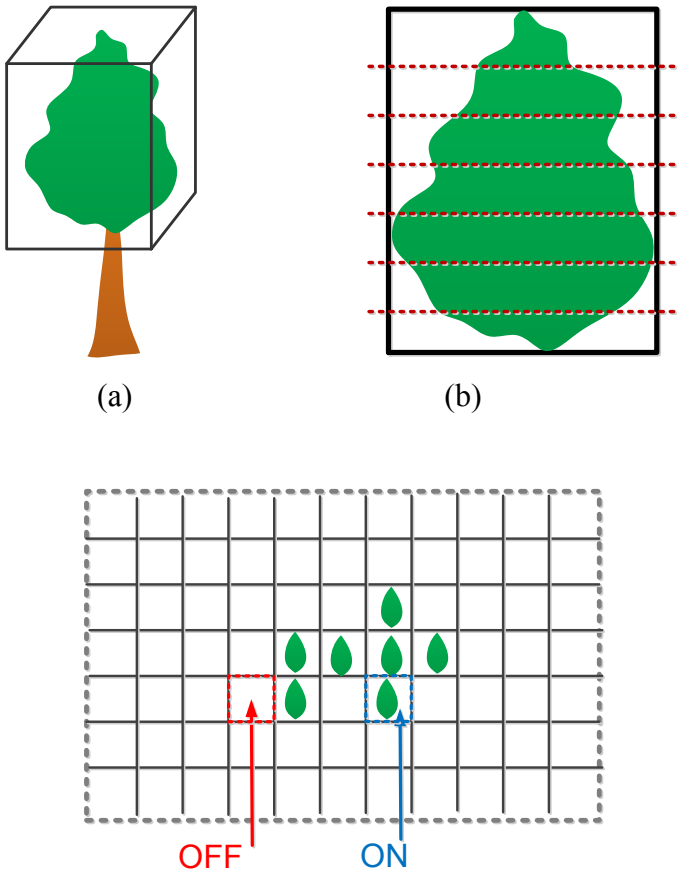

Figure 4.2 Conventional voxelization method; (a) Confining box boundary (b) Horizontal slices (c) ON and OFF voxels in a slice which includes many redundant OFF pixels. The slice boundary is shown in dashed gray line.

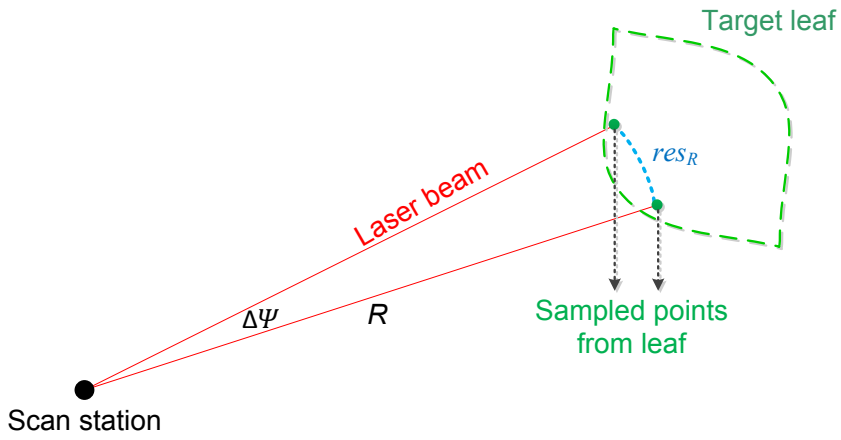

Figure 4.3 2D schematic of sampling resolution on a target leaf.

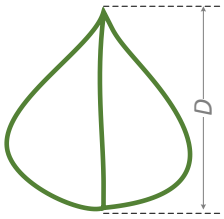

Figure 4.4 Sample leaf of *Populus tremuloides* and its sizes.

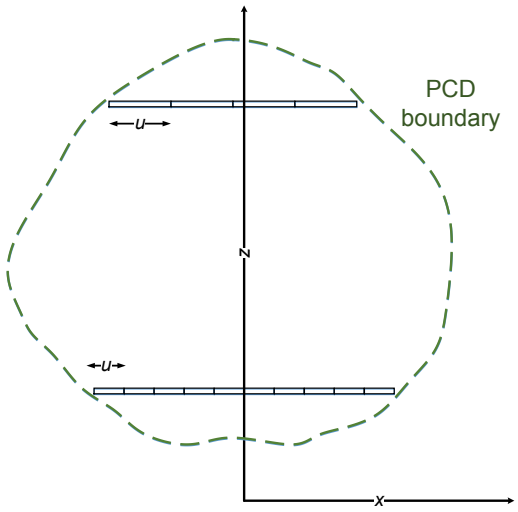

Figure 4.5 Side view of the tree crown pixelization schematic in proposed algorithm.

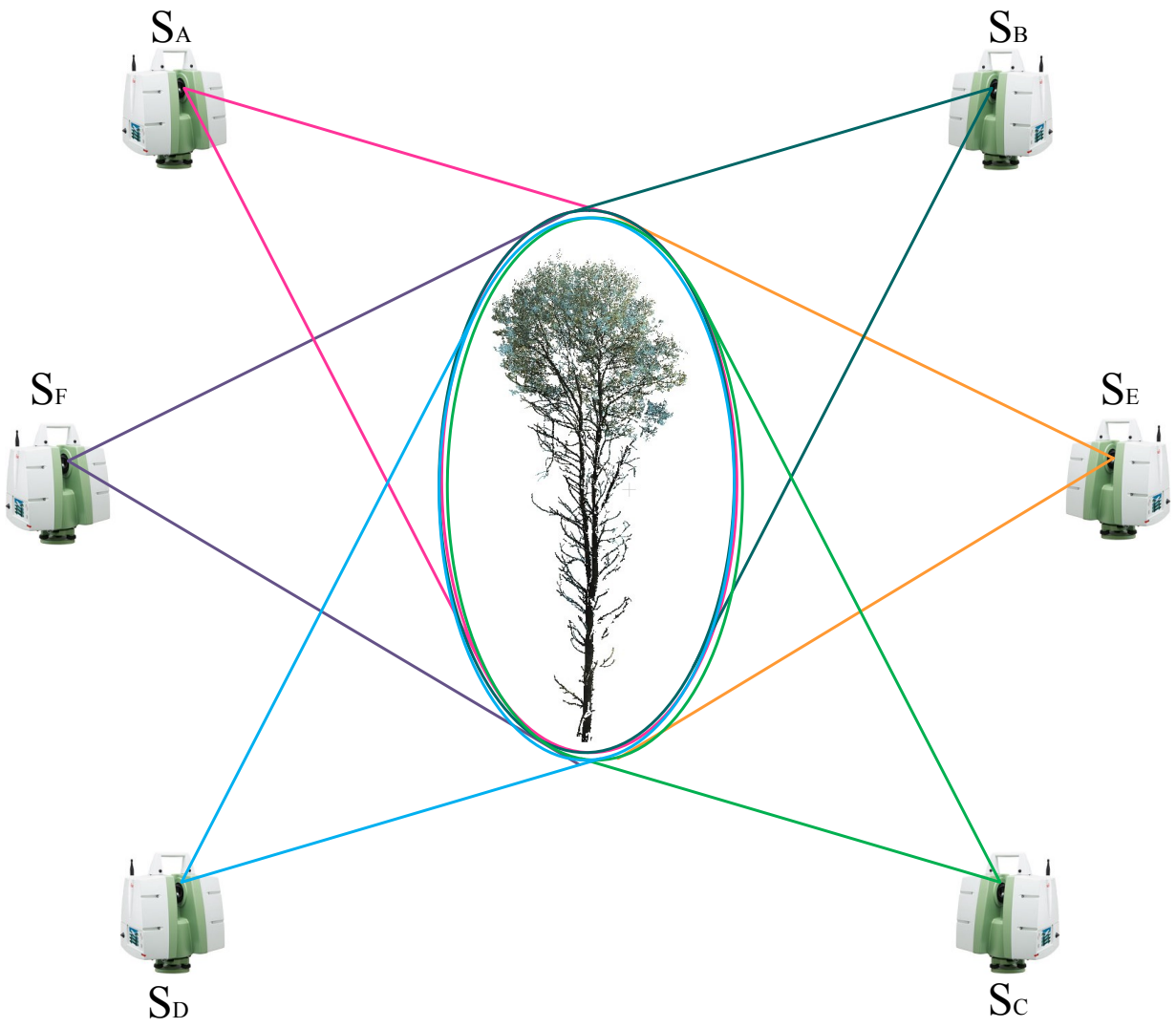

Figure 4.6 Schematic of an individual tree scanning from six stations (A-B-C-D-E-F) around it.

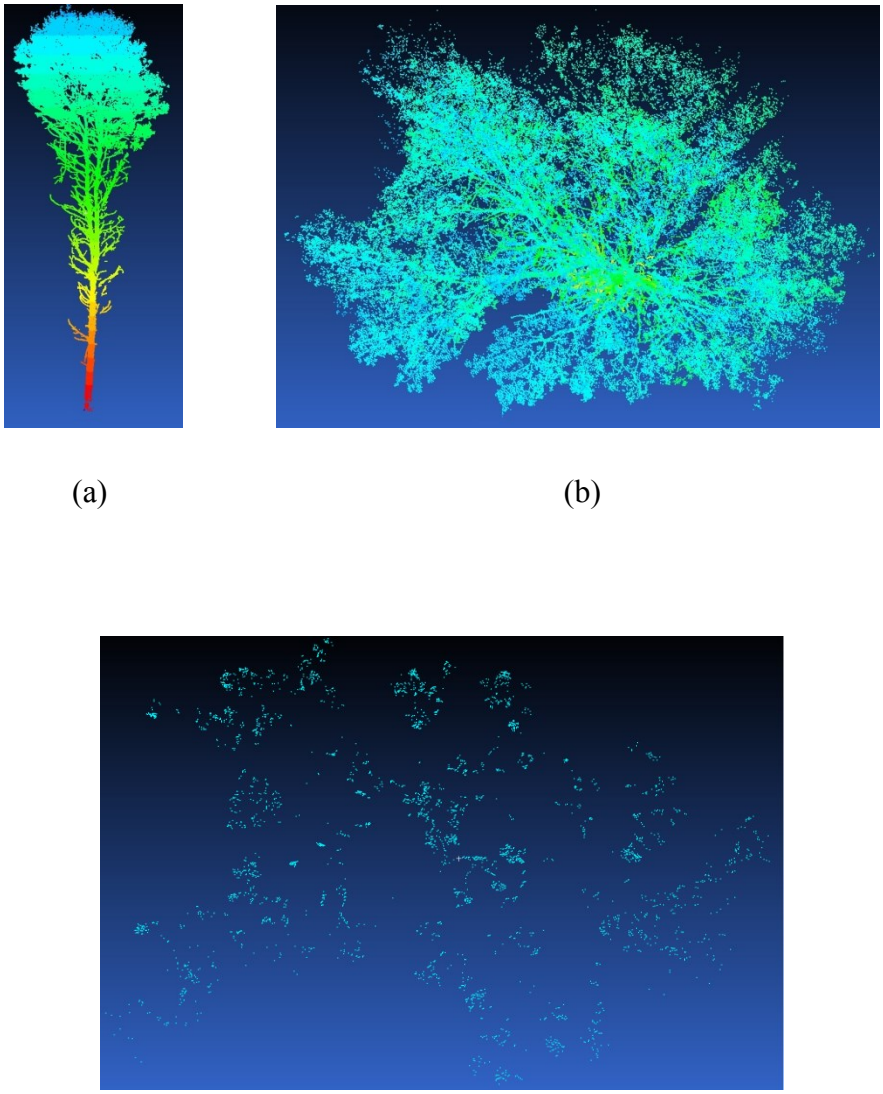

(a) (b)

(c)

Figure 4.7 Illustrations of the LiDAR point clouds for a single tree in Cyclone; (a) Side view (b) Top view (c) Point cloud acquired from slice 81.

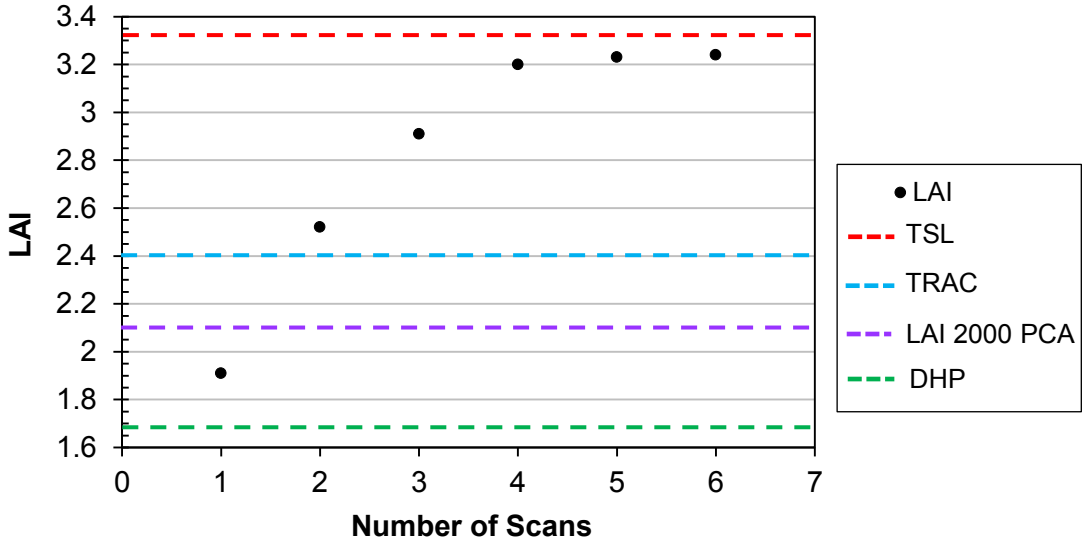

Figure 4.8 LAI calculations of six stations for a single tree and comparison with LAI values obtained by TLS and other optical sensors. The black dots represent the LAI measured in this study by LiDAR using one to six scan stations. The dashed red line shows the LAI value (3.32) from TLS, the dashed blue line is the LAI value (2.4) from TRAC, the dashed purple line shows the LAI value of 2.1 from the LAI-2000 Plant Canopy Analyzer, and the dashed green line is the LAI value (1.67) by DHP.

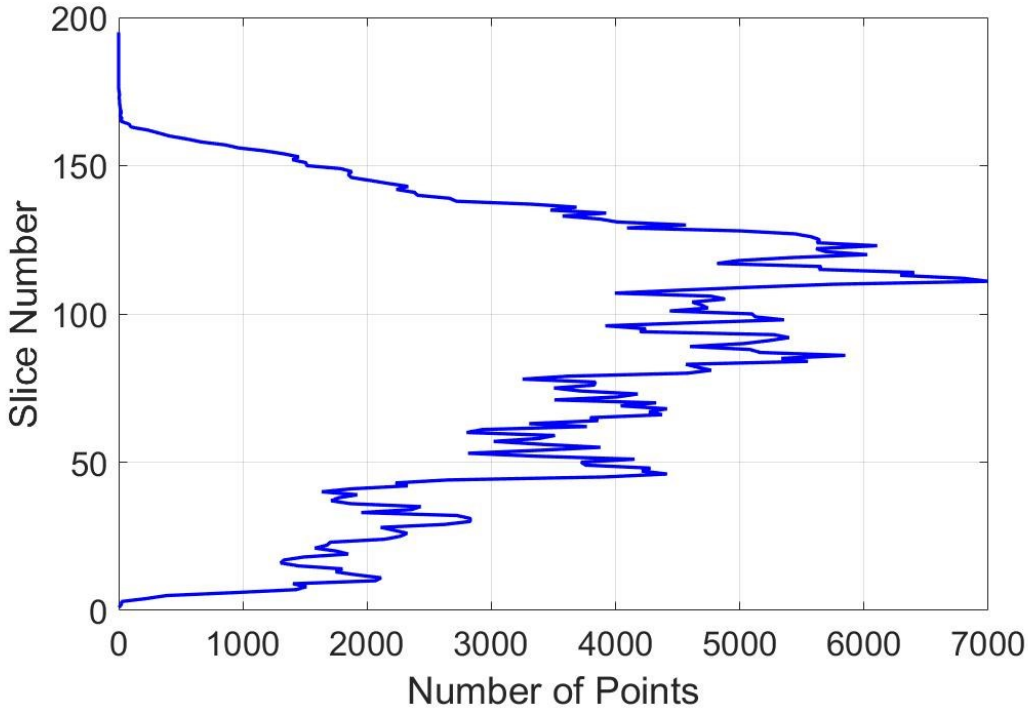

Figure 4.9 Point density profile along a single slice. The number of points processed at each slice.

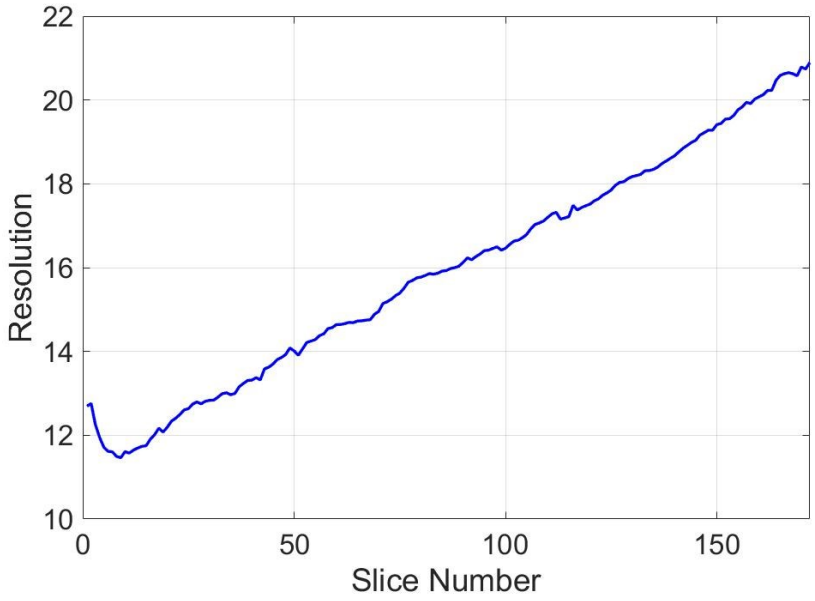

Figure 4.10 Sampling resolution at the middle voxel in *mm* used for defining *u* in each slice.

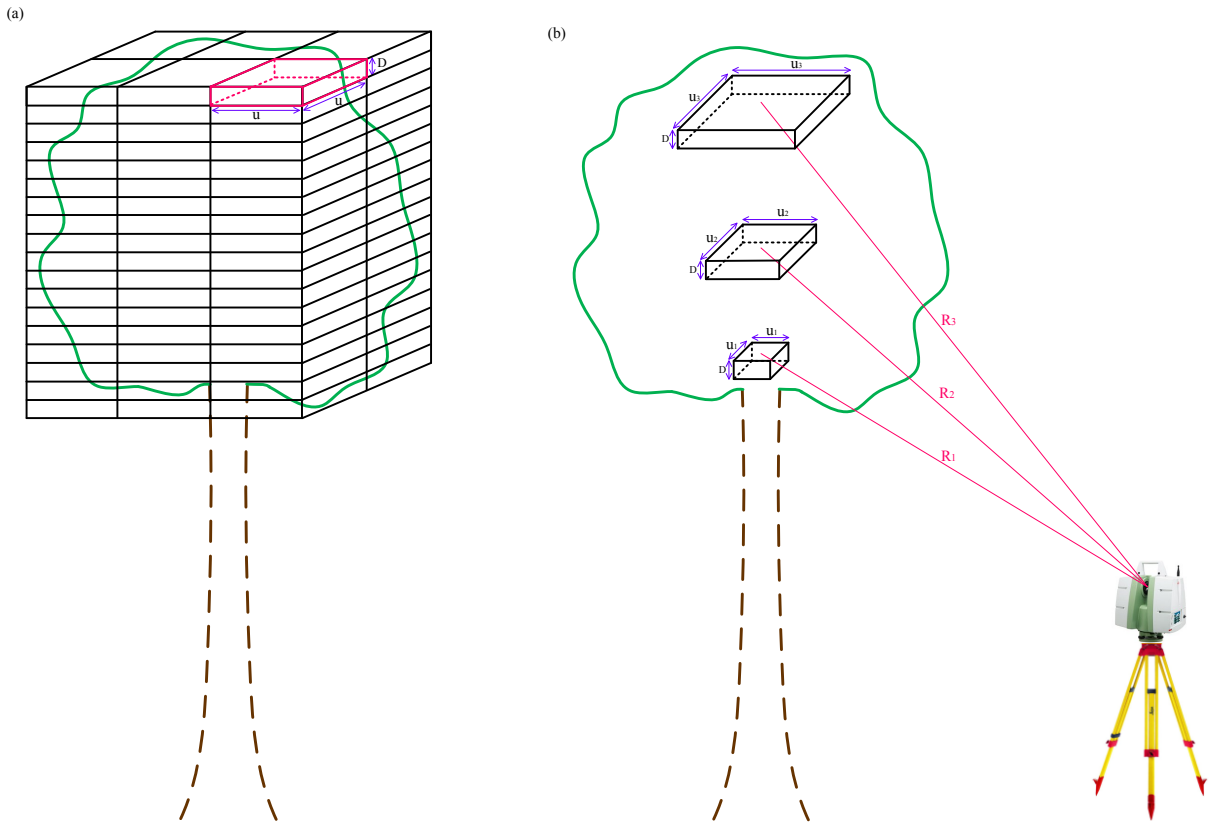

Figure 4.11 Different voxelization techniques; (a) fixed size voxels (u × u × D) (b) voxels of adaptive size ($u_1 \times u_1 \times D$), ($u_2 \times u_2 \times D$), and ($u_3 \times u_3 \times D$) depending on their distance from scan station.

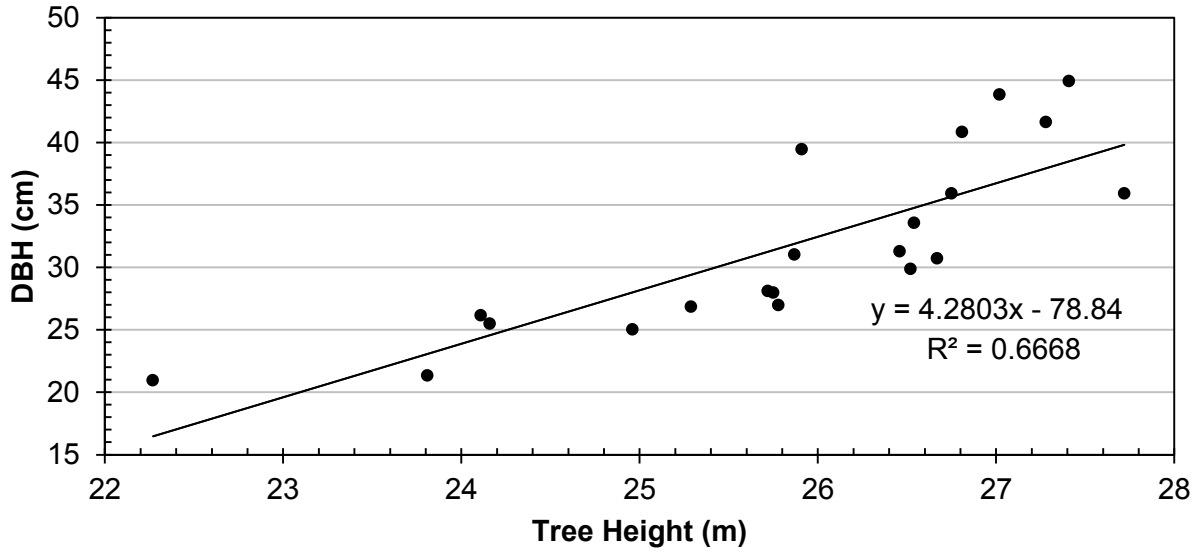

Figure 4.12 Diameter at Breast Height (DBH) versus Leaf Area Index (LAI) for the 21 sampled Trees derived from PCD data in summer season.

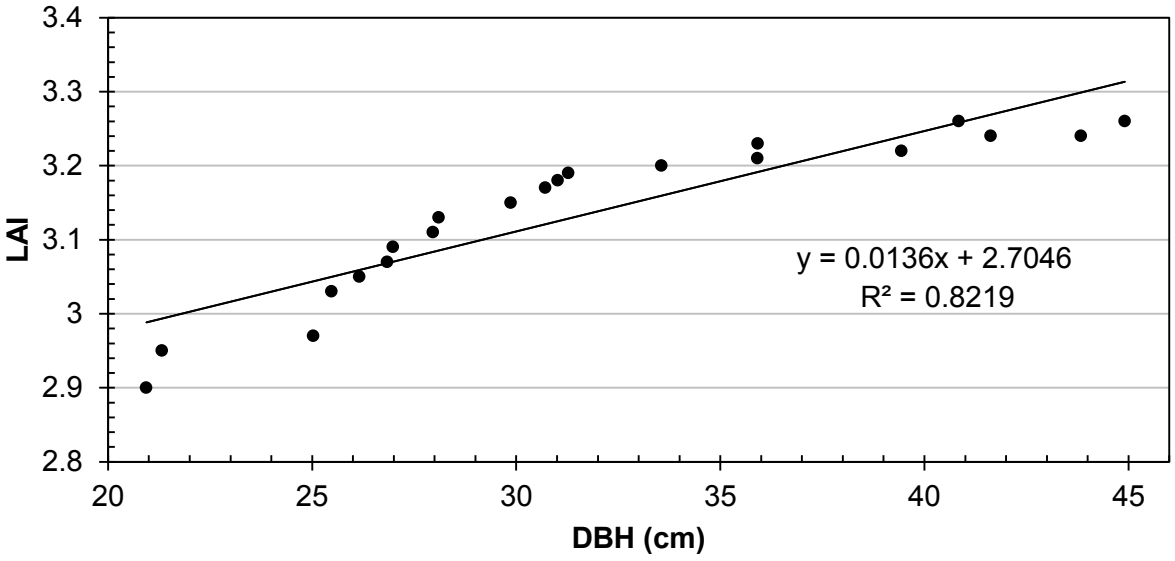

Figure 4.13 Scatter plot of LAI as a function of DBH with a linear regression line (21 trees) in summer season.

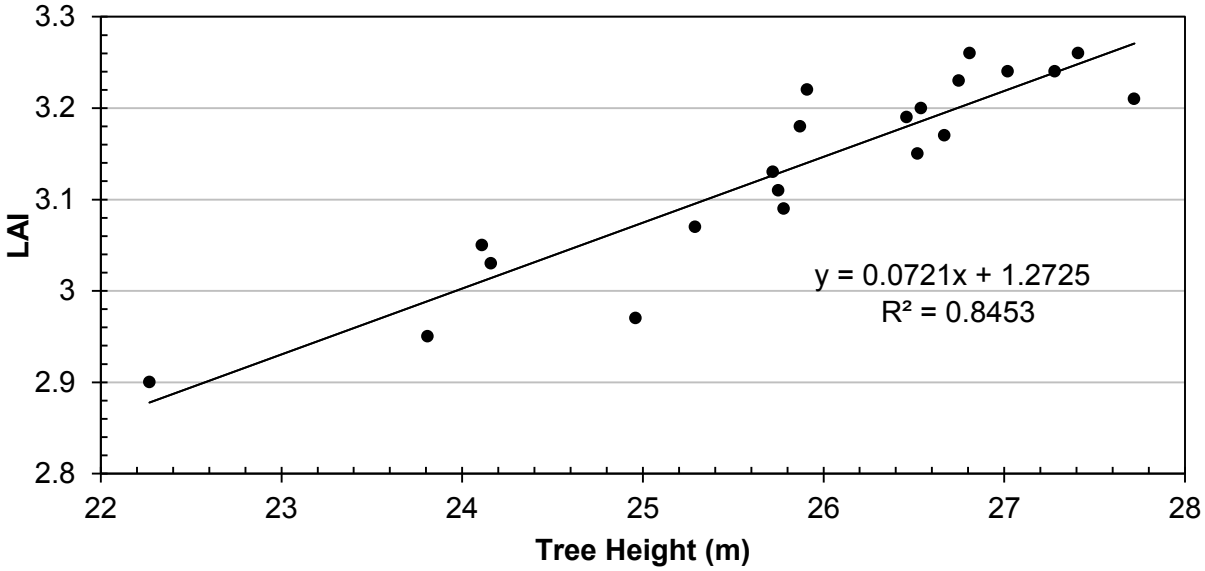

Figure 4.14 Scatter plot of LAI as a function of tree height with a linear regression line (21 trees) in summer season.

References

Asner, G.P., Scurlock, J.M. and A Hicke, J. 2003. Global synthesis of leaf area index observations: implications for ecological and remote sensing studies. *Global Ecology and Biogeography*, 12(3), pp.191-205.

Barclay, H. J. 2001. Distribution of leaf orientations in six conifer species. *Canadian Journal of Botany*, 79 (4), 389-397.

Barr, A.G., Black, T.A., Hogg, E.H., Kljun, N., Morgenstern, K., and Nesic, Z. 2004. Inter-annual variability in the leaf area index of a boreal aspen-hazelnut forest in relation to net ecosystem production. *Agricultural and forest meteorology*, 126 (3), 237-255.

Beland, M., Widlowski, J.L., Fournier, R.A., Côté, J.F. and Verstraete, M.M. 2011. Estimating leaf area distribution in savanna trees from terrestrial LiDAR measurements. Agricultural and Forest Meteorology, 151(9), 1252-1266.

Beland, M., Widlowski, J.L. and Fournier, R.A. 2014a. A model for deriving voxel-level tree leaf area density estimates from ground-based LiDAR. Environmental Modelling and Software, 51, 184-189.

Beland, M., Baldocchi, D.D., Widlowski, J.L., Fournier, R.A. and Verstraete, M.M. 2014b. On seeing the wood from the leaves and the role of voxel size in determining leaf area distribution of forests with terrestrial LiDAR. *Agricultural and Forest Meteorology*, 184, 82-97.

Bourque, C.P.A., and Quazi, H.K. 2008. Leaf Area Index Review and Determination for the Greater Athabasca Oil Sands Region of Northern Alberta, Canada. *Report, Cumulative Environmental Management Association. Fort McMurray, Alberta*, 1-40.

Chen, J.M. and Black, T.A. 1991. Measuring leaf area index of plant canopies with branch architecture. *Agricultural and Forest Meteorology*, 57(1-3), 1-12.

Chen, J.M., and Black, T.A. 1992. Defining leaf area index for non-flat leaves. *Plant Cell and Environment*, 15, 421-429.

Chen, J.M., Rich, P.M., Gower, S.T., Norman, J.M., and Plummer, S. 1997a. Leaf area index of boreal forests: Theory, techniques, and measurements. Journal of Geophysical Research, 102(D24), 29429-29443.

Chen, J.M., Chen, X.Y., Ju, W.M., and Geng, X.Y. 2005. Distributed hydrological model for mapping evapotranspiration using remote sensing inputs. *Journal of Hydrology*, 305, 15-39.

Cleugh, H.A., Leuning, R., Mu, Q.Z., and Running, S.W. 2007. Regional evaporation estimates from flux tower and MODIS satellite data. *Remote Sensing of Environment*, 106, 285-304.

Davidson, D.P., Hall, R.J., Peddle, D.R. and Johnsonl, R.L.2000. A Comparison of Optical Methods for Estimating Leaf Area Index in Forest Stands. *22nd Annual Canadian Remote Sensing Symposium*, Canada, 653-659.

Dietz, J., Holscher, D., and Leuschner, C. 2006. Rainfall partitioning in relation to forest structure in differently managed montane forest stands in Central Sulawesi, Indonesia. *Forest Ecology and Management*, 237, 170-178.

Duchemin, B., Hadria, R., Erraki, S., Boulet, G., Maisongrande, P., Chehbouni, A., Escadafal, R., Ezzahar, J., Hoedjes, J.C.B., Kharrou, M.H., Khabba, S., Mougenot, B., Olioso, A., Rodriguez, J.C., and Simonneaux, V. 2006. Monitoring wheat phenology and irrigation in Central Morocco: on the use of relationships between evapotranspiration, crops coefficients, leaf area index and remotely-sensed vegetation indices. *Agricultural Water Management*, 79, 1-27.

Dufrene, E., Davi, H., Francois, C., Le Dantec, G., and Granier, A. 2005. Modelling carbon and water cycles in a beech forest: part I: Model description and uncertainty analysis on modelled NEE. *Ecological Modeling*, 185, 407-436.

Duursma, R.A., Kolari, P., Perämäki, M., Pulkkinen, M., Mäkelä, A., and Nikinmaa, E. 2009. Contributions of climate: leaf area index and leaf physiology tovariation in gross primary production of six coniferous forests across Europe: amodel-based analysis. *Tree Physiology*, 29, 621-639.

Eriksson, H., Eklundh, L., Hall, K., and Lindroth, A. 2005. Estimating LAI in deciduous forest stands. *Agricultural and Forest Meteorology*, 129(1), 27-37.

Fang, H., Li, W., Wei, S. and Jiang, C. 2014. Seasonal variation of leaf area index (LAI) over paddy rice fields in NE China: Intercomparison of destructive sampling, LAI-2200, digital hemispherical photography (DHP), and AccuPAR methods. *Agricultural and Forest Meteorology*, 198, 126-141.

Feng, D., Chen, J. M., Plummer, S., Chen, M., and Pisek, J. 2006. Algorithm for global leaf area index retrieval using satellite imagery. *IEEE Transactions Geoscience Remote Sensing*, 44 (8), 2219-2229.

Gobron, N. 2008. Leaf Area Index (LAI). *Terrestrial Essential Climate Variables for Climate Change Assessment, Mitigation and Adaptation, GTOS*, 52. FAO.

Gower, S.T., Vogel, J., Norman, J.M., Kucharik, C.J., Steele, S.J., and Stow, T.K. 1997. Carbon distribution and net primary production of aspen, jack pine and black spruce BOREAS forests. *Journal of Geophysical Research*, 102(D24), 29029-29041.

Hosoi, F. and Omasa, K. 2009. Factors contributing to accuracy in the estimation of the woody canopy leaf area density profile using 3D portable LiDAR imaging. *Journal of Experimental Botany*, 58(12), 3463-3473.

Hosoi, F. and Omasa, K. 2012. Estimation of vertical plant area density profiles in a rice canopy at different growth stages by high-resolution portable scanning LiDAR with a lightweight mirror. *ISPRS journal of photogrammetry and remote sensing*, 74, 11-19.

Hosoi, F., Nakai, Y. and Omasa, K. 2013. 3-D voxel-based solid modeling of a broad-leaved tree for accurate volume estimation using portable scanning LiDAR. *ISPRS journal of photogrammetry and remote sensing*, 82, 41-48.

Ishihara, M.I., and Hiura, T. 2011. Modeling leaf area index from litter collection and tree data in a deciduous broadleaf forest. *Agricultural and Forest Meteorology*, 151(7), 1016-1022.

Kim, A.M., Olsen, R.C. and Béland, M. 2015. Simulation of small footprint full waveform LIDAR propagation through a tree canopy in 3D. In *SPIE Defense+ Security* (pp. 94650K-94650K). International Society for Optics and Photonics.

Kucharik, C.J., Norman, J.M., Murdock, L.M., and Gower, S.T., 1997. Characterizing canopy non-randomness with a multiband vegetation imager (MVI). Journal of Geophysical Research, 102(D24), 29455-29473.

Kucharik, C.J., Norman, J.M., and Gower, S.T. 1998. Measurements of leaf orientation, light distribution and sunlit leaf area in a boreal aspen forest. *Agricultural and Forest Meteorology*, 91, 127-148.

Law, B.E., Van Tuyl, S., Cescatti, A. and Baldocchi, D.D. 2001. Estimation of leaf area index in open-canopy ponderosa pine forests at different successional stages and management regimes in Oregon. *Agricultural and Forest Meteorology*, 108(1), 1-14.

Leblanc, S.G., and Fournier, R.A. 2014. Hemispherical photography simulations with an architectural model to assess retrieval of leaf area index. *Agricultural and Forest Meteorology*, 194, 64-76.

Lefsky, M. A., Cohen, W. B., Acker, S. A., Parker, G. G., Spies, T. A., and Harding, D. 1999. LiDAR remote sensing of the canopy structure and biophysical properties of Douglas-fir western hemlock forests. *Remote Sensing of Environment*, 70(3), 339-361.

Lovell, J.L., Jupp, D.L.B., Culvenor, D.S., and Coops, N.C. 2003. Using airborne and ground-based ranging LiDAR to measure canopy structure in Australian forests. *Canadian Journal of Remote Sensing*, 29 (5), 607-622.

Lovell, J.L., Jupp, D.L.B., Newnham, G.J., and Culvenor, D.S. 2011. Measuring tree stem diameters using intensity profiles from ground-based scanning LiDAR from a fixed viewpoint. *ISPRS Journal of Photogrammetry and Remote Sensing*, 66(1), 46-55.

Ma, L., Zheng, G., Eitel, J.U., Magney, T.S. and Moskal, L.M. 2016a. Determining woody-to-total area ratio using terrestrial laser scanning (TLS). *Agricultural and Forest Meteorology*, 228, 217-228.

Ma, L., Zheng, G., Eitel, J.U., Moskal, L.M., He, W. and Huang, H. 2016b. Improved salient feature-based approach for automatically separating photosynthetic and nonphotosynthetic components within terrestrial LiDAR point cloud data of forest canopies. *IEEE Transactions on Geoscience and Remote Sensing*, 54(2), 679-696.

Maass, J., Vose, J.M., Swank, W.T., and Martínez-Yrízar, A. 1995. Seasonal changes of leaf area index (LAI) in a tropical deciduous forest in west Mexico. *Forest Ecology and Management*, 74(1), 171-180.

Macfarlane, C., Hoffman, M., Eamus, D., Kerp, N., Higginson, S., McMurtrie, R. and Adams, M. 2007. Estimation of leaf area index in eucalypt forest using digital photography. *Agricultural and Forest Meteorology*, 143(3), 176-188.

Martínez, B., García-Haro, F.J. and Camacho-de Coca, F. 2009. Derivation of high-resolution leaf area index maps in support of validation activities: Application to the cropland Barrax site. *Agricultural and forest meteorology*, 149 (1), 130-145.

McIntosh, A.C.S., Gray, A.N., and Garman, S.L. 2009. Canopy Structure on Forest Lands in Western Oregon: Differences Among Forest Types and Stand Ages. United States

Department of Agriculture, Forest Service, Pacific Northwest Research Station, General Technical Report PNW-GTR-794 August 2009.

Morsdorf, F., Kotz, B., Meier, E., Itten, K., Allgower, B., 2006. Estimation of LAI and fractional cover from small footprint airborne laser scanning data based on gap fraction. *Remote Sensing of Environment*. 104, 50-61.

Nasahara, K.N., Muraoka, H., Nagai, S. and Mikami, H. 2008. Vertical integration of leaf area index in a Japanese deciduous broad-leaved forest. *Agricultural and forest meteorology*, 148 (6), 1136-1146.

Norman, J.M. and Campbell, G.S. 1989. Canopy structure. In 'Plant physiological ecology: field methods and instrumentation'.(Eds RW Pearcy, J Ehleringer, HA Mooney, PW Rundel) 301–325.

Olivas, P.C., Oberbauer, S.F., Clark, D.B., Clark, D.A., Ryan, M.G., O'Brien, J.J. and Ordonez, H. 2013. Comparison of direct and indirect methods for assessing leaf area index across a tropical rain forest landscape. *Agricultural and forest meteorology*, 177, 110-116.

Olsoy, P. J., Glenn, N.F., Clark, P.E., and Derryberry, D.R. 2014. Aboveground total and green biomass of leaf-off land shrub derived from terrestrial laser scanning. *ISPRS Journal of Photogrammetry and Remote Sensing*, 88, 166-173.

Riaño, D., Valladares, F., Condés, S. and Chuvieco, E. 2004. Estimation of leaf area index and covered ground from airborne laser scanner (LiDAR) in two contrasting forests. *Agricultural and Forest Meteorology*, 124 (3), 269-275.

Ross, J. 1981. The radiation regime and architecture of plant stands. *The Hague*, 391.

Ryu, Y., Sonnentag, O., Nilson, T., Vargas, R., Kobayashi, H., Wenk, R., and Baldocchi, D.D. 2010. How to quantify tree leaf area index in an open savanna ecosystem: a multi-instrument and multi-model approach. *Agriculture and Forest Meteorology*, 150 (1), 63-76.

Sainte-Marie, J., Saint-André, L., Nouvellon, Y., Laclau, J.P., Roupsard, O., Le Maire, G., Delpierre, N., Henrot, A. and Barrandon, M. 2014. A new probabilistic canopy dynamics model (SLCD) that is suitable for evergreen and deciduous forest ecosystems. *Ecological modeling*, 290,121-133.

Schleppi, P., Conedera, M., Sedivy, I. and Thimonier, A. 2007. Correcting non-linearity and slope effects in the estimation of the leaf area index of forests from hemispherical photographs. *Agricultural and Forest Meteorology*, 144 (3), 236-242.

Song, Y., Maki, M., Imanishi, J. and Morimoto, Y. 2011. Voxel-based estimation of plant area density from airborne laser scanner data. In Proceedings of the ISPRS Workshop Laser Scanning, Calgary, Canada 38 (5/W12).

Strahler, A. H., Jupp, D. L. B., Woodcock, C. E., Schaaf, C. B., Yao, T., Zhao, F., Yang, X., Lovell, J., Culvenor, D., Newnham, G., Ni-Miester, W., and Boykin-Morris, W. 2008. Retrieval of forest structural parameters using a ground-based LiDAR instrument (Echidna (R). *Canadian Journal of Remote Sensing*, 34(2), S426-S440.

Styers, D.M., Moskal, L.M., Richardson, J.J. and Halabisky, M.A. 2014. Evaluation of the contribution of LiDAR data and post classification procedures to object-based classification accuracy. *Journal of Applied Remote Sensing*, 8(1), 1-17.

Takeda, T., Oguma, H., Sano, T., Yone, Y. and Fujinuma, Y. 2008. Estimating the plant area density of a Japanese larch (Larix kaempferi Sarg.) plantation using a ground-based laser scanner. *Agricultural and Forest Meteorology*, 148(3), 428-438.

Watson, D.J. 1947. Comparative physiological studies on the growth of field crops. I. Variation in net assimilation rate and leaf area between species and varieties, and within and between years. *Australian Journal of Botany*, 11, 41-76.

Weiss, M., Baret, F., Smith, G.J., Jonckheere, I. and Coppin, P. 2004. Review of methods for in situ leaf area index (LAI) determination: Part II. Estimation of LAI, errors and sampling. *Agricultural and Forest Meteorology*, 121(1), 37-53.

Widlowski, J.L., Côté, J.F. and Béland, M. 2014. Abstract tree crowns in 3D radiative transfer models: Impact on simulated open-canopy reflectances. *Remote Sensing of Environment*, 142, 155-175.

Yue, C., Ciais, P., Luyssaert, S., Cadule, P., Harden, J., Randerson, J., Bellassen, V., Wang, T., Piao, S., Poulter, B., and Viovy, N. 2013. Simulating boreal forest carbon dynamics after stand-replacing fire disturbance: insights from a global process-based vegetation model. *Biogeoscience*, 10, 8233-8252.

Zhao, K., García, M., Liu, S., Guo, Q., Chen, G., Zhang, X., Zhou, Y. and Meng, X. 2015. Terrestrial LiDAR remote sensing of forests: Maximum likelihood estimates of canopy

profile, leaf area index, and leaf angle distribution. *Agricultural and Forest Meteorology*, 209, 100-113.

Zheng, G., Chen, J.M., Tian, Q., Ju, W.M., and Xia, X.Q. 2007. Combining remote sensing imagery and forest age inventory for biomass mapping. Journal of Environmental Management, 85, 616-623.

Zheng, G. and Moskal, L.M. 2012a. Computational-geometry-based retrieval of effective leaf area index using terrestrial laser scanning. *IEEE Transactions on Geoscience and Remote Sensing*, 50(10), 3958-3969.

Zheng, G. and Moskal, L.M. 2012b. Leaf orientation retrieval from terrestrial laser scanning (TLS) data. *IEEE Transactions on Geoscience and Remote Sensing*, 50(10), 3970-3979.

Zheng, G. and Moskal, L.M. 2012c. Spatial variability of terrestrial laser scanning based leaf area index. *International Journal of Applied Earth Observation and Geoinformation*, 19, 226-237.

Zheng, G., Moskal, L.M. and Kim, S.H. 2013. Retrieval of effective leaf area index in heterogeneous forests with terrestrial laser scanning. IEEE Transactions on Geoscience and Remote Sensing, 51(2), 777-786.

Zheng, G., Ma, L., He, W., Eitel, J.U., Moskal, L.M. and Zhang, Z. 2016. Assessing the contribution of woody materials to forest angular gap fraction and effective leaf area index using terrestrial laser scanning data. *IEEE Transactions on Geoscience and Remote Sensing*, 54(3), 1475-1487.

CHAPTER 5

Contributions, Conclusions, and Future Work

5.1 Conclusions

The main objective of this Ph.D. dissertation was to develop new algorithms to assess the forest structure properties using terrestrial LiDAR data in a Canadian boreal forest. In this context, this study mainly focuses on developing new algorithms for creating high-resolution Digital Terrain Model (DTM) in a dense forest, separating photosynthetic and non-photosynthetic components in Point Cloud Data (PCD) and finally a calculation of the Leaf Area Index (LAI) which is a significant forest structure parameter. The main contributions, conclusions, and related future work for each chapter in the present thesis are summarized as follows;

Chapter 2. Retrieving a Digital Terrain Model (DTM) in a Boreal Forest Using Ground-Based LiDAR

The PCD collected by discrete Ground-based LiDAR from a forest has the potential for generation of DTM with a high spatial resolution due to its fixed platform and high data density (Slob and Hack, 2004; Prokop, 2008; Entwistle et al, 2009; Ergun, 2010; Abellán e al. 2014). This is generally a challenging task since discrete LiDAR only records the first reflection of a laser beam and hence ground points under the vegetation might be missed (Tyagur and Hollaus, 2016). However, appropriate application of mathematical tools in our proposed algorithm solves this problem. A new simple algorithm in MATLAB® software was developed for automatic DTM generation. It utilizes median filtering for retrieving missed ground points and introduces a new score for assessment of the quality of DTM profile which is based on local slopes. The input of the algorithm is the high spatial resolution PCD which is slightly post-processed for removing noise such as sun glare. The errors associated with LiDAR classification on different data contexts, such as point density, terrain slope, shadowing effect, and land cover type, were assessed. The accuracy analysis of filtering results from the random sample datasets showed that

only 0.07 % errors were committed by the filter algorithm. The algorithm was successful in processing the PCD from various cross-sections of a plot study at the Peace River Environmental Monitoring Super Site, Peace River (PR-EMSS), Alberta. Our study plot consists of a terrain with different surface areas offering very low qualitative and quantitative (omission/commission) errors. The algorithm performance was acceptable in the low complexity of land features such as smooth slopes, light vegetation and high density of visible ground points. This work is the first application of discrete ground-based LiDAR on a forest area for DTM.

The core of the proposed algorithm can be modified for generation of other topographic maps such as Canopy Height Model (CHM) and Canopy Surface Model (CSM). These maps are essential for forest management and industrial planning (Fisher and Tate, 2006; Farid et al. 2008; Gonzalez et al. 2010). However, generation of DTM is a prerequisite for CHM and CSM.

Chapter 3. Automatic Separation of Photosynthetic and Non-Photosynthetic Components in a Point Cloud Data from a Boreal Forest Canopy

Accurate separation of photosynthetic and non-photosynthetic components is an essential step for calculation of significant canopy assessment parameters such as leaf area index and also green biomass (Beland et al. 2011). Without separation of photosynthetic from non-photosynthetic components, a different parameter (plant area index) is calculated instead of leaf area index (Takeda et al. 2008; Olivasa et al. 2013; Pueschel et al. 2014).

This chapter is focused on developing an algorithm for automatic, simple, and efficient separation of photosynthetic from non-photosynthetic materials. The algorithm doesn't require the collection of extra information on temporal characteristics such as seasonal data, laser wavelength, or tree distance. The algorithm is based on an absorption intensity parameter which is calculated for every point using its raw intensity and its distance to the station. To evaluate the performance of the filtering method and examine the errors, both qualitative and quantitative analyses were employed in this study (Sithole and Vosselman, 2004). The separated photosynthetic PCD is ready for processing by the algorithm developed in chapter 4 for calculation of LAI.

Chapter 4. Calculation of Leaf Area Index in a Canadian Boreal Forest Using Ground-Based LiDAR

LAI is an indicator of forest dynamics and ecological processes such as balance of the global carbon exchange, energy cycle in photosynthesis, evapotranspiration mechanisms, precipitation interception, and water/nutrient cycling (Chen et al. 2005; Dufrene et al. 2005; Dietz et al. 2006; Cleugh et al. 2007; Zheng et al. 2007; Gobron, 2008; Duursma et al. 2009; Yue et al. 2013; Sainte-Marie et al. 2014). The current state of the art offers algorithms for LAI calculation from ground-based LiDAR PCD. These methods divide the PCD into smaller equisize cubic collections called voxels. Then, they take advantage of intermediate auxiliary mathematical models such as radiative transfer and gap fraction model for indirect calculation of LAI (Chen and Black, 1991; Eriksson et al. 2005; Hosoi and Omasa, 2009; Widlowski et al. 2014; Fang et al. 2014; Beland et al. 2014a). The mentioned methods are complicated and prone to a high level of error. A common denominator from these studies is that the effect of LiDAR scan sampling resolution is ignored.

In this chapter, these aforementioned drawbacks are addressed and a new algorithm is developed. Instead of using auxiliary models, LAI is calculated directly. This algorithm calculates LAI simply. The green PCD generated by the separation algorithm in chapter 3 is delivered to the LAI algorithm developed in this chapter. In the proposed algorithm, the PCD of an individual tree is divided into *adaptive* voxels which gradually vary in lateral size from the bottom of the trunk to the top of crown; the proposed voxelization scheme doesn't need a large outer confining box. Instead, PCD is vertically sliced and then divided to an array of pixels. Also, the redundant voxels are minimized and the number of empty voxels doesn't affect the calculations. LAI is calculated directly from each voxel, in order to remove the errors associated with radiative transfer model, gap fraction, and extinction factor.

The results of the present study also show that one scanning station is not appropriate for delivering the spatial distribution of point density to estimate LAI. With an increase of scan stations from 1 to 6 the LAI changes from 1.91 to 3.24. LAI values from 4 stations are well within the range of 3.32 presented in the literature for boreal forests. We recommend using at least 4 scan stations to keep the LAI measurement and calculation error within minimum error while minimizing the occlusion effect. The results from this chapter also showed that using larger adaptive voxels results in very large LAI values. With adaptive voxeling ($u = 10.res_k$), the average voxel size is 96% larger that the voxels of fixed size ($u = 10\overline{res}$). Hence, the total number of voxels required to process the whole PCD is lower. This is of ultimate significance

especially in case of assessment of a forest stand with a wide area which shall result in a point cloud with tens of millions of points.

5.2 Limitations to Research Projects

There are several sources of error that affect the accuracy of LiDAR measurements. Potential sources of error are the water drops, wind, sun-glare, co-registration, and topography.

Water drops: The presence of water drops on leaves, branches, and trunk originating from dew or rain shower can severely affect the reflection of the laser beam and disrupt the PCD. Hence, some points might be eliminated from PCD due to absorption of the laser in water. Even if the laser beam survives the extra attenuation, the point intensity is highly affected by the water droplet. This can affect the procedure of separation of photosynthetic from non-photosynthetic components.

Wind: Wind breeze can cause slight trembling and movement of leaves and thin branches. This can result in an inaccurate PCD or generate extra points which cause a problem in data processing.

Sun glare: Sunbeam contains all wavelengths of visible light including 532 nm. While scanning, as the laser transmitter/receiver points toward the sun, a lot of energy are received which adds a huge amount of points in an approximately conical shape to the PCD. Hence, the data collection is recommended to be carried out on cloudy days. As an alternative, the points belonging to sun glare can be manually omitted from PCD before the processing steps.

Co-registration: When an operator tries to manually collect the PCD's gathered from several stations into a single PCD, several reference targets are used. This manual operation in Cyclone or Cloud Compare® software might involve some level of error depending on operator skills.

Topography: For forest stands over hilly areas, some tree features might be missed by LiDAR laser beams. This results in an incomplete PCD which leads to inaccurate canopy parameters. Especially in case of DTM generation, some land extents might be missed.

5.3 Future Work

5.3.1 Retrieving Canopy Height Model (CHM) and Above Ground Biomass (AGB)

Forest attributes such as canopy height can be directly retrieved from LiDAR data. Retrieving canopy height provides data to estimate canopy volume and above-ground biomass. The vertical structure of forest ecosystems also provides opportunities for enhanced forest management, monitoring, and planning. As a future work, a canopy height model can be developed to estimate above-ground biomass. Also, future research can be dedicated to the analysis of the error distribution in DTM generation, as this error can be transmitted consequently into derived products including Canopy Height Models, vegetation biomass, Leaf Area Index (LAI), and carbon storage.

5.3.2 Enhancing the Algorithm Performance in the Context of Noise Removing and Leaf Identification Features

Current versions of the algorithms require slight pre-processing of the PCD. As an example, sun-glare is manually omitted from the PCD. This is a simple task which can be carried out by any software with the 3D visual representation of point clouds. As a future work, with the objective of having fully automated algorithms, instead of manual sun-glare removal, an extra module can be designed and added to the beginning of current algorithms. This extra module should have the ability to detect sun-glare points based on their usual overall geometry, point intensity, or point elevation and omit them from the PCD.

As another future work, to enhance the algorithm performance, several extra modules can be added to the code. As an example, machine learning techniques can be applied for leaf identification inside each voxel. To do this, a sample leaf is scanned by LiDAR at several different angles of 0°, 45°, and 90° in relation to laser beam direction. Then, the leaf identifier module is trained by prototype PCD from scanned leaves. Finally, this module can search inside every voxel and find the leaves based on their specifications.

5.3.3 Correcting for the Angle of Incidence and the Wind Effect

As a future work, the methods developed in this chapter can be improved to consider more practical settings such as the incidence angle of the laser beam and the wind effect. In the current state of the art, these factors are ignored due to the complexity in considering their effect in the PCD. To consider the effect of beam angle, the physical phenomena of laser beam reflection over biomass should be studied and modeled. This phenomenon generally depends on the texture of the target surface which might be soft, stiff, or rough, the laser beam diameter, and the normal vector of the target surface. Since the PCD offers a high point density data, the hitting surface can be identified using neighboring points and the normal vector can be calculated by analytical geometry techniques. This procedure can be added to current algorithms as an extra module.

The wind can also strongly disturb the recorded PCD. As an example, if wind gusts cause movement of a single leaf, laser beam might hit it in more points than usual. This will result in more points in PCD, higher leaf area and consequently the calculated leaf area index will be larger. As a future project, the effect of wind can be minimized by identifying repeated points in PCD. The signature of every single point is its point intensity. This can be done by examining the intensity of a point and comparing it with adjacent points.

5.3.4 Expanding the Sample Species and Sites

The application of the proposed method to a cross-section of the forest from a single and multiple scan stations shall be the subject of a future work, where we shall compare the calculated canopy parameters of different individual trees with forest stands of various areas. In the present study, only perpendicular sunbeam radiation over canopy ($\theta = 0$) is studied. Oblique sunbeam shall be the topic of a future research.

As a future industrial direction, the three algorithms developed in this thesis can be integrated into the software of commercial LiDAR scan stations for simple access, quick processing, and widespread use.

References

Abellán, A., Oppikofer, T., Jaboyedoff, M. Rosser, N.J., Lim, M., and Lato, M.J. 2014. Terrestrial laser scanning of rock slope instabilities. *Earth Surface Processes and Landforms*, 39, 80-97.

Beland, M., Widlowski, J.L. and Fournier, R.A. 2014a. A model for deriving voxel-level tree leaf area density estimates from ground-based LiDAR. *Environmental Modelling and Software*, 51, 184-189.

Beland, M., Widlowski, J.L., Fournier, R.A., Côté, J. F., and Verstraete, M.M. 2011. Estimating leaf area distribution in savanna trees from terrestrial LiDAR measurements. *Agricultural and Forest Meteorology*, 151, 1252-1266.

Chen, J.M. and Black, T.A. 1991. Measuring leaf area index of plant canopies with branch architecture. *Agricultural and Forest Meteorology*, 57(1-3), 1-12.

Chen, J.M., Rich, P.M., Gower, S.T., Norman, J.M., and Plummer, S. 1997. Leaf area index of boreal forest: theory, techniques, and measurements. *Journal of Geophysical Research*, 102 (D24), 29429-29443.

Cleugh, H.A., Leuning, R., Mu, Q.Z., and Running, S.W. 2007. Regional evaporation estimates from flux tower and MODIS satellite data. *Remote Sensing of Environment*, 106, 285-304.

Dietz, J., Holscher, D., Leuschner, C., and Hendrayanto, 2006. Rainfall partitioning in relation to forest structure in differently managed montane forest stands in Central Sulawesi, Indonesia. *Forest Ecology and Management*, 237, 170-178.

Dufrene, E., Davi, H., Francois, C., Le Dantec, G., and Granier, A. 2005. Modelling carbon and water cycles in a beech forest: part I: Model description and uncertainty analysis on modeled NEE. *Ecological Modeling*, 185, 407-436.

Duursma, R.A., Kolari, P., Perämäki, M., Pulkkinen, M., Mäkelä, A., and Nikinmaa, E. 2009. Contributions of climate: leaf area index and leaf physiology to variation in gross primary production of six coniferous forests across Europe: a model-based analysis. *Tree Physiology*, 29, 621-639.

Entwistle, J., McCaffrey, K., and Abrahams, P. 2009. Three-dimensional (3D) visualisation: The application of terrestrial laser scanning in the investigation of historical Scottish farming townships. *Journal of Archaeological Science*, 36, 860–866.

Ergun, B. 2010. A novel 3D geometric object filtering function for application in indoor area with terrestrial laser scanning data. *Optics and Laser Technology*, 42, 799–804.

Eriksson, H., Eklundh, L., Hall, K., and Lindroth, A. 2005. Estimating LAI in deciduous forest stands. *Agricultural and Forest Meteorology*, 129(1), 27-37.

Fang, H., Li, W., Wei, S. and Jiang, C. 2014. Seasonal variation of leaf area index (LAI) over paddy rice fields in NE China: Intercomparison of destructive sampling, LAI-2200, digital hemispherical photography (DHP), and AccuPAR methods. *Agricultural and Forest Meteorology*, 198, 126-141.

Farid, A., Goodrich, D.C., Bryant, R., and Sorooshian, S. 2008. Using airborne lidar to predict leaf area index in cottonwood trees and refine riparian water-use estimates. *Journal of Arid Environments*, 72, 1-15.

Fisher, P.F., and Tate, N.J. 2006. Causes and consequences of error in digital elevation models. *Progress in Physical Geography*, 30, 467-489.

Gobron, N. 2008. Leaf Area Index (LAI). *Terrestrial Essential Climate Variables for Climate Change Assessment, Mitigation and Adaptation, GTOS*, 52. FAO.

Gonzalez, P., Asner, G.P., Battles, J.J., Lefsky, M.A., Waring, K.M., and Palace, M. 2010. Forest carbon densities and uncertainties from lidar, QuickBird, and field measurements in California. *Remote Sensing of Environment*, 114, 1561-1575.

Hosoi, F. and Omasa, K. 2009. Factors contributing to accuracy in the estimation of the woody canopy leaf area density profile using 3D portable LiDAR imaging. *Journal of Experimental Botany*, 58(12), 3463-3473.

Olivasa, P.C., Oberbauera, S.F., Clarkc, D.B., Clarkc, D.A., Ryand, M.G., O'Brienf, J.J., and Ordo˜nezg, H. 2013. Comparison of direct and indirect methods for assessing leaf area index across a tropical rain forest landscape. *Agricultural and Forest Meteorology*, 177, 110-116.

Pirotti, F., and Tarolli, P. 2010. Suitability of LiDAR point density and derived landform curvature maps for channel network extraction. *Hydrological Processes*, 24, 1187-1197.

Prokop, A. 2008. Assessing the applicability of terrestrial laser scanning for spatial snow depth measurements. *Cold Regions Science and Technology*, 54, 155-163.

Pueschel, P., Newnham, G., and Hill, J. 2014. Retrieval of Gap Fraction and Effective Plant Area Index from Phase-Shift Terrestrial Laser Scans. *Remote Sensing*, 6, 2601-2627.

Sainte-Marie, J., Saint-André, L., Nouvellon, Y., Laclau, J.P., Roupsard, O., Le Maire, G., Delpierre, N., Henrot, A. and Barrandon, M. 2014. A new probabilistic canopy dynamics model (SLCD) that is suitable for evergreen and deciduous forest ecosystems. *Ecological modeling*, 290,121-133.

Slob, S., Hack, R. 2004. 3D terrestrial laser scanning as a new field measurement and monitoring technique. *Engineering geology for infrastructure planning in Europe*, 179-189.

Takeda, T., Oguma, H., Sano, T., Yone, Y., and Fujinuma, Y. 2008. Estimating the plant area density of a Japanese larch (Larix kaempferi Sarg.) plantation using a ground-based laser scanner. *Agriculture and Forest Meteorology*, 148 (3), 428-438.

Tyagur, N. and Hollaus, M. 2016. Digital terrain models from mobile laser scanning data in Moravian Karst. *International Archives of the Photogrammetry, Remote Sensing and Spatial Information Sciences*, 387-394.

Widlowski, J.L., Côté, J.F. and Béland, M. 2014. Abstract tree crowns in 3D radiative transfer models: Impact on simulated open-canopy reflectances. *Remote Sensing of Environment*, 142, 155-175.

Yue, C., Ciais, P., Luyssaert, S., Cadule, P., Harden, J., Randerson, J., Bellassen, V., Wang, T., Piao, S., Poulter, B., and Viovy, N. 2013. Simulating boreal forest carbon dynamics after stand-replacing fire disturbance: insights from a global process-based vegetation model. *Biogeoscience*, 10, 8233-8252.

Zheng, G., Chen, J.M., Tian, Q., Ju, W.M., and Xia, X.Q. 2007. Combining remote sensing imagery and forest age inventory for biomass mapping. *Journal of Environmental Management*, 85, 616-623.

BIBLIOGRAPHY

Abellán, A., Oppikofer, T., Jaboyedoff, M. Rosser, N.J., Lim, M., and Lato, M.J. 2014. Terrestrial laser scanning of rock slope instabilities. *Earth Surface Processes and Landforms*, 39, 80-97.

Andersen, H.E., Reutebuch, R.E., and McGaughey, R.J. 2006. A rigorous assessment of tree height measurements obtained using airborne lidar and conventional field methods. *Canadian Journal of Remote Sensing*, 32, 355-366.

Anjin, C., Yongmin, K., Yongil, K. and Yangdam, E. 2012. Estimation of individual tree biomass from airborne lidar data using tree height and crown diameter. *Disaster Advances*, 5(4), 360-365.

Arnold, N., Rees, W., Devereux, B., and Amable, G. 2006. Evaluating the potential of high-resolution airborne LIDAR data in glaciology. *International Journal of Remote Sensing*, 27, 1233-1251.

Askne, J.I.H., Soja, M.J., and Ulander, L.M.H. 2017. Biomass estimation in a boreal forest from TanDEM-X data, lidar DTM, and the interferometric water cloud model. *Remote Sensing of Environment*, 196, 265-278.

Asner, G.P., Scurlock, J.M. and A Hicke, J. 2003. Global synthesis of leaf area index observations: implications for ecological and remote sensing studies. *Global Ecology and Biogeography*, 12(3), pp.191-205.

Axelsson, P. 1999. Processing of laser scanner data algorithms and applications. *ISPRS Journal of Photogrammetry and Remote Sensing*, 54 (2–3), 138-147.

Axelsson, P. 2000. DEM Generation from Laser Scanner Data Using Adaptive TIN Models. *International Archive of Photogrammetry, Remote Sensing and Spatial Information Sciences (ISPRS)*, 33 (B4), 110-117.

Bamber, J.L., and Rivera, A. 2007. A review of remote sensing methods for glacier mass balance determination. *Global Planet Change*, 59, 138-148.

Barclay, H. J. 2001. Distribution of leaf orientations in six conifer species. *Canadian Journal of Botany*, 79 (4), 389-397.

Barr, A.G., Black, T.A., Hogg, E.H., Kljun, N., Morgenstern, K., and Nesic, Z. 2004. Inter-annual variability in the leaf area index of a boreal aspen-hazelnut forest in relation to net ecosystem production. *Agricultural and forest meteorology*, 126 (3), 237-255.

Bartels, M., Wei, H., and Mason, D. C. 2006. DTM Generation from LIDAR Data using Skewness Balancing. *Proceedings of the 18th International Conference on Pattern Recognition (ICPR'06)* 0-7695-2521-0/06. IEEE.

Bartels, M., and Wei, H. 2010. Threshold-free object and ground point separation in LiDAR data. *Pattern Recognition Letters*, 31 (10), 1089-1099.

Bauwens, S., Bartholomeus, H., Calders, K., and Lejeune, P. (2016). Forest Inventory with Terrestrial LiDAR: A Comparison of Static and Hand-Held Mobile Laser Scanning. *Forests*, 7 (127), 1-17.

Beaumier, C., and Idrissa, M. 2016. Digital terrain models derived from digital surface model uniform regions in urban areas. *International Journal of Remote Sensing*, 37 (15), 3477-3493. http://dx.doi.org/10.1080/01431161.2016.1182666.

Beer, C., Reichstein, M., Tomelleri, E., Ciais, P., Jung, M., Carvalhais, N., Rödenbeck, C., Arain, M.A., Baldocchi, D., Bonan, G.B. and Bondeau, A. 2010. Terrestrial gross carbon dioxide uptake: global distribution and covariation with climate. *Science*, 329(5993), 834-838.

Behera, M. D., and Roy, P. S. 2002. Lidar remote sensing for forestry applications: The Indian context. *Current Science*, 83 (11), 1320-1328.

Beland, M., Widlowski, J.L., Fournier, R.A., Côté, J. F., and Verstraete, M.M. 2011. Estimating leaf area distribution in savanna trees from terrestrial LiDAR measurements. *Agricultural and Forest Meteorology*, 151, 1252-1266.

Beland, M., Widlowski, J.L. and Fournier, R.A. 2014a. A model for deriving voxel-level tree leaf area density estimates from ground-based LiDAR. *Environmental Modelling and Software*, 51, 184-189.

Beland, M., Baldocchi, D.D., Widlowski, J.L., Fournier, R.A. and Verstraete, M.M. 2014b. On seeing the wood from the leaves and the role of voxel size in determining leaf area distribution of forests with terrestrial LiDAR. *Agricultural and Forest Meteorology*, 184, 82-97.

Beumier, C., and Idrissa, M. 2016. Digital terrain models derived from digital surface model uniform regions in urban areas. *International Journal of Remote Sensing*, 37 (15), 3477-3493.

Bourque, C.P.A., and Quazi, H.K. 2008. Leaf Area Index Review and Determination for the Greater Athabasca Oil Sands Region of Northern Alberta, Canada. *Report, Cumulative Environmental Management Association. Fort McMurray, Alberta*, 1-40.

BreÂda, N.J.J. 2003. Ground-based measurements of leaf area index: a review of methods, instruments and current controversies. *Journal of Experimental Botany*, 54 (392), 2403-2417.

Brovelli, M.A., Cannata, M., and Longoni, U.M. 2002. Managing and processing LIDAR data within GRASS. *Proceedings of the Open source GIS* - GRASS users conference, Trento, Italy.

Brown, M.J., and Parker, G.G. 1994. Canopy light transmittance in a chronosequence of mixed-species deciduous forests. *Canadian Journal of Forest Research*, *24*(8), 1694-1703.

Chehata, N., Guo, L., and Mallet, C. 2009. Airborne LIDAR feature selection for urban classification using random forests. *International Archive of Photogrammetry, Remote Sensing and Spatial Information Sciences*, 38, 207-212.

Chen, J.M. and Black, T.A. 1991. Measuring leaf area index of plant canopies with branch architecture. *Agricultural and Forest Meteorology*, 57(1-3), 1-12.

Chen, J.M., and Black, T.A. 1992. Defining leaf area index for non-flat leaves. *Plant Cell and Environment*, 15, 421-429.

Chen, J. M., Rich, P. M., Gower, S. T., Norman, J. M., and Plummer, S. 1997. Leaf area index of boreal forests: Theory, techniques, and measurements. *Geophysical Research Atmospheres*, 102 (D24), 29429-29443.

Chen, J.M., Chen, X.Y., Ju, W.M., and Geng, X.Y. 2005. Distributed hydrological model for mapping evapotranspiration using remote sensing inputs. *Journal of Hydrology*, 305, 15-39.

Chen, Q. 2007. Airborne LIDAR data processing and information extraction. *Photogrammetric Engineering and Remote Sensing*, 73, 109–112.

Chen, Z., Xu, B., and Gao, B. 2016. An Image-Segmentation-Based Urban DTM Generation Method Using Airborne LiDAR Data. *IEEE, journal of selected topics in applied earth observations and remote sensing*, 9 (1), 496-506.

Clawges, R., Vierling, L., Calhoon, M., and Toomey, M. 2007. Use of a ground based scanning lidar for estimation of biophysical properties of western larch (*Larix occidentalis*). *International Journal of Remote Sensing*, 28 (19), 4331-4344.

Cleugh, H.A., Leuning, R., Mu, Q.Z., and Running, S.W. 2007. Regional evaporation estimates from flux tower and MODIS satellite data. *Remote Sensing of Environment*, 106, 285-304.

Cleveland, W.S., and Loader, C.L. 1996. Smoothing by local regression: Principles and methods. In *Statistical Theory and Computational Aspects of Smoothing*. New York, NY, USA: Springer-Verlag, 10-49.

Côté, J.F., Fournier, R.A., Frazer, G.W. and Niemann, K.O. 2012. A fine-scale architectural model of trees to enhance LiDAR-derived measurements of forest canopy structure. *Agricultural and Forest Meteorology*, 166, 72-85.

Cothrun C. The Technical Side: Dual Axis Compensators. Available online: http://www.krcmar.ca/sites/default/files/1995_Spring_Dual%20Axis%20Compensators_1.pdf (accessed on 18 December 2016).

Danson, F.M., and Curran, P.J. 1993. Factors affecting the remotely sensed response of coniferous forest plantations. *Remote Sensing of Environment*, 43, 55-65.

Danson, F.M., Hetherington, D., Morsdorf, F., Koetz, B., and Allgower, B. 2007. Forest canopy gap fraction from terrestrial laser scanning. *IEEE Geoscience and Remote Sensing Letter*, 4, 157-160.

Davidson, D.P., Hall, R.J., Peddle, D.R. and Johnsonl, R.L.2000. A Comparison of Optical Methods for Estimating Leaf Area Index in Forest Stands. *22nd Annual Canadian Remote Sensing Symposium*, Canada, 653-659.

Dietz, J., Holscher, D., and Leuschner, C. 2006. Rainfall partitioning in relation to forest structure in differently managed montane forest stands in Central Sulawesi, Indonesia. *Forest Ecology and Management*, 237, 170-178.

Donoghue, D.N.M., Watt, P.J., Cox, N.J., and Wilson, J. 2007. Remote sensing of species mixtures in conifer plantations using LiDAR height and intensity data. *Remote Sensing of Environment*, 110, 509-522.

Drake, J.B., Dubayah, R.O., Clark, D.B., Knox, R.G., Blair, J.B., Hofton, M.A., and Prince, S. 2002. Estimation of tropical forest structural characteristics using large footprint lidar. *Remote Sensing of Environment*, 79 (2), 305-319.

Dubayah R.O., and Drake J.B. (2000). LiDAR Remote Sensing for Forestry. *Journal of Forestry*, 98 (6), 44-46.

Ducey, M.J., Astrup, R., Seifert, S., Pretzsch, H., Larson, B.C., and Coates, K.D. 2013. Comparison of forest attributes derived from two terrestrial Lidar systems. *Photogrammetric Engineering and Remote Sensing*, 79 (3):245-257.

Duchemin, B., Hadria, R., Erraki, S., Boulet, G., Maisongrande, P., Chehbouni, A., Escadafal, R., Ezzahar, J., Hoedjes, J.C.B., Kharrou, M.H., Khabba, S., Mougenot, B., Olioso, A., Rodriguez, J.C., and Simonneaux, V. 2006. Monitoring wheat phenology and irrigation in Central Morocco: on the use of relationships between evapotranspiration, crops coefficients, leaf area index and remotely-sensed vegetation indices. *Agricultural Water Management*, 79, 1-27.

Dufrene, E., Davi, H., Francois, C., Le Dantec, G., and Granier, A. 2005. Modelling carbon and water cycles in a beech forest: part I: Model description and uncertainty analysis on modelled NEE. *Ecological Modeling*, 185, 407-436.

Duursma, R.A., Kolari, P., Perämäki, M., Pulkkinen, M., Mäkelä, A., and Nikinmaa, E. 2009. Contributions of climate: leaf area index and leaf physiology tovariation in gross primary production of six coniferous forests across Europe: amodel-based analysis. *Tree Physiology*, 29, 621-639.

Eitel, J.U.H., Long, D.S., Gessler, P.E., Hunt, E.R., and Brown, D.J. 2009. Sensitivity of ground-based remote sensing estimates of wheat chlorophyll content to variation in soil reflectance. *Soil Science Society of America Journal*, 73, 1715-1723.

Eitel, J.U.H., Vierling, L.A., and Long, D.S. 2010. Simultaneous measurements of plant structure and chlorophyll content in broadleaf saplings with a terrestrial laser scanner. Remote Sensing of Environment, 114, 2229-2237.

Eitel, J.U.H., Magney, T.S., Vierling, L. A., and Dittmar, G. 2014. Assessment of crop foliar nitrogen using a novel dual-wavelength laser system and implications for conducting laser-based plant physiology. *ISPRS Journal of Photogrammetry and Remote Sensing*, 97, 229-240.

Elmqvist, M. 2002. Ground Surface Estimation from Airborne Laser Scanner Data Using Active Shape Models. *International Archives of the Photogrammetry, Remote Sensing and Spatial Information Sciences*, 34 (3A), Commission III, 09–13, Graz, Austria, 115-118.

El-Sheimy, N., Valeo, C., and Habib, A. 2005. *Digital Terrain Modeling*. Artech House, Boston, Mass. pp. 266.

Entwistle, J., McCaffrey, K., and Abrahams, P. 2009. Three-dimensional (3D) visualisation: The application of terrestrial laser scanning in the investigation of historical Scottish farming townships. *Journal of Archaeological Science*, 36, 860–866.

Ergun, B. 2010. A novel 3D geometric object filtering function for application in indoor area with terrestrial laser scanning data. *Optics and Laser Technology*, 42, 799–804.

Eriksson, H., Eklundh, L., Hall, K., and Lindroth, A. 2005. Estimating LAI in deciduous forest stands. *Agricultural and Forest Meteorology*, 129(1), 27-37.

Evans, J.S., and Hudak, A.T. 2007. A multiscale curvature algorithm for classifying discrete return LiDAR in forested environments. *IEEE Transactions on Geoscience and Remote Sensing*, 45 (4), 1029-1038.

Fang, H., Li, W., Wei, S. and Jiang, C. 2014. Seasonal variation of leaf area index (LAI) over paddy rice fields in NE China: Intercomparison of destructive sampling, LAI-2200, digital hemispherical photography (DHP), and AccuPAR methods. *Agricultural and Forest Meteorology*, 198, 126-141.

FAO, 2006. Global Forest Resources Assessment 2005. FAO Forestry Paper 147, Food and Agriculture Organization of the United Nations, Rome, Italy.

Farid, A., Goodrich, D.C., Bryant, R., and Sorooshian, S. 2008. Using airborne lidar to predict leaf area index in cottonwood trees and refine riparian water-use estimates. *Journal of Arid Environments*, 72, 1-15.

Feng, D., Chen, J. M., Plummer, S., Chen, M., and Pisek, J. 2006. Algorithm for global leaf area index retrieval using satellite imagery. *IEEE Transactions Geoscience Remote Sensing*, 44 (8), 2219-2229.

Filin, S., and Pfeifer, N. 2006. Segmentation of airborne laser scanning data using a slope adaptive neighborhood. *ISPRS International Archives of the Photogrammetry, Remote Sensing and Spatial Information Sciences*, 60, 71–80.

Fisher, P.F., and Tate, N.J. 2006. Causes and consequences of error in digital elevation models. *Progress in Physical Geography*, 30, 467-489.

Flood, M., and Gutelis, B. 1997. Commercial implications of topographic terrain mapping using scanning airborne laser radar. *Photogrammetric Engineering and Remote Sensing*, 63, 327-366.

Food Agric. Organ. (FAO). 2010. Global forest resources assessment. *Forestry Paper* 163, FAO, Rome, Italy.

Fournier, R.A., Mailly, D., Walter, J.M.N. and Soudani, K. 2003. Indirect measurement of forest canopy structure from in situ optical sensors. *Remote sensing of forest environments,* 77-113, Springer US.

Franklin, J. 1986. Thematic mapper analysis of coniferous forest structure and composition. *International Journal of Remote Sensing*, 7, 1287-1301.

Gao, B. 1996. NDWI- A normalized difference water index for remote sensing of vegetation liquid water from space. *Remote Sensing of Environment*, 58 (3), 257-266.

Gemmell, F.M. 1995. Effects of forest cover, terrain and scale on timber volume estimation with thematic mapper data in a Rocky Mountain site. *Remote Sensing of Environment*, 51, 291-305.

Gobron, N. 2008. Leaf Area Index (LAI). *Terrestrial Essential Climate Variables for Climate Change Assessment, Mitigation and Adaptation, GTOS*, 52. FAO.

Goetz, S.J., Prince, S.D., Small, J., and Gleason, A.C.R., 2000. Interannual variability of global terrestrial primary production: results of a model driven with satellite observations. *Journal of Geophysical Research-Atmospheres,* 105, 20077-20091.

Gonzalez, P., Asner, G.P., Battles, J.J., Lefsky, M.A., Waring, K.M., and Palace, M. 2010. Forest carbon densities and uncertainties from lidar, QuickBird, and field measurements in California. *Remote Sensing of Environment*, 114, 1561-1575.

Gower, S.T., Vogel, J., Norman, J.M., Kucharik, C.J., Steele, S.J., and Stow, T.K. 1997. Carbon distribution and net primary production of aspen, jack pine and black spruce BOREAS forests. *Journal of Geophysical Research*, 102(D24), 29029-29041.

Greaves, H.E., Vierling, L.A., Eitel, J.U.H., Boelman, N.T., Magney, T.S., Prager, C.M., and Griffin, K.L. 2015. Estimating aboveground biomass and leaf area of low-stature arctic shrubs with terrestrial lidar. *Remote Sensing of Environment*, 164, 26-35.

GSA BIM Guide for 3D Imaging. 2009. Available online: https://www.gsa.gov/portal/mediaId%20/226819/fileName/GSA_BIM_Guide_Series_03.action (accessed 18 December 2016).

Gullison, R.E., Frumhoff, P., Canadell, J., Field, C.B., Nepstad, D.C., Hayhoe, K., Avissar, R., Curran, L.M., Friedlingstein, P., Jones, C.D., and Nobre, C. 2007. Tropical forests and climate policy. *Science*, 316, 985-986.

Hancock, S., Essery, R., Reid, T., Carle, J., Baxter, R., Rutter, N. and Huntley, B. 2014. Characterising forest gap fraction with terrestrial lidar and photography: An examination of relative limitations. *Agricultural and forest meteorology*, 189, 105-114.

Haralick, R., and Shapiro, L. 1992. *Computer and Robot Vision*. Addison Wesley, Reading, Mass.

Harding, D.J., Lefsky, M.A., Parker, G.G., and Blair J.B. 2001. Laser altimeter canopy height profiles: methods and validation for closed-canopy, broadleaf forests. *Remote Sensing of Environment*, 76 (3), 283-297.

Haugerud, R.A., and Harding D.J. 2001. Some Algorithms for Virtual Deforestation (VDF) of LiDAR Topographic Survey Data. Proceedings of the ISPRS workshop on Land Surface Mapping and Characterization Using Laser Altimetry. Annapolis, Maryland, *International Archives of the Photogrammetry, Remote Sensing and Spatial Information Sciences*, 34 (3/W4), Commission III, 203-209.

Hauglin, M., Astrup, R., Gobakken, T., and Næsset, E. 2013. Estimating single-tree branch biomass of Norway spruce with terrestrial laser scanning using voxel-based and crown dimension features. *Scandinavian Journal of Forest Research*, 28 (5), 1-14.

Hebert, M., and Vandapel, N. 2003. Terrain classification techniques from ladar data for autonomous navigation. *Robotics Institute*, 411.

Herzfeld, U.C., Lingle, C.S. and Lee, L.H. 1993. Geostatistical evaluation of satellite radar altimetry for high-resolution mapping of Lambert Glacier, Antarctica. *Annals of Glaciology*, 17(1), 77-85.

Hollaus, M., Wagner, W., Eberhofer, C., and Karel, W. 2006. Accuracy of large-scale canopy heights derived from LiDAR data under operational constraints in a complex alpine environment. *ISPRS Journal of Photogrammetry and Remote Sensing*, 60 (5), 323-338.

Holopainen, M., Vastaranta, M., Kankare, V., Räty, M., Vaaja, M., Liang, X., Yu, X., Hyyppä, J., Hyyppä, H., Viitala, R. and Kaasalainen, S., 2011. Biomass estimation of individual trees using stem and crown diameter TLS measurements. *ISPRS-International Archives of the Photogrammetry, Remote Sensing and Spatial Information Sciences*, 38(12), 91-95.

Hong, S.H., Cho, H.S., Kim, N.H., and Sohn, H.G. 2015. 3D indoor modeling based on terrestrial laser scanning. *Journal of the Korean Society of Civil Engineers*, 35, 525-531.

Hopkinson, C., Lovell, J., Chasmer, L., Jupp, D., Kljun, N. and van Gorsel, E. 2013. Integrating terrestrial and airborne lidar to calibrate a 3D canopy model of effective leaf area index. *Remote Sensing of Environment*, 136, 301-314.

Horaud, R., Hansard, M., Evangelidis, G. and Ménier, C. 2016. An overview of depth cameras and range scanners based on time-of-flight technologies. *Machine Vision and Applications*, 27(7), 1005-1020.

Hosoi, F. and Omasa, K. 2009. Factors contributing to accuracy in the estimation of the woody canopy leaf area density profile using 3D portable LiDAR imaging. *Journal of Experimental Botany*, 58(12), 3463-3473.

Hosoi, F. and Omasa, K. 2009. Factors contributing to accuracy in the estimation of the woody canopy leaf area density profile using 3D portable LiDAR imaging. *Journal of Experimental Botany*, 58(12), 3463-3473.

Hosoi, F., and Omasa, K. 2006. Voxel-based 3-D modeling of individual trees for estimating leaf area density using high-resolution portable scanning lidar. *IEEE transactions on geoscience and remote sensing*, 44(12), 3610-3618.

Hosoi, F., and Omasa, K. 2007. Factors contributing to accuracy in the estimation of the woody canopy leaf area density profile using 3D portable lidar imaging. *Journal of Experimental Botany*, 58(12), 3463-3473.

Hosoi, F., and Omasa, K. 2009. Estimating vertical plant area density profile and growth parameters of a wheat canopy at different growth stages using three-dimensional portable lidar imaging. *ISPRS Journal of Photogrammetry and Remote Sensing*, 64(2), 151-158.

Hosoi, F. and Omasa, K. 2012. Estimation of vertical plant area density profiles in a rice canopy at different growth stages by high-resolution portable scanning LiDAR with a lightweight mirror. *ISPRS journal of photogrammetry and remote sensing*, 74, 11-19.

Hosoi, F., Nakai, Y., and Omasa, K. 2010. Estimation and error analysis of woody canopy leaf area density profiles using 3-D airborne and ground-based scanning lidar remote-sensing techniques. *IEEE Transactions on Geoscience and Remote Sensing*, 48(5), 2215-2223.

Hosoi, F., Nakai, Y. and Omasa, K. 2013. 3-D voxel-based solid modeling of a broad-leaved tree for accurate volume estimation using portable scanning LiDAR. *ISPRS journal of photogrammetry and remote sensing*, 82, 41-48.

Huang, P., and Pretzsch, H. 2010. Using terrestrial laser scanner for estimating leaf areas of individual trees in a conifer forest. *Trees*, 24 (4), 609-619.

Hyyppa, J., Kelle, O., Lehikoinen, M. and Inkinen, M. 2001. A segmentation-based method to retrieve stem volume estimates from 3-D tree height models produced by laser scanners. *IEEE Transactions on geoscience and remote sensing*, 39, 969-975.

Ishihara, M.I., and Hiura, T. 2011. Modeling leaf area index from litter collection and tree data in a deciduous broadleaf forest. *Agricultural and Forest Meteorology*, 151(7), 1016-1022.

Jaboyedoff, M., Oppikofer, T., Abellán, A., Derron, M. H., Loye, A., Metzger, R., and Pedrazzini, A. 2012. Use of LIDAR in landslide investigations: A review. *Natural Hazards*, 61, 5-28.

Jackson, R.B., Jobbágy, E.G., Avissar, R., Roy, S.B., Barrett, D.J., Cook, C.W., Farley, K.A., Le Maitre, D.C., McCarl, B.A. and Murray, B.C. 2005. Trading water for carbon with biological carbon sequestration. *Science*, 310(5756), 1944-1947.

Jacobsen, K., and Lohmann, P. 2003. Segmented filtering of laser scanner DSMs. *International Archives of Photogrammetry and Remote Sensing*, 34 (3/W13).

Jaw, J.J., and Chuang, T.Y. 2008. Registration of ground-based LIDAR point clouds by means of 3D line features. *Journal of the Chinese Institute of Engineers*, 31, 1031-1045.

Jones, L. 2006. Monitoring landslides in hazardous terrain using terrestrial LIDAR: An example from Montserrat. *Quarterly Journal of Engineering Geology and Hydrogeology*, 39, 371-373.

Jupp, D.L.B., Culvenor, D.S., Lovell, J.L., Newnham, G.J., Strahler, A.H., and Woodcock, C.E. 2009. Estimating forest LAI profiles and structural parameters using a ground based laser called 'Echidna (R)'. *Tree Physiology*, 29 (2), 171-181.

Kato, A., Moskal, L.M., Schiess, P., Swanson, M.E., Calhoun, D., and Stuetzle, W. 2009. Capturing tree crown formation through implicit surface reconstruction using airborne lidar data. *Remote Sensing of Environment*, 113 (6), 1148-1162.

Kelbe, D., Romanczyk, P., van Aardt, J. and Cawse-Nicholson, K. 2013. Reconstruction of 3D tree stem models from low-cost terrestrial laser scanner data. *SPIE Defense, Security, and Sensing*, 873106-873106.

Kilian, J., N. Haala, and M. English, 1996. Capture and Evaluation of Airborne Laser Scanner Data. *International Archives of Photogrammetry and Remote Sensing*, 31 (B3), Vienna, 383-388.

Kim, A.M., Olsen, R.C. and Béland, M. 2015. Simulation of small footprint full waveform LIDAR propagation through a tree canopy in 3D. In *SPIE Defense+ Security* (pp. 94650K-94650K). International Society for Optics and Photonics.

Kim, Y., Chang, A., Kim, Y., Song, J. and Kim, C. 2012. Estimation of forest biomass from airborne LiDAR data as measures against Global Warming-Individual Tree Unit and Forest Stand Unit. *Disaster Advances*, *5*(4), 295-299.

Kindermann, G., McCallum, I., Fritz, S. and Obersteiner, M. 2008. A global forest growing stock, biomass and carbon map based on FAO statistics. *Silva Fennica*, 42(3), 387-396.

Koetz, B., Morsdorf, F., Sun, G., Ranson, K.J., Itten, K., and Allgower, B. 2006. Inversion of a lidar waveform model for forest biophysical parameter estimation. *IEEE Geoscience and Remote Sensing Letter,* 3 (1), 49-53.

Kraus, K., and Mikhail, E.M., 1972. Linear least squares interpolation. 1016–1029.

Kraus, K., and Pfeifer, N. 1998. Determination of terrain models in wooded areas with airborne laser scanner data. *ISPRS International Archives of the Photogrammetry, Remote Sensing and Spatial Information Sciences*, 53, (4), 193-203.

Kraus, K., Karel, W., Briese, C. and Mandlburger, G. 2006. Local accuracy measures for digital terrain models. *The Photogrammetric Record*, 21 (116), 342-354.

Kucharik, C.J., Norman, J.M., Murdock, L.M., and Gower, S.T., 1997. Characterizing canopy non-randomness with a multiband vegetation imager (MVI). Journal of Geophysical Research, 102(D24), 29455-29473.

Kucharik, C.J., Norman, J.M., and Gower, S.T. 1998. Measurements of leaf orientation, light distribution and sunlit leaf area in a boreal aspen forest. *Agricultural and Forest Meteorology*, 91, 127-148.

Lalonde, J.F., Vandapel, N., Huber, D. F., and Hebert, M. 2006. Natural terrain classification using three-dimensional lidar data for ground robot mobility. *Journal of Field Robotics*, 23(10), 839-861.

Law, B.E., Van Tuyl, S., Cescatti, A. and Baldocchi, D.D. 2001. Estimation of leaf area index in open-canopy ponderosa pine forests at different successional stages and management regimes in Oregon. *Agricultural and Forest Meteorology*, 108(1), 1-14.

Leblanc, S.G., and Fournier, R.A. 2014. Hemispherical photography simulations with an architectural model to assess retrieval of leaf area index. *Agricultural and Forest Meteorology*, 194, 64-76.

Lee, H.S., and Younan, N. 2003. DTM extraction of LiDAR returns via adaptive processing. *IEEE Transactions on Geoscience and Remote Sensing*, 41 (9), 2063-2069.

Lefsky, M. A., Cohen, W. B., Acker, S. A., Parker, G. G., Spies, T. A., and Harding, D. 1999. LiDAR remote sensing of the canopy structure and biophysical properties of Douglas-fir western hemlock forests. *Remote Sensing of Environment*, 70(3), 339-361.

Lefsky, M., and McHale, M. 2008. Volume estimates of trees with complex architecture from terrestrial laser scanning. *Journal of Applied Remote Sensing*, 2(1), 023521-023521.

Lefsky, M.A., Cohen W.B., Parker G.G., and Harding D.J. 2002. LiDAR Remote Sensing for Ecosystem Studies. *BioScience*, 52(1), 19-30.

Lefsky, M.A., Cohen, W.B. and Spies, T.A. 2001. An evaluation of alternate remote sensing products for forest inventory, monitoring, and mapping of Douglas-fir forests in western Oregon. *Canadian journal of forest research*, 31(1), 78-87.

Lefsky, M.A., Cohen, W.B., Acker, S.A., Parker, G.G., Spies, T.A., and Harding, D.J. 1999. LiDAR remote sensing of the canopy structure and biophysical properties of Douglas-fir western hemlock forests. *Remote Sensing of Environment*, 70(3), 339-361.

Li, Z., Douglas, E., Strahler, A., Schaaf, C., Yang, X., Wang, Z., Yao, T., Zhao, F., Saenz, E. J., Paynter, I., and Woodcock C.E. 2013. Separating leaves from trunks and branches with Dual_Wavelenght Terrestrial Lidar Scanning. *In Geoscience and Remote Sensing Symposium (IGARSS) IEEE,* 3383- 3386.

Liang, X., Kankare, V., Hyyppä, J., Wang, Y., Kukko, A., Haggrén, H., Yu, X., Kaartinen, H., Jaakkola, A., Guan, F., Holopainen, M., Vastaranta, M. 2016. Terrestrial laser scanning in forest inventories. *ISPRS Journal of Photogrammetry and Remote Sensing*, 115, 63-77.

Liang, X.L., Litkey, P., Hyyppa, J., Kaartinen, H., Vastaranta, M., and Holopainen, M. 2012. Automatic stem mapping using single-scan terrestrial laser scanning. *IEEE Transactions on Geoscience and Remote Sensing*, 50(2), 661-670.

Lim, K., Treitz, P., Wulder, M., St-Onge, B. and Flood, M. 2003. LiDAR remote sensing of forest structure. *Progress in physical geography*, 27(1), 88-106.

Lin, Y., and Herold, M. 2016. Tree species classification based on explicit tree structure feature parameters derived from static terrestrial laser scanning data. *Agricultural and Forest Meteorology*, 216, 105-114.

Lin, Y., and West, G. 2016. Retrieval of effective leaf area index (LAIe) and leaf area density (LAD) profile at individual tree level using high density multi-return airborne LiDAR. *International Journal of Applied Earth Observation and Geoinformation*, 50, 150-158.

Liu, X. 2008. Airborne LIDAR for DEM generation: Some critical issues. *Progress in Physical Geography*, 32, 31-49.

Liu, Z., and Jin, G. 2017. Importance of woody materials for seasonal variation in leaf area index from optical methods in a deciduous needle leaf forest. *Scandinavian Journal of Forest Research*, 1-11.

Lohmann, P., Koch, A., and Schaeffer, M. 2000. Approaches to the filtering of laser scanner data. *International Archives of Photogrammetry and Remote Sensing*, 33(B3/1), 534-541.

Loudermilk, E.L., Hiers, J.K., O'Brien, J.J., Mitchell, R.J., Singhania, A., Fernandez, J.C., and Slatton, K.C. 2009. Ground-based LIDAR: a novel approach to quantify fine scale fuel bed characteristics. *International Journal Wildland Fire*, 18 (6), 676-685.

Lovell, J.L., Jupp, D.L.B., Culvenor, D.S., and Coops, N.C. 2003. Using airborne and ground-based ranging LiDAR to measure canopy structure in Australian forests. *Canadian Journal of Remote Sensing*, 29 (5), 607-622.

Lovell, J.L., Jupp, D.L.B., Newnham, G.J., and Culvenor, D.S. 2011. Measuring tree stem diameters using intensity profiles from ground-based scanning LiDAR from a fixed viewpoint. *ISPRS Journal of Photogrammetry and Remote Sensing*, 66(1), 46-55.

Ma, L., Zheng, G., Eitel, J. U. H., Moskal, M., He, W., and Huang, H. 2016. Improved Salient Feature-Based Approach for Automatically Separating Photosynthetic and Nonphotosynthetic Components Within Terrestrial Lidar Point Cloud Data of Forest Canopies. *IEEE Transaction on Geoscience and Remote Sensing*, 54(2), 679-696.

Ma, L., Zheng, G., Eitel, J.U., Magney, T.S. and Moskal, L.M. 2016a. Determining woody-to-total area ratio using terrestrial laser scanning (TLS). *Agricultural and Forest Meteorology*, 228, 217-228.

Ma, L., Zheng, G., Eitel, J.U., Moskal, L.M., He, W. and Huang, H. 2016b. Improved salient feature-based approach for automatically separating photosynthetic and nonphotosynthetic components within terrestrial LiDAR point cloud data of forest canopies. *IEEE Transactions on Geoscience and Remote Sensing*, 54(2), 679-696.

Maas, H-G., Bienert, A., Scheller, S., and Keane, E. 2008. Automatic forest inventory parameter determination from terrestrial laser scanner data. *International Journal of Remote Sensing*, 29(5), 1579-1593.

Maass, J., Vose, J.M., Swank, W.T., and Martínez-Yrízar, A. 1995. Seasonal changes of leaf area index (LAI) in a tropical deciduous forest in west Mexico. *Forest Ecology and Management*, 74(1), 171-180.

Macfarlane, C., Hoffman, M., Eamus, D., Kerp, N., Higginson, S., McMurtrie, R. and Adams, M. 2007. Estimation of leaf area index in eucalypt forest using digital photography. *Agricultural and Forest Meteorology*, 143(3), 176-188.

Maguya, A. S., Junttila, V. and Kauranne, T. 2014. Algorithm for Extracting Digital Terrain Models under Forest Canopy from Airborne LiDAR Data. *Remote Sensing*, 6, 6524-6548.

Margolis, H.A., Nelson, R.F., Montesano, P.M., Beaudoin, A., Sun, G., Andersen, H.E. and Wulder, M.A. 2015. Combining satellite lidar, airborne lidar, and ground plots to estimate the amount and distribution of aboveground biomass in the boreal forest of North America. *Canadian Journal of Forest Research*, 45(7), 838-855.

Martínez, B., García-Haro, F.J. and Camacho-de Coca, F. 2009. Derivation of high-resolution leaf area index maps in support of validation activities: Application to the cropland Barrax site. *Agricultural and forest meteorology*, 149(1), 130-145.

MATLAB R2016b, the MathWorks lnc., Natick, Massachusetts, United States, 2016.

McIntosh, A.C., Gray, A.N. and Garman, S.L. 2009. Canopy structure on forest lands in western Oregon: Differences among forest types and stand ages. United States Department of Agriculture, Forest Service, Pacific Northwest Research Station, General Technical Report PNW-GTR-794 August 2009.

McKinley, D.C., Ryan, M.G., Birdsey, R.A., Giardina, C.P., Harmon, M.E., Heath, L.S., Houghton, R.A., Jackson, R.B., Morrison, J.F., Murray, B.C. and Pataki, D.E. 2011. A synthesis of current knowledge on forests and carbon storage in the United States. *Ecological Applications*, 21(6), pp.1902-1924.

MEA, M.E.A. 2005. Ecosystems and human well-being: synthesis. *Island, Washington, DC*.

Meng, X., Currit, N., and Zhao, K. 2010. Ground filtering algorithms for airborne LiDAR data: A review of critical issues. *Remote Sensing*, 2 (3), 833-860.

Miller, C. and LaFelamme, R.A. 1958. The digital terrain model theory and applications. *Photogrammetric Engineering*, 24 (3), 433-442.

Moholdt, G., Nuth, C., Hagen, J.O., and Kohler, J. 2010. Recent elevation changes of Svalbard glaciers derived from ICES at laser altimetry. *Remote Sensing of Environment*, 114, 2756-2767.

Mongus, D., and Zalik, B. 2012. Parameter-free ground filtering of LiDAR data for automatic DTM generation. *ISPRS Journal of Photogrammetry and Remote Sensing*, 67, 1-12.

Monsi, M., and Saeki, T. 2005. On the factor light in plant communities and its importance for matter production. *Annals of Botany*, 95 (3), 549-567.

Montealegre, A.L., Lamelas, M.T., and de la Riva, J. 2015. A Comparison of Open-Source LiDAR Filtering Algorithms in a Mediterranean Forest Environment. *IEEE Journal of Selected Topics in Applied Earth Observations and Remote Sensing*, 8(8), 4072-4085.

Moorthy, I., Miller, J.R., Hu, B.X., Chen, J., and Li, Q.M. 2008. Retrieving crown leaf area index from an individual tree using ground-based LiDAR data. *Canadian Journal of Remote Sensing*, 34 (3), 320-332.

Morsdorf, F., Kotz, B., Meier, E., Itten, K., Allgower, B., 2006. Estimation of LAI and fractional cover from small footprint airborne laser scanning data based on gap fraction. *Remote Sensing of Environment*, 104, 50-61.

Morsdorf, F., Nichol, C., Malthus T., and Woodhouse, I.H..2009. Assessing forest structural and physiological information content of multi-spectral LiDAR waveforms by radiative transfer modelling. *Remote Sensing of Environment*,113, 2152-2163.

Næsset, E. 1997. Determination of mean tree height of forest stands using airborne laser scanner data. *ISPRS Journal of Photogrammetry and Remote Sensing,* 52, 49-56.

Næsset, E., Gobakken, T., Holmgren, J., Hyyppä, H., Hyyppä, J., Maltamo, M., Nilsson, M., Olsson, H., Persson, Å. and Söderman, U. 2004. Laser scanning of forest resources: the Nordic experience. *Scandinavian Journal of Forest Research*, 19(6), 482-499.

Nardinocci, C., Forlani, G., and Zingaretti, P. 2003. Classification and filtering of laser data. *International Archives of Photogrammetry and Remote Sensing*, 34.3/W13.

Nasahara, K.N., Muraoka, H., Nagai, S. and Mikami, H. 2008. Vertical integration of leaf area index in a Japanese deciduous broad-leaved forest. *Agricultural and forest meteorology*, 148 (6), 1136-1146.

Nilsson, M. 1996. Estimation of tree heights and stand volume using an airborne LIDAR system. *Remote Sensing of Environment*, 56, 1-7.

Norman, J.M. and Campbell, G.S. 1989. "Canopy structure," in Plant Physiological Ecology. Field Methods and Instrumentation, J. E. R. W. Pearcy, H. A. Mooney, and P. W. Rundel, Eds. New York: Chapman and Hall, 301-325.

NRC (2007). Earth science and applications from space: National imperatives for the next decade and beyond, 2007. Washington, D.C., The National Academies Press, 426 pp.

Nurunnabi, A., West, G., and Belton, D. 2016. Robust Locally Weighted Regression Techniques for Ground Surface Points Filtering in Mobile Laser Scanning Three Dimensional Point Cloud Data. *IEEE, transactions on geoscience and remote sensing*, 54 (4), 2181-2193.

Olivas, P.C., Oberbauer, S.F., Clark, D.B., Clark, D.A., Ryan, M.G., O'Brien, J.J. and Ordonez, H. 2013. Comparison of direct and indirect methods for assessing leaf area index across a tropical rain forest landscape. *Agricultural and forest meteorology*, 177, 110-116.

Olsoy, P. J., Glenn, N.F., Clark, P.E., and Derryberry, D.R. 2014. Aboveground total and green biomass of leaf-off land shrub derived from terrestrial laser scanning. *ISPRS Journal of Photogrammetry and Remote Sensing*, 88, 166-173.

Olsoy, P.J., Glenn, N.F., and Clark, P.E. 2014b. Estimating sagebrush biomass using terrestrial laser scanning (TLS). *Rangeland Ecology and Management*, 67(2), 224-228.

Omasa, K., Hosoi, F., and Konishi, A. 2006. 3D lidar imaging for detecting and understanding plant responses and canopy structure. *Journal of experimental botany*, 58(4), 881-898.

Omasa, K., Hosoi, F., and Konishi, A. 2007. 3D lidar imaging for detecting and understanding plant responses and canopy structure. *Journal of Experimental Botany*, 58 (4), 881-898.

Pan, Y., Birdsey, R.A., Fang, J., Houghton, R., Kauppi, P.E., Kurz, W.A., Phillips, O.L., Shvidenko, A., Lewis, S.L., Canadell, J.G. and Ciais, P. 2011. A large and persistent carbon sink in the world's forests. *Science*, 333(6045), 988-993.

Parker, G.G. 1995. Structure and microclimate of forest canopies. In: Lowman, M., Madkarni, N. (Eds.), Forest Canopies. *Academic Press, California, USA*, 73-106.

Petrie, G. and Kennie T.J.M. 1987. Terrain Modeling in surveying and Civil Engineering. *Computer-Aided Design*, 19 (4), 171-187.

Pfeifer, N. and Mandlburger, G. 2009. LiDAR data filtering and DTM generation. *Topographic Laser Ranging and Scanning*, 307–334.

Pfeifer, N., Reiter, T., Briese, C., and Rieger, W. 1999. Interpolation of high quality ground models from laser scanner data in forested areas. *International Archives of Photogrammetry and Remote Sensing*, 32 (3/W14), 31-36.

Pfennigbauer, M., and A. Ullrich, 2010. Improving quality of laser scanning data acquisition through calibrated amplitude and pulse deviation measurement. *Proceedings of SPIE*, 7684.

Pirotti, F., and Tarolli, P. 2010. Suitability of LiDAR point density and derived landform curvature maps for channel network extraction. *Hydrological Processes*, 24, 1187-1197.

Pope, A., Willis, I., Rees, W., Arnold, N., and Pálsson, F. 2013. Combining airborne LIDAR and landsat ETM+ data with photoclinometry to produce a digital elevation model for Langjökull, Iceland. *International Journal of Remote Sensing*, 34, 1005-1025.

Popescu, S.C., Wynne, R.H., and Nelson, R.F. 2003. Measuring individual tree crown diameter with LIDAR and assessing its influence on estimating forest volume and biomass. *Canadian Journal of Remote Sensing*, 29, 564-577.

Pozar, D.M., 2006. Microwave engineering. *Publishing House of Electronics Industry*.

Prince, S.D., and Goward, S.N. 1995. Global primary production: a remote sensing approach. *Journal of Biogeography,* 22, 815-835.

Prokop, A. 2008. Assessing the applicability of terrestrial laser scanning for spatial snow depth measurements. *Cold Regions Science and Technology*, 54, 155-163.

Pueschel, P., Newnham, G., and Hill, J. 2014. Retrieval of Gap Fraction and Effective Plant Area Index from Phase-Shift Terrestrial Laser Scans. *Remote Sensing*, 6, 2601-2627.

Raber, G.T., Jensen, J.R. Schill, S.R. and Schuckman, K. 2002. Creation of Digital Terrain Models Using an Adaptive LiDAR Vegetation Point Removal Process. *Photogrammetric Engineering and Remote Sensing*, 68 (12), 1307-1316.

Radtke, P.J., and Bolstad, P.V. 2001. Laser point-quadrat sampling for estimating foliage-height profiles in broad-leaved forests. *Canadian Journal of Forest Research*, 31 (3), 410-418.

Reutebuch, S.E., Andersen, H.E. and McGaughey, R.J. 2005. Light detection and ranging (LIDAR): an emerging tool for multiple resource inventory. *Journal of Forestry*, 103(6), 286-292.

Reutebuch, S.E., McGaughey, R. J., Andersen, H. E., and Carson, W.W. 2003. Accuracy of a high-resolution LiDAR terrain model under a conifer forest canopy. *Canadian Journal of Remote Sensing*, 29 (5), 527-535.

Reutebuch, S.E., McGaughey, R. J., Andersen, H. E., and Carson, W.W. 2003. Accuracy of a high-resolution LiDAR terrain model under a conifer forest canopy. *Canadian Journal of Remote Sensing*, 29 (5), 527-535.

Riaño, D., Valladares, F., Condés, S. and Chuvieco, E. 2004. Estimation of leaf area index and covered ground from airborne laser scanner (LiDAR) in two contrasting forests. *Agricultural and Forest Meteorology*, 124 (3), 269-275.

Roering, J.J., Stimely, L.L., Mackey, B.H., and Schmidt, D.A. 2009. Using DInSAR, airborne LIDAR, and archival air photos to quantify landsliding and sediment transport. *Geophysical Research Letters*, 36, 1-5.

Roggero, M. 2001. Airborne laser scanning: clustering in raw data. *International Archives of the Photogrammetry, Remote Sensing and Spatial Information Sciences,* 34 (3/W4), 227- 232.

Roncella, R., Saletti, R., and Terreni, P. 1991. A novel bit-level systolic array median filter. In Solid-State Circuits Conference, ESSCIRC'91. Proceedings-Seventeenth European. *IEEE*. 1, 97-100.

Ross, J. 1981. The radiation regime and architecture of plant stands. *The Hague*, 391.

Running, S.W., Thornton, P.E., Nemani, R. and Glassy, J.M. 2000. Global terrestrial gross and net primary productivity from the Earth Observing System. *Methods in ecosystem science*, 3, 44-45.

Ryu, Y., Sonnentag, O., Nilson, T., Vargas, R., Kobayashi, H., Wenk, R., and Baldocchi, D.D. 2010. How to quantify tree leaf area index in an open savanna ecosystem: a multi-instrument and multi-model approach. *Agriculture and Forest Meteorology*, 150 (1), 63-76.

Sainte-Marie, J., Saint-André, L., Nouvellon, Y., Laclau, J.P., Roupsard, O., Le Maire, G., Delpierre, N., Henrot, A. and Barrandon, M. 2014. A new probabilistic canopy dynamics model (SLCD) that is suitable for evergreen and deciduous forest ecosystems. *Ecological modeling*, 290,121-133.

Schilling, A., Schmidt, A., and Maas, H.G. 2012. Tree topology representation from TLS point clouds using depth-first search in voxel space. *Photogrammetric Engineering and Remote Sensing*, 78(4), 383-392.

Schleppi, P., Conedera, M., Sedivy, I. and Thimonier, A. 2007. Correcting non-linearity and slope effects in the estimation of the leaf area index of forests from hemispherical photographs. *Agricultural and Forest Meteorology*, 144 (3), 236-242.

Scholes, R.J., Frost, P.G.H., and Tian, Y. 2004. Canopy structure in savannas along a moisture gradient on Kalahari sands. *Global Change Biology*, 10, 292-302.

Sellers, P.J., Dickinson, R.E., Randall, D.A., Betts, A.K., Hall, F.G., Berry, J.A., Collatz, G.J., Denning, A.S., Mooney, H.A., Nobre, C.A. and Sato, N. 1997. Modeling the exchanges of energy, water, and carbon between continents and the atmosphere. *Science*, 275(5299), pp.502-509.

Serifoglu, C., Gungor, O., and Yilmaz V. 2016. Performance evaluation of different ground filtering algorithms for UAV-based point clouds. *The International Archives of the Photogrammetry, Remote Sensing and Spatial Information Sciences*, 41.

Sexton, J.O., Bax, T., Siqueir, Paul., Swenson, J.J., and Hensley, S. 2009.A comparison of lidar, radar, and field measurements of canopy height in pine and hardwood forests of southeastern North America. *Forest Ecology and Management*, 257, 1136-1147.

Shan, J. and Sampath, A. 2005. Urban DEM generation from raw LiDAR data: A labelling algorithm and its performance. *Photogrammetric Engineering and Remote Sensing*, 71(2), 217-226.

Sheng, Y., Gong, P., and Biging, G.S. 2003. Orthoimage production for forested areas from large-scale aerial photographs. *Photogrammetric Engineering and Remote Sensing*, 69, 259-66.

Simonse, M., Aschoff, T., Spiecker, H. and Thies, M. 2003. Automatic determination of forest inventory parameters using terrestrial laser scanning. *In Proceedings of the scandlaser scientific workshop on airborne laser scanning of forests,* 252-258.

Sims, D.A., and Gamon, J.A. 2003. Estimation of vegetation water content and photosynthetic tissue area from spectral reflectance: a comparison of indices based on liquid water and chlorophyll absorption features. *Remote Sensing of Environment*, 84 (4), 526-537.

Sithole, G. 2001. Filtering of Laser Altimetry Data Using a Slope Adaptive Filter. *International Archives of Photogrammetry Remote Sensing and Spatial Information Sciences*, 34(3/W4), 203-210.

Sithole, G. 2005. Segmentation and classification of airborne laser scanner data.

Sithole, G. and Vosselman, G. 2004. Experimental comparison of filter algorithms for bare earth extraction from airborne laser scanning point clouds. *ISPRS Journal of Photogrammetry and Remote Sensing*, 59, 85-101.

Slob, S., Hack, R. 2004. 3D terrestrial laser scanning as a new field measurement and monitoring technique. *Engineering geology for infrastructure planning in Europe*, 179-189.

Sohn, G., and Dowman, I. 2002. Terrain surface reconstruction by the use of tetrahedron model with the MDL criterion. *International Archives of the Photogrammetry, Remote Sensing and Spatial Information Sciences*, 34 (3A), 336-344.

Song, Y., Maki, M., Imanishi, J. and Morimoto, Y. 2011. Voxel-based estimation of plant area density from airborne laser scanner data. *In Proceedings of the ISPRS Workshop Laser Scanning, Calgary, Canada,* 38, (5/W12), 209-212.

Stoker, J. 2009. Visualization of multiple-return lidar data: using voxels. *Photogrammetric Engineering and Remote Sensing*, 75 (2), 109-112.

Strahler, A.H., Jupp, D.L., Woodcock, C.E., Schaaf, C.B., Yao, T., Zhao, F., Yang, X., Lovell, J., Culvenor, D., Newnham, G. and Ni-Miester, W. 2008. Retrieval of forest structural

parameters using a ground-based lidar instrument (Echidna®). *Canadian Journal of Remote Sensing*, 34(S2), 426-440.

Streutker, D., and Glenn, N. 2006. LiDAR measurement of sagebrush steppe vegetation heights. *Remote Sensing of Environment*, 102 (1–2), 135-145.

Styers, D.M., Moskal, L.M., Richardson, J.J. and Halabisky, M.A. 2014. Evaluation of the contribution of LiDAR data and post classification procedures to object-based classification accuracy. *Journal of Applied Remote Sensing*, 8(1), 1-17.

Takeda, T., Oguma, H., Sano, T., Yone, Y. and Fujinuma, Y. 2008. Estimating the plant area density of a Japanese larch (Larix kaempferi Sarg.) plantation using a ground-based laser scanner. *Agricultural and Forest Meteorology*, 148(3), 428-438.

Thoren, D., and Schmidhalter, U. 2009. Nitrogen status and biomass determination of oilseed rape by laser-induced chlorophyll fluorescence. *European Journal of Agronomy*, 30, 238-242.

Tóvári, D. and Pfeifer, N., 2005. Segmentation based robust interpolation-a new approach to laser data filtering. *International Archives of Photogrammetry, Remote Sensing and Spatial Information Sciences*, 36(3/19), 79-84.

Tyagur, N. and Hollaus, M. 2016. Digital terrain models from mobile laser scanning data in Moravian Karst. *International Archives of the Photogrammetry, Remote Sensing and Spatial Information Sciences*, 41, 387-394.

Vandapel, N., Huber, D.F., Kapuria, A., and Hebert, M. 2004.Natural terrain classification using 3-D lidar data. *in Proc. IEEE ICRA, New York, NY, USA*, 1–5, 5117-5122.

Vosselman, G. 2000. Slope based filtering of laser altimetry data. *International Archives of the Photogrammetry, Remote Sensing and Spatial Information Sciences*, 33 (B3), 935-942.

Vosselman, G., and Mass, H. 2001. Adjustment and Filtering of Raw Laser Altimetry Data. In *Proceedings of OEEPE Workshop on Airborne Laserscanning and Interferometric SAR for Detailed Digital Terrain Models, Stockholm, Sweden*.

Vosselman, G., and Maas, H. G. 2010. *Airborne and Terrestrial Laser Scanning*. CRC Press, 2010.

Wack, R., and Wimmer, A. 2002. Digital terrain models from airborne laser scanner data- a grid based approach. *International Archives of the Photogrammetry, Remote Sensing and Spatial Information Sciences*, 34 (3B), 293-296.

Wang, Y., Mercer, B., Tao, C., Sharma, J., and Crawford, S. 2001. Automatic Generation of Bald Earth Digital Elevation Models from Digital Surface Models Created Using Airborne IFSAR. In *Proceedings of 2001 ASPRS Annual Conference* (23-27).

Wang, Y., Weinacker, H. and Koch, B. 2008. A lidar point cloud based procedure for vertical canopy structure analysis and 3D single tree modeling in forest. *Sensors*, 8(6), 3938-3951.

Wang, Z., Li, H., and Wu, L. 2010. Geodesics-based topographical feature extraction from airborne LIDAR data for disaster management. In *Geoinformatics, 2010 18th International Conference on* (pp. 1-5). IEEE.

Warren Wilson, J. 1959. Analysis of the spatial distribution of foliage by two dimensional point quadrats. *New Phytologist*, 58 (1), 92-99.

Warren Wilson, J. 1960. Inclined point quadrats. *New Phytologist*, 59 (1), 1-8.

Warren Wilson, J., 1963. Errors resulting from thickness of point quadrats. *Australian Journal of Botany*, 11, 178-188.

Watson, D.J. 1947. Comparative physiological studies on the growth of field crops. I. Variation in net assimilation rate and leaf area between species and varieties, and within and between years. *Australian Journal of Botany*, 11, 41-76.

Watt, P.J., and Donoghue, D.N.M. 2005. Measuring forest structure with terrestrial laser scanning. *International Journal of Remote Sensing*, 26 (7), 1437-1446.

Weiss, M., Baret, F., Smith, G.J., Jonckheere, I. and Coppin, P. 2004. Review of methods for in situ leaf area index (LAI) determination: Part II. Estimation of LAI, errors and sampling. *Agricultural and Forest Meteorology*, 121(1), 37-53.

White, S.A., and Wang, Y. 2003. Utilizing dems derived from LiDAR data to analyze morphologic change in the North Carolina coastline. *Remote Sensing of Environment*, 85 (1), 39-47.

Whitford, K., Colquhoun, I., Lang, A., and Harper, B. 1995. Measuring leaf area index in a sparse eucalypt forest: A comparison of estimates from direct measurement, hemispherical photography, sunlight transmittance and allometric regression. *Agricultural Forest Meteorology*, 74(3), 237–249.

Whitman, D., Zhang, K., Leatherman, S.P., and Robertson, W. 2003. Airborne laser topographic mapping: application to hurricane storm surge hazards. *Earth Science in the City: A Reader*, 363-376.

Widlowski, J.L., Côté, J.F. and Béland, M. 2014. Abstract tree crowns in 3D radiative transfer models: Impact on simulated open-canopy reflectances. *Remote Sensing of Environment*, 142, 155-175.

Woolard, J.W., and Colby, J.D. 2002. Spatial characterization, resolution, and volumetric change of coastal dunes using airborne LIDAR: Cape Hatteras, North Carolina. *Geomorphology*, 48, 269-287.

Wu, J.Y., Cawse-Nicholson, K., and Aardt, J.V. 2013. 3D Tree reconstruction from simulated small footprint waveform lidar. *Photogrammetric Engineering and Remote Sensing*, 79 (12), 1147-1157.

Wulder, M.A., Bater, C.W., Coops, N.C., Hilker, T. and White, J.C. 2008. The role of LiDAR in sustainable forest management. *The Forestry Chronicle*, 84(6), 807-826.

Wulder, M.A., White, J.C., Bater, C.W., Coops, N.C., Hopkinson, C. and Chen, G. 2012a. Lidar plots -A new large-area data collection option: Context, concepts, and case study. *Canadian Journal of Remote Sensing*, 38(05), 600-618.

Wulder, M.A., White, J.C., Nelson, R.F., Næsset, E., Ørka, H.O., Coops, N.C., Hilker, T., Bater, C.W. and Gobakken, T. 2012. Lidar sampling for large-area forest characterization: A review. *Remote Sensing of Environment*, 121, 196-209.

Yu, B., Liu, H., Wu, J., Hu, Y., and Zhang, L. 2010. Automated derivation of urban building density information using airborne LIDAR data and object-based method. *Landscape and Urban Planning*, 98, 210-219.

Yu, X., Hyyppä, J., Kaartinen, H. and Maltamo, M. 2004. Automatic detection of harvested trees and determination of forest growth using airborne laser scanning. *Remote Sensing of Environment*, 90(4), 451-462.

Yue, C., Ciais, P., Luyssaert, S., Cadule, P., Harden, J., Randerson, J., Bellassen, V., Wang, T., Piao, S., Poulter, B., and Viovy, N. 2013. Simulating boreal forest carbon dynamics after stand-replacing fire disturbance: insights from a global process-based vegetation model. *Biogeoscience*, 10, 8233-8252.

Zakˇsek, K. and Pfeifer, N. 2006. An improved morphological filter for selecting relief points from a LIDAR point cloud in steep areas with dense vegetation. *Luubljana, Slovenia and Innsbruck, Austria: Institute of Anthropological and Spatial Studies, Scientific Research*

Centre of the Slovenian Academy of Sciences and Arts, and Institute of Geography, Innsbruck University.

Zhang, C. 2003. A progressive morphological filter for removing nonground measurements from airborne LIDAR data. *IEEE Transactions on Geoscience and Remote Sensing*, 41(4), 872-882.

Zhang, J., and Lin, X. 2013. Filtering airborne LiDAR data by embedding smoothness-constrained segmentation in progressive TIN densification. *ISPRS International Archives of the Photogrammetry, Remote Sensing and Spatial Information Sciences*, 81, 44-59.

Zhang, K., and Whitman, D. 2005. Comparison of three algorithms for filtering airborne LiDAR data. *Photogrammetric Engineering and Remote Sensing*, 71 (3), 313–324.

Zhang, K., Chen, S., Whitman, D., Shyu, M., Yan, J., and Zhang, C. 2003. A progressive morphological filter for removing nonground measurements from airborne LIDAR data. *IEEE Transactions on Geoscience and Remote Sensing*, 41(4), 872–882.

Zhao, F., Yang, X., Schull, M.A., Roman-Colon, M., Yao, T., and Wang, Z. 2011. Measuring effective leaf area index foliage profile, and stand height in New England forest stands using a full-waveform ground-based lidar. *Remote Sensing of Environment*, 115, 2954-2964.

Zhao, K., García, M., Liu, S., Guo, Q., Chen, G., Zhang, X., Zhou, Y. and Meng, X. 2015. Terrestrial LiDAR remote sensing of forests: Maximum likelihood estimates of canopy profile, leaf area index, and leaf angle distribution. *Agricultural and Forest Meteorology*, 209, 100-113.

Zheng, D.L., Rademacher, J., Chen, J.Q., Crow, T., Bresee, M., le Moine, J., and Ryu, S.R. 2004. Estimating aboveground biomass using Landsat 7 ETM+ data across a managed landscape in northern Wisconsin, USA. *Remote Sensing of Environment,* 93, 402-411.

Zheng, G. and Moskal, L.M. 2012a. Computational-geometry-based retrieval of effective leaf area index using terrestrial laser scanning. *IEEE Transactions on Geoscience and Remote Sensing*, 50(10), 3958-3969.

Zheng, G. and Moskal, L.M. 2012b. Leaf orientation retrieval from terrestrial laser scanning (TLS) data. *IEEE Transactions on Geoscience and Remote Sensing*, 50(10), 3970-3979.

Zheng, G. and Moskal, L.M. 2012c. Spatial variability of terrestrial laser scanning based leaf area index. *International Journal of Applied Earth Observation and Geoinformation*, 19, 226-237.

Zheng, G., and Moskal, L.M. 2012. Spatial variability of terrestrial laser scanning based leaf area index. *International Journal of Applied Earth Observation and Geoinformation*, 19, 226-237.

Zheng, G., Chen, J.M., Tian, Q., Ju, W.M., and Xia, X.Q. 2007. Combining remote sensing imagery and forest age inventory for biomass mapping. Journal of Environmental Management, 85, 616-623.

Zheng, G., Ma, L., He, W., Eitel, J.U., Moskal, L.M. and Zhang, Z. 2016. Assessing the contribution of woody materials to forest angular gap fraction and effective leaf area index using terrestrial laser scanning data. *IEEE Transactions on Geoscience and Remote Sensing*, 54(3), 1475-1487.

Zheng, G., Moskal, L.M. and Kim, S.H. 2013. Retrieval of effective leaf area index in heterogeneous forests with terrestrial laser scanning. *IEEE Transactions on Geoscience and Remote Sensing*, 51(2), 777-786.

Zhou, X. and Hemstrom, M.A. 2009. Estimating aboveground tree biomass on forest land in the Pacific Northwest: a comparison of approaches.